Argonne NATIONAL LABORATORY

ANL/LWRS-15/02

Tensile and Fatigue Testing and Material Hardening Model Development for 508 LAS Base Metal and 316 SS Similar Metal Weld under In-air and PWR Primary Loop Water Conditions

Nuclear Engineering Division

About Argonne National Laboratory

Argonne is a U.S. Department of Energy laboratory managed by UChicago Argonne, LLC under contract DE-AC02-06CH11357. The Laboratory's main facility is outside Chicago, at 9700 South Cass Avenue, Argonne, Illinois 60439. For information about Argonne and its pioneering science and technology programs, see www.anl.gov.

ANL/LWRS-15/02

Tensile and Fatigue Testing and Material Hardening Model Development for 508 LAS Base Metal and 316 SS Similar Metal Weld under In-air and PWR Primary Loop Water Conditions

Subhasish Mohanty, William Soppet, Saurin Majumdar, and Ken Natesan

Nuclear Engineering Division, Argonne National Laboratory

September 2015

This page intentionally left blank

ABSTRACT

This report provides an update on an assessment of environmentally assisted fatigue for light water reactor components under extended service conditions. This report is a deliverable in September 2015 under the work package for environmentally assisted fatigue under DOE's Light Water Reactor Sustainability program. In an April 2015 report we presented a baseline mechanistic finite element model of a two-loop pressurized water reactor (PWR) for system-level heat transfer analysis and subsequent thermal-mechanical stress analysis and fatigue life estimation under reactor thermal-mechanical cycles. In the present report, we provide tensile and fatigue test data for 508 low-alloy steel (LAS) base metal, 508 LAS heat-affected zone metal in 508 LAS–316 stainless steel (SS) dissimilar metal welds, and 316 SS-316 SS similar metal welds. The test was conducted under different conditions such as in air at room temperature, in air at 300 ^{o}C, and under PWR primary loop water conditions. Data are provided on materials properties related to time-independent tensile tests and time-dependent cyclic tests, such as elastic modulus, elastic and offset strain yield limit stress, and linear and nonlinear kinematic hardening model parameters. The overall objective of this report is to provide guidance to estimate tensile/fatigue hardening parameters from test data. Also, the material models and parameters reported here can directly be used by industry for finite element fatigue and ratcheting evaluation of reactor components under in-air and PWR water conditions.

This page intentionally left blank

TABLE OF CONTENTS

Tensile and Fatigue Testing and Material Hardening Model Development for 508 LAS Base Metal and 316 SS Similar Metal Weld under In-air and PWR Primary Loop Water Conditions i

ABSTRACT i

Table of Contents iii

List of Figures v

List of TABLES x

Abbreviations xii

Acknowledgments xiii

1 Introduction 1

2 Time-Dependent Material Models Based on Cyclic Plasticity: Theoretical Background 3

2.1 Cyclic Plasticity Model 3

2.2 Estimation of Time-dependent Elastic Modulus, Elastic Limit, and Offset Strain Yield Stress 4

2.3 Modeling of Intra-Cycle Hardening and Estimation of Time-Dependent Kinematic Hardening Parameters 5

3 Test Specimens and Experimental Setup 11

3.1 Test Specimen Material and Geometry 11

3.2 Experimental Setup 14

3.2.1 In-air tensile/fatigue test setup 14

3.2.2 PWR water loop fatigue test setup 16

4 Results from 508 LAS Base and HAZ Metal Tensile Test and Material Model 21

4.1 Test Conditions for 508 LAS Base and HAZ Metal Tensile Tests 21

4.2 Estimated Stress-Strain Curves for 508 LAS Base and HAZ Metal 24

4.3 Estimated Tensile Test and Kinematic Hardening Properties for 508 LAS Base and HAZ Metal 26

5 Results of 508 LAS Base Metal Fatigue Test and Material Model 29

5.1 Test Conditions for 508 LAS Base Metal Fatigue Tests 29

5.2 Bulk Fatigue Life and Maximum/Minimum Stress Time Histories for 508 LAS Base Metal Fatigue Tests 34

5.3 Elastic Modulus and Various Strain Range Time Histories for 508 LAS Base Metal Fatigue Tests 36

5.4 Elastic Limit Stress and Kinematic Hardening Parameters for 508 LAS Base Metal Fatigue Tests 40

5.5 Comparison of 0.05% Offset Yield Limit Stress and Kinematic Hardening Parameters for 508 LAS Base Metal Fatigue Tests 43

6 Results of 316 SS - 316 SS Similar Metal Tensile Test and Material Model 47

6.1 Test Conditions for Tensile Test of 316 SS-316 SS Weld Specimens 47

6.2 Estimated Stress-Strain Curves for 316 SS-316 SS Similar Metal Welds..... 50

6.3 Estimated Tensile Test and Kinematic Hardening Properties for 316 SS-316 SS Welds 51

7 Results of 316 SS-316 SS Similar Metal Fatigue Test and Material Model 53

7.1 Test Conditions for 316 SS-316 SS Weld Fatigue Tests 53

7.2 Bulk Fatigue Life and Maximum/Minimum Stress Histories for 316 SS-316 SS Weld Specimens..... 54

7.3 Elastic Modulus and Strain Range Histories for 316 SS-316 SS Welds 56

7.4 Elastic Limit Stress and Kinematic Hardening Parameters for 316 SS-316 SS Welds 61

7.5 Comparison of 0.05% Offset Yield Limit Stress and Corresponding Kinematic Hardening Parameters for 316 SS-316 SS Weld 65

8 Summary and Future Study 69

LIST OF FIGURES

Figure 2. 1 Equivalent monotonic stress-strain curves estimated from engineering ("Engg.") stress-strain data of a typical fatigue test for first quarter cycle and upward and downward cycles over the first 49 cycles. Also shown are the curve from the corresponding temperature tensile test (T03) data, various offset yield lines, and corresponding elastic and yield limit stresses. 5
Figure 2. 2 Schematic showing linear vs. nonlinear intra-cycle hardening stress (kinematic hardening stress) and the evolution at the center of yield surface (the back stress) 6
Figure 3. 1 Computer modeling schematic of a PWR showing different metals and welds used in the reactor pressure vessel, RCS pipe, and their joints. 12
Figure 3. 2 Location of the 508 LAS (heat-affected zone) specimen. 12
Figure 3. 3 Location of the 316 SS-316 SS similar weld specimen (with respect to 316 SS-316 SS similar metal weld plates). 13
Figure 3. 4 Geometry of hourglass type specimens. 13
Figure 3. 5 a) Test section with induction heating coil, b) LEPEL induction heating system, and c) close view of induction heating coil and specimen and extensometer location. 15
Figure 3. 6 LABVIEW screen shot showing examples of temperature history at different locations of a specimen and pull rod during the heatup and temperature stabilization procedures. 15
Figure 3. 7 LABVIEW screen shot showing examples of temperature profile along the length of specimen (specimen gauge center at origin) and pull rod during the heatup procedure. 16
Figure 3. 8 Environmental test loop showing different subsystems. 17
Figure 3. 9 Water pressure history measured during heatup for a PWR environment fatigue test of a 508 LAS specimen (Test EN-F20). 18
Figure 3. 10 Example water flow rate measured during heatup and temperature stabilization for a PWR environment fatigue test of a 508 LAS specimen (Test EN-F20). 19
Figure 3. 11 Example temperature histories measured during heatup and temperature stabilization for a PWR environment fatigue test of a 508 LAS specimen (Test EN-F20). 19
Figure 3. 12 Example temperature profile along the length of 508 LAS specimen and pull rod during a PWR environment fatigue test (Test EN-F20). 20
Figure 3. 13 Example loop water conductivity (measured through ECP sensor channel with a multiplication factor of 10^{-2}) time history during initial loop pressurization, heatup, temperature stabilization, and main fatigue test. 20
Figure 4. 1 Example temperature histories (measured through different thermocouples) during heatup, temperature stabilization, main tensile test, and cooldown for a 508 LAS HAZ specimen (Test T09). 22
Figure 4. 2 Magnified version of Figure 4.1 showing temperature measured at gauge center thermocouple. 23

Figure 4. 3 Example stress readings during only heatup and temperature stabilization for a 508 LAS HAZ specimen (Test T09). 23

Figure 4. 4 Example strain history during only heatup and temperature stabilization for a 508 LAS HAZ specimen (Test T09). 24

Figure 4. 5 Engineering stress-strain curves estimated from tensile test data of 508 LAS base and HAZ metal specimens under different conditions. 25

Figure 4. 6 True stress-strain curves (up to ultimate strain) estimated from tensile test data of 508 LAS base and HAZ metal specimens under different conditions. 25

Figure 5. 1 a) FE mesh of tensile test specimen and pull rods, b) maximum principal strain distribution at the end of FE simulation of T06 tensile test, and c) Von Mises stress distribution at the end of FE simulation. 30

Figure 5. 2 Stroke versus strain data obtained from T06 FE model and comparison with experimental (T06 tensile test) results. 30

Figure 5. 3 Strain versus Von Mises stress data obtained from T06 FE model and comparison with experimental (T06 tensile test) results. 31

Figure 5. 4 Strain versus maximum principal stress data from T06 FE model and comparison with experimental (T06 tensile test) results. 31

Figure 5. 5 a) Maximum principal strain distribution at the end of FE simulation of T08 tensile test and b) Von Mises stress distribution at the end of FE simulation. 32

Figure 5. 6 Stroke versus strain data obtained from T08 FE model and comparison with experimental (T08 tensile test) results. 32

Figure 5. 7 Strain versus Von Mises stress data obtained from T08 FE model and comparison with experimental (T08 tensile test) results. 33

Figure 5. 8 Strain versus maximum principal stress data obtained from T08 FE model and comparison with experimental (T08 tensile test) results. 33

Figure 5. 9 Fatigue lives for 508 LAS base metal specimens fatigue tested under different conditions. 34

Figure 5. 10 Maximum and minimum stress for 508 LAS base metal specimens fatigue tested under different conditions. 35

Figure 5. 11 Magnified version of Figure 5.10 showing the cyclic stress hardening/softening in 508 LAS base metal specimens under different conditions. 35

Figure 5. 12 Equivalent monotonic stress-strain curves estimated from upward/downward cycle (for first 50 cycles) stress-strain data of RT-F23 (22 ^{o}C, In-air condition) fatigue test and comparison with T06 (22 ^{o}C, in-air condition) tensile test data. Also the figure shows offset yield lines and corresponding elastic and yield limit stresses. 36

Figure 5. 13 Equivalent monotonic stress-strain curves estimated from upward/downward cycle (for first 50 cycles) stress-strain data for ET-F24 (300 ^{o}C, in air) fatigue test and comparison with T08 (300 ^{o}C, in air) tensile test data. Also given are the offset yield lines and corresponding elastic and yield limit stresses 37

Figure 5. 14 Equivalent monotonic stress-strain curves estimated from upward/downward cycle (for first 50 cycles) stress-strain data for EN-F20 (300 ^{o}C, PWR Water)

fatigue test and comparison with T08 (300 °C, in air) tensile test data. Also given are the offset yield lines and corresponding elastic and yield limit stresses. 37
Figure 5. 15 Elastic modulus for 508 LAS base metal specimens fatigue tested under different conditions. 38
Figure 5. 16 Total strain range for 508 LAS base metal specimens fatigue tested under different conditions. 38
Figure 5. 17 Elastic strain range for 508 LAS base metal specimens fatigue tested under different conditions. 39
Figure 5. 18 Plastic strain range for 508 LAS base metal specimens fatigue tested under different conditions. 39
Figure 5. 19 Accumulated plastic strain for 508 LAS base metal specimens fatigue tested under different conditions. 40
Figure 5. 20 Elastic limit stress for 508 LAS base metal specimens fatigue tested under different conditions. 41
Figure 5. 21 Linear kinematic hardening parameter C1 (elastic limit stress used as yield stress) for 508 LAS base metal specimens fatigue tested under different conditions. 41
Figure 5. 22 Nonlinear kinematic hardening parameter C1 (elastic limit stress used as yield stress) for 508 LAS base metal specimens fatigue tested under different conditions. 42
Figure 5. 23 Nonlinear kinematic hardening parameter γ1 (elastic limit stress used as yield stress) for 508 LAS base metal specimens fatigue tested under different conditions. 42
Figure 5. 24 Offset-strain (0.05%) yield limit stress for 508 LAS base metal specimens fatigue tested under different conditions. 44
Figure 5. 25 Linear kinematic hardening parameter C1 (0.05% offset strain stress used as yield stress) for 508 LAS base metal specimens fatigue tested under different conditions. 44
Figure 5. 26 Nonlinear kinematic hardening parameter C1 (0.05% offset strain stress used as yield stress) for 508 LAS base metal specimens fatigue tested under different conditions. 45
Figure 5. 27 Nonlinear kinematic hardening parameter γ 1 (0.05% offset strain stress used as yield stress) for 508 LAS base metal specimens fatigue tested under different conditions. 45
Figure 6. 1 Example temperature histories (measured through different thermocouples) during heatup, temperature stabilization, main tensile test, and cooldown for a 316 SS-316 SS weld specimen (Test T05). 48
Figure 6. 2 Magnified version of Figure 6.1 showing temperature measured at gauge-center thermocouple. 48
Figure 6. 3 Example stress history during only heatup and temperature stabilization for a 316 SS-316 SS weld specimen (Test T05). 49
Figure 6. 4 Example strain history during only heatup and temperature stabilization for a 316 SS-316 SS weld specimen (Test T05). 49
Figure 6. 5 Engineering stress-strain curves estimated from tensile test data of 316 SS-316 SS weld specimens, which were tensile tested at room temperature and 300 °C. 50

Figure 6. 6 True stress-strain curves (up to ultimate strain) estimated from tensile test data of 316 SS-316 SS weld specimens, which were tensile tested at room temperature and 300 ^{o}C. 50

Figure 7. 1 Stroke versus strain data estimated from T05 (conducted at 300 ^{o}C and in-air condition for 316 SS-316 SS weld specimen) results. 54

Figure 7. 2 Fatigue lives for 316SS-316SS weld specimens fatigue tested under different conditions. 55

Figure 7. 3 Maximum and minimum stress for 316SS-316SS weld specimens fatigue tested under different conditions. 55

Figure 7. 4 Magnified version of Figure 7.3 showing level of cyclic stress hardening/softening in 316SS-316SS weld specimens under different conditions. .. 56

Figure 7. 5 Equivalent monotonic stress-strain curves estimated from upward/downward cycle (first 49 cycles) stress-strain data for ET-F08 fatigue test and T03 tensile test data. Also shown are the offset yield lines and elastic and yield limit stress. 57

Figure 7. 6 Equivalent monotonic stress-strain curves estimated from upward/downward cycle (first 49 cycles) stress-strain data for ET-F07 fatigue test and T05 tensile test data. Also shown are various offset yield lines and the elastic and yield limit stress. 57

Figure 7. 7 Equivalent monotonic stress-strain curves estimated from upward/downward cycle (first 50 cycles) stress-strain data for ET-F17 fatigue test and T05 tensile test data. Also shown are various offset yield lines and the elastic and yield limit stress. 58

Figure 7. 8 Equivalent monotonic stress-strain curves estimated from upward/downward cycle (first 50 cycles) stress-strain data for EN-F18 fatigue test and T05 tensile test data. Also shown are various offset yield lines and elastic and yield limit stress. 58

Figure 7. 9 Elastic modulus for 316SS-316SS weld specimens fatigue tested under different conditions. 59

Figure 7. 10 Total strain range for 316SS-316SS weld specimens fatigue tested under different conditions. 59

Figure 7. 11 Elastic strain range for 316SS-316SS weld specimens fatigue tested under different conditions. 60

Figure 7. 12 Plastic strain range for 316SS-316SS weld specimens fatigue tested under different conditions. 60

Figure 7. 13 Accumulated plastic strain for 316SS-316SS weld specimens fatigue tested under different conditions. 61

Figure 7. 14 Elastic limit stress for 316SS-316SS weld specimens fatigue tested under different conditions. 62

Figure 7. 15 Linear kinematic hardening parameter C1 (elastic limit stress used as yield stress) for 316SS-316SS weld specimens fatigue tested under different conditions. 62

Figure 7. 16 Nonlinear kinematic hardening parameter C1 (elastic limit stress used as yield stress) for 316SS-316SS weld specimens fatigue tested under different conditions. 63

Figure 7. 17 Nonlinear kinematic hardening parameter γ1 (elastic limit stress used as yield stress) for 316SS-316SS weld specimens fatigue tested under different conditions. 63

Figure 7. 18 Offset strain (0.05%) yield limit stress for 316SS-316SS weld specimens fatigue tested under different conditions. 65
Figure 7. 19 Linear kinematic hardening parameter C1 (0.05% offset strain stress used as yield stress) for 316SS-316SS weld specimens fatigue tested under different conditions. 66
Figure 7. 20 Nonlinear kinematic hardening parameter C1 (0.05% offset strain stress used as yield stress) for 316SS-316SS weld specimens fatigue tested under different conditions. 66
Figure 7. 21 Nonlinear kinematic hardening parameter γ1 (0.05% offset strain stress used as yield stress) for 316SS-316SS weld specimens fatigue tested under different conditions. 67

LIST OF TABLES

Table 4. 1 Test conditions for 508 LAS base and HAZ metal tensile tests. 22
Table 4. 2 Estimated tensile test material properties for 508 LAS base and HAZ metal specimens tensile tested under different conditions. 26
Table 4. 3 Estimated (or assumed) elastic limit and associated kinematic hardening properties for 508 LAS base and HAZ metal specimens tensile tested under different conditions. 27
Table 4. 4 Estimated 0.05% offset yield limit and associated kinematic hardening properties for 508 LAS base and HAZ metal specimens tensile tested under different conditions. 27
Table 4. 5 Estimated 0.1% offset yield limit and associated kinematic hardening properties for 508 LAS base and HAZ metal specimens tensile tested under different conditions. 27
Table 4. 6 Estimated 0.2% offset yield limit and associated kinematic hardening properties for 508 LAS base and HAZ metal specimens tensile tested under different conditions. 28
Table 5. 1 Test conditions for 508 LAS base metal fatigue tests. 29
Table 5. 2 Material model parameters (elastic limit stress as yield limit stress) for 508 LAS base metal specimens, at selected fatigue cycles and comparison with tensile test parameters. 43
Table 5. 3 Material model parameters (0.05% offset strain stress used as yield limit stress) for 508 LAS base metal specimens, at selected fatigue cycles and comparison with tensile test parameters. 46
Table 6. 1 Test conditions for 508 LAS base and HAZ metal tensile tests. 47
Table 6. 2 Estimated tensile test material properties for 316 SS-316 SS weld specimens, which were tensile tested under different conditions. 51
Table 6. 3 Estimated (or assumed) elastic limit and associated kinematic hardening properties for 316 SS-316 SS weld specimens, which were tensile tested under different conditions. 51
Table 6. 4 Estimated 0.05% offset yield limit and associated kinematic hardening properties for 316 SS-316 SS weld specimens, which were tensile tested under different conditions. 52
Table 6. 5 Estimated 0.1% offset yield limit and associated kinematic hardening properties for 316 SS-316 SS similar weld specimens, which were tensile tested under different conditions. 52
Table 6. 6 Estimated 0.2% offset yield limit and associated kinematic hardening properties for 316 SS-316 SS weld specimens, which were tensile tested under different conditions. 52
Table 7. 1 Test conditions for 316 SS-316 SS weld fatigue tests. 53

Table 7. 2 Material model parameters (elastic limit stress used as yield limit stress) for 316 SS-316 SS weld specimens, at selected fatigue cycles and comparison with tensile test parameters. 64
Table 7. 3 Material model parameters (0.05% offset strain stress used as yield limit stress)for 316 SS-316 SS weld specimens, at selected fatigue cycles and comparison with tensile test parameters. 68

ABBREVIATIONS

ANL	Argonne National Laboratory
ASME	American Society of Mechanical Engineers
DO	Dissolved Oxygen
DOE	Department of Energy
ECP	Electrochemical Potential
FE	Finite Element
FEA	Finite Element Analysis
HAZ	Heat Affected Zone
LAS	Low Alloy Steel
LWR	Light Water Reactor
LWRS	Light Water Reactor Sustainability
PWR	Pressurized Water Reactor
RCS	Reactor Coolant System
SS	Stainless Steel

ACKNOWLEDGMENTS

This research was supported through the U.S. Department of Energy's Light Water Reactor Sustainability program under the work package of environmental fatigue study, program manager Dr Jeremy Busby (FY 2015) and Dr. Keith Leonard (FY 2016).

This page intentionally left blank

1 Introduction

In our previous report [1] we presented a baseline mechanistic (finite element) model for cyclic stress analysis of PWR components. In this earlier work, heat transfer and cyclic thermal-structural analysis were performed for an assembly-level PWR model. By using the assembly-level results from cyclic thermal-structural analysis along with ASME and NUREG-6909 fatigue evaluation criteria, we estimated the fatigue life for example components such as the hot leg and cold leg. In performing the thermal-structural stress analysis, we used elastic material properties. This approach is in line with present industry approaches for fatigue evaluation of nuclear power plant components [2, 3]. The relevant design codes allow elastic-analysis-based shakedown or ratcheting analysis of nuclear reactor and pressure components to check against progressive damage due to fatigue. However, as reported in literature [4], large uncertainties exist in fatigue life evaluations that use current elastic stress analysis [4]. Theoretically, if stress and strain stay below the elastic limit, no fatigue will occur in the reactor components. However, safety-critical reactor components often fail due to fatigue damage associated with the reactor loading cycles. This failure could be due to non-elastic and non-recoverable plastic yield in the reactor metal. The fatigue damage in reactor components could be aggravated by the harsh reactor environment. As a result, estimates of the fatigue life of reactor components should be based on the results of elastic-plastic stress analysis rather than pure elastic stress analysis.

Elastic-plastic analysis by means of finite element (FE) modeling requires modeling the material behavior through isotropic or kinematic models or a combination of isotropic and kinematic models. Although component stress analysis under monotonic load can accurately be modeled through isotropic models alone, stress analysis under cyclic load requires both isotropic and kinematic models. However, most of the presently available FE models are based on isotropic and kinematic hardening models, which are based on fixed or time-independent stress-strain data from tensile tests or from half-life stress-strain data from fatigue tests. Although for stress analysis under monotonic loading it may be sufficient to use time-independent stress-strain data, stress analysis under cyclic loading using fixed stress-strain data may not be adequate. Under long-duration cyclic loading, the intrinsic stress-strain properties of reactor materials evolve over time and do not remain fixed as is the case with monotonic loading under static or quasi-static conditions. Hence, it is essential to characterize and model this time-dependent behavior of reactor materials under cyclic loading and under different environmental conditions. It is our assumption that a time-dependent material model will improve the accuracy of mechanistic FE models for stress analysis of reactor components under cyclic loading. This stress analysis would improve the fatigue life prediction.

Most of the presently available fatigue modeling literature has focused on improving the stress-life data set and related empirical fatigue design curves [5-7] for estimating fatigue life given the stress/strain state of a component. A few studies [8-14] have given emphasis to the more mechanistic aspects of fatigue life prediction, such as through-ratcheting or shakedown analysis of reactor component by means of FE models based on nonlinear kinematic hardening. Most of the models discussed in these studies are based on the monotonic stress–strain curve obtained from a tension specimen. However, a quasi-static tensile test based model alone may not capture the time-dependent behavior of reactor material under cyclic thermal-mechanical loading.

As part of the Department of Energy's Light Water Reactor Sustainability (DOE/LWRS) program, we are developing time-independent material models based on tensile tests and time-dependent material models based on cyclic tests for different reactor materials, such as 316 stainless steel (SS), 508 low-alloy steel (LAS) base metal, 316 SS-316 SS similar metal welds, and 316 SS-508 LAS dissimilar metal welds. Also, materials models are being developed under different environmental conditions, such as in air (at room temperature and 300 ^{o}C) and PWR primary loop water (at 300 ^{o}C). In our previous work, we presented time-dependent material models for 316 SS base metals [15-17]. In this report, we present tensile and fatigue test results and associated material models under different test and environmental conditions for 508 LAS base metal and 316 SS-316 SS similar metal welds.

This report is organized into following chapters:

1. Introduction
2. Cyclic Plasticity Based Time-Dependent Material Models: Theoretical Background
3. Test Specimens and Experimental Setup
4. Results of 508 LAS Base and HAZ Metal Tensile Test and Material Model
5. Results of 508 LAS Base Metal Fatigue Test and Material Model
6. Results of 316 SS-316 SS Similar Metal Tensile Test and Material Model
7. Results of 316 SS-316 SS Similar Metal Fatigue Test and Material Model
8. Conclusion and Future Direction

The overall objective of this report is to provide guidance for estimating hardening parameters based on tensile/fatigue tests. Also, the material models and parameters given in this report can directly be used by industry for fatigue and ratcheting evaluation of reactor components.

2 Time-Dependent Material Models Based on Cyclic Plasticity: Theoretical Background

In the present work, a time-dependent plasticity model is proposed to model reactor materials such as 508 LAS base metal and 316 SS-316 SS metal weld. In the proposed model it is assumed that the material yield surface and the corresponding hardening and softening behavior evolved over time. It is essential to characterize this behavior under various loading and environmental conditions and then to estimate relevant material parameters. These material parameters can be estimated from cyclic stress-strain data obtained through uni-axial fatigue tests conducted under relevant environmental conditions and temperatures. These macroscopic and time-dependent material parameters can be used to develop a component-level FE model of PWR piping and other components. In turn, this model can be used for predicting the stress-strain evolution over time under multi-axial and thermal-mechanical cyclic loading. We discussed similar approaches to material modeling in our previous work [15-17] for 316 SS base metal. However, for completeness of this report in the following section, the theoretical background behind the time-dependent material model and associated parameter estimation techniques is briefly discussed.

2.1 Cyclic Plasticity Model

As a material undergoes cyclic loading in a reactor environment, it no longer behaves similarly to monotonic loading. In the case of monotonic loading, the yield surface only expands/contracts (isotropic hardening/softening). In the case of cyclic loading, the yield surface translates in stress space (kinematic hardening/softening), in addition to its expansion/contraction (isotopic hardening/softening). Hence, combined isotropic and kinematic hardening is appropriate for modeling of plastic-deformation-related damage in reactor steel due to cyclic loading. Within an individual cycle, the kinematic hardening is the dominant plastic deformation process, in which the material yielding depends on the accumulated plastic strain associated with that particular cycle. However, most of this intra-cycle hardening can be recovered during stress reversal, leading to a dynamic recovery or memory effect (Bauschinger effect). However, over multiple fatigue cycles (inter-cycle behavior) the material also hardens or softens due to remnant intra-cycle plastic deformation, which leads to the expansion/contraction of the yield surface. This inter-cycle expansion/contraction of the yield surface is referred as the "isotropic hardening component" in the cyclic plasticity model. In the present work, a time-dependent plasticity model based on Von-Mises stress criteria is proposed. The corresponding yield function can be expressed as

$$f(\boldsymbol{\sigma}_i^j - \boldsymbol{\alpha}_i^j) = \sigma_i^y \tag{2.1}$$

where $\boldsymbol{\sigma}_i^j$ is jth instance of the stress vector in the ith fatigue cycle, and $\boldsymbol{\alpha}_i^j$ corresponds to the jth instance of the back stress vector. The back stress vector represents an intra-cycle memory effect (kinematic hardening stress). In Eq. (2.1), σ_i^y is the yield stress of the ith fatigue cycle, which can be represented through isotopic hardening/softening stress. For pressure-independent J2 plasticity, the equivalent Von-Mises stress in Eq. (2.1) can be expressed as

$$f(\boldsymbol{\sigma}_i^j - \boldsymbol{\alpha}_i^j) = \sqrt{\frac{3}{2}(\boldsymbol{\sigma}^{dev}{}_i^j - \boldsymbol{\alpha}^{dev}{}_i^j):(\boldsymbol{\sigma}^{dev}{}_i^j - \boldsymbol{\alpha}^{dev}{}_i^j)} \tag{2.2}$$

where $\boldsymbol{\sigma}^{dev}{}_i^j$ and $\boldsymbol{\alpha}^{dev}{}_i^j$ represent the jth instance of the deviatoric portion of the primary and back stress vector in the ith fatigue cycle, respectively. To accurately model the cyclic behavior of a reactor component, it is essential to ascertain the evolution of elastic properties (e.g., elastic modulus), the back stress vector (α_i^j in Eq. 2.1), and the cyclic yield stress (σ_i^y in Eq. 2.1). The cyclic back stress α_i^j can be estimated in a FE code if the cyclic or time-dependent constants related to the kinematic hardening behavior of the concern materials are known. By contrast, the cyclic evolution of the isotropic component of the stress tensor in a FE code can be estimated if the cyclic or time-dependent yield stresses of the concern materials are known. These parameters and related material models are the basic building blocks in a FE-based evaluation models for elastic-plastic fatigue and must be estimated for different reactor materials and under prototypical conditions. These parameters can be estimated from cyclic stress-strain data obtained through a uni-axial fatigue test. The procedure and theoretical background to estimate these parameters are discussed below.

2.2 Estimation of Time-dependent Elastic Modulus, Elastic Limit, and Offset Strain Yield Stress

It is essential to know whether the elastic properties, such as elastic modulus, evolve over time due to cyclic loading and whether environmental factors affect these parameters. In the present work, the cycle-by-cycle elastic moduli are estimated for respective fatigue tests conducted under different environmental conditions. First, the stress-strain curve in each cycle is divided into two, such as the upward and downward portion of the stress-strain curve. Second, the divided portions are shifted and scaled (by half) such that both curves resemble a tensile test curve based on monotonic stress-strain. Figure 2.1 shows the resulting equivalent monotonic stress-strain curves for a symmetric strain-control fatigue test with 0.5% as the maximum strain amplitude. Third, the elastic portion (linear portion) of the stress-strain curve is selected based on an assumed elastic limit strain (refer to Figure 2.1). The elastic limit strain is assumed based on engineering judgment after observation of the trends of overlapped equivalent monotonic stress-strain curves. The selected elastic limit strain was assumed fixed over the entire fatigue life while the other time-dependent material parameters were estimated, such as elastic limit stress, elastic modulus, yield limit stress, and kinematic hardening parameters. Once the elastic portions of the upward and downward stress-strain curves are selected, the corresponding upward and downward elastic moduli are estimated by a linear least squares technique. Finally, these upward and downward elastic constants are averaged to estimate the average elastic modulus in a particular fatigue cycle. Similar to estimation of the cyclic elastic modulus, the evolution of elastic limit stress and offset-strain yield stress were estimated for individual fatigue cycles by using the above-mentioned upward/downward stress-strain curves. All these time-dependent parameters were estimated automatically using a MATLAB-based material modeler code developed by Argonne National Laboratory (ANL). For the kinematic hardening parameter estimation in the cyclic loading case, 0.05% offset-strain yield limit was considered compared to the usual 0.2% offset yield strain. This is because 0.2% offset strain may fall outside the cyclic stress-strain curve, as shown in Figure 2.1. Also selecting higher offset strain limit may exclude the substantial inelastic region of stress-strain curve, as can also be seen from Figure 2.1. To avoid this situation, a lower value of 0.05% offset strain was considered to

estimate the corresponding offset yield stress. The estimated cyclic elastic modulus can be fed to a FE code to model the elastic component of stress under cyclic loading. Moreover, the cyclic elastic limit or offset yield limit stress can be fed to a FE code to model the isotropic component of the stress tensor.

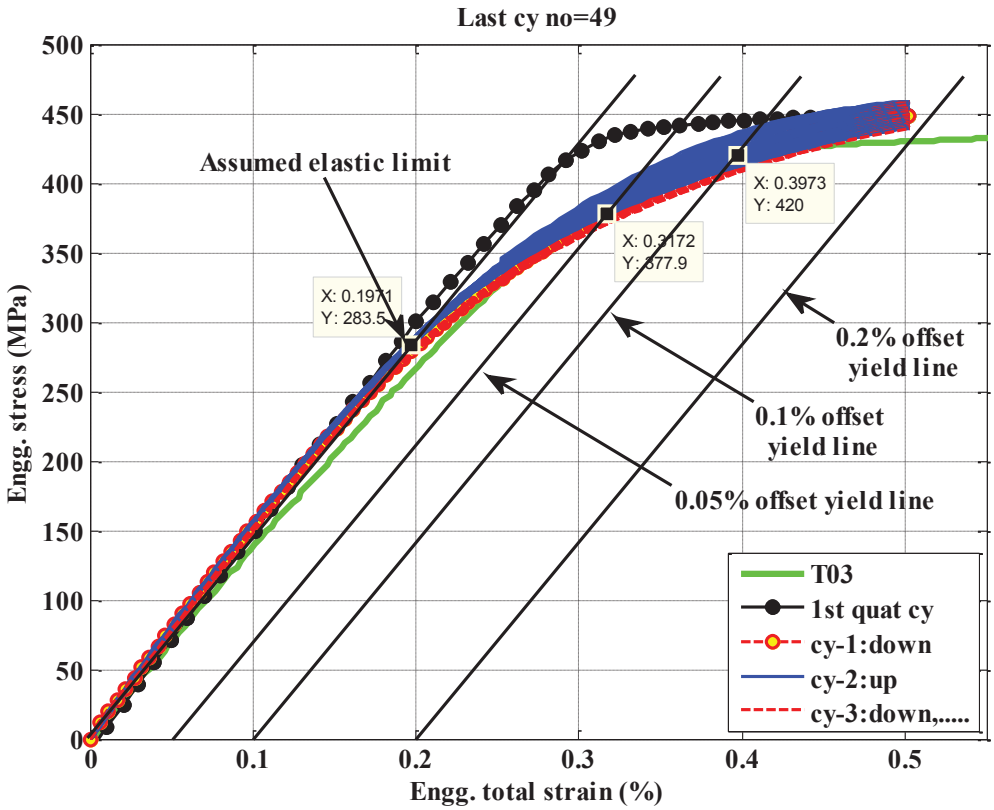

Figure 2. 1 Equivalent monotonic stress-strain curves estimated from engineering ("Engg.") stress-strain data of a typical fatigue test for first quarter cycle and upward and downward cycles over the first 49 cycles. Also shown are the curve from the corresponding temperature tensile test (T03) data, various offset yield lines, and corresponding elastic and yield limit stresses.

2.3 Modeling of Intra-Cycle Hardening and Estimation of Time-Dependent Kinematic Hardening Parameters

Kinematic hardening parameters are required to model the intra-cycle hardening stress, such as back stress in materials due to loading/unloading within a fatigue cycle. At a given instant j within a particular fatigue cycle i, the back stress α_i^j (refer to Eq. 2.1) is estimated in an FE code. The evolution of the intra-cycle hardening stress beyond the corresponding cycle yield stress is equivalent to the evolution of the center of the yield surface (refer to Figure 2.2) in the form of back stress α_i^j. The intra-cycle back stress is dependent on the accumulated plastic strain within a cycle, as well as on kinematic hardening parameters. These predetermined parameters can be used for modeling cyclic evolution of back stress in an FE code. Unlike monotonic loading, for the case of cycling loading, a fixed set of parameters may not completely describe the hardening/softening behavior for the entire loading envelope. Due to the dependence of material deformation on number of cycles, the kinematic hardening

behavior within all cycles may not be represented by a single set of kinetic hardening parameters. Rather, the kinematic hardening parameters may evolve over time. Hence, we need to understand how these macroscopic hardening parameters evolve over time and how they are affected by different loading conditions (e.g., load amplitude and loading rate) and environmental conditions (e.g., room temperature versus elevated temperate, in-air condition versus PWR coolant water chemistry, etc.).

As seen in Figure 2.2, the stress at selected cycle number (beyond that for the corresponding cycle yield stress, σ_i^y) can be described either by a linear or nonlinear mapping of accumulated plastic strain within that cycle.

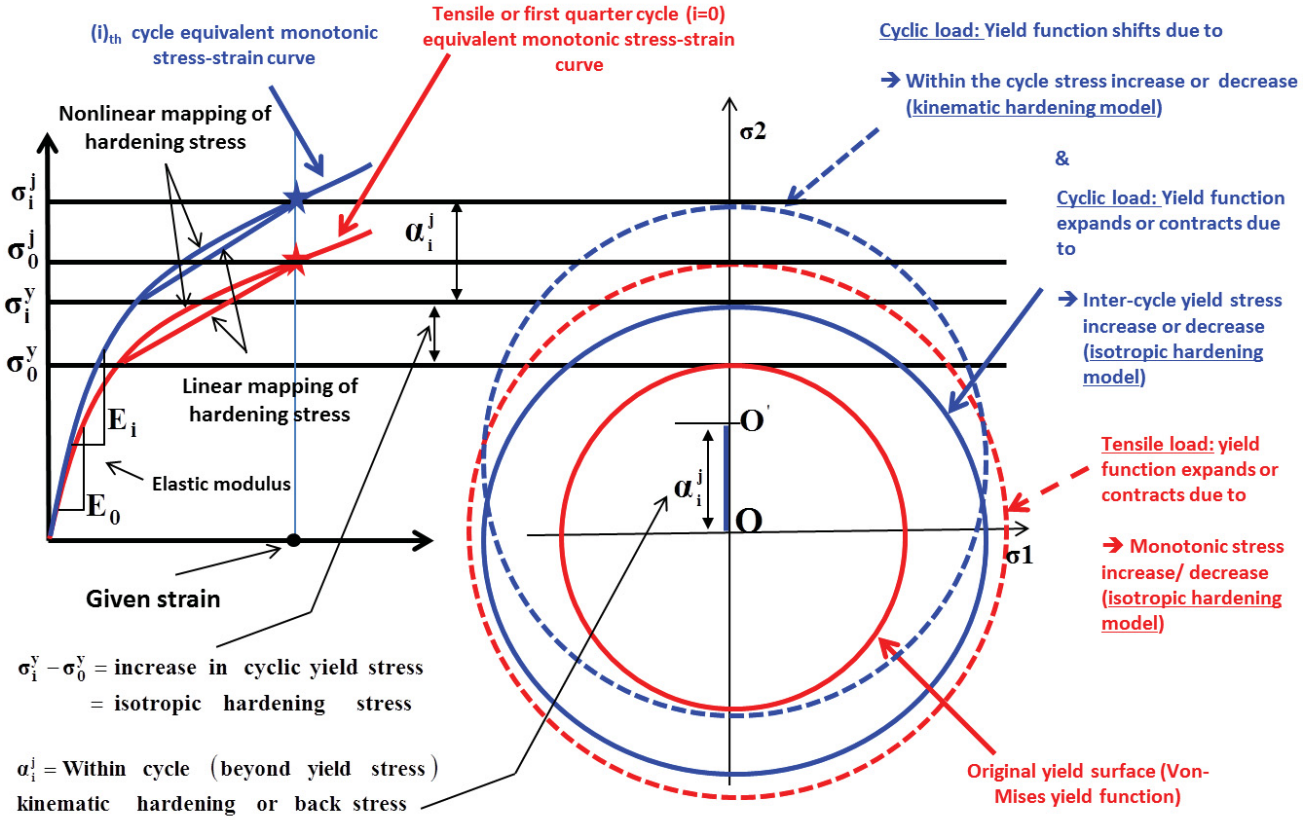

Figure 2. 2 Schematic showing linear vs. nonlinear intra-cycle hardening stress (kinematic hardening stress) and the evolution at the center of yield surface (the back stress)

We mapped the intra-cycle kinematic hardening stress both linearly and nonlinearly. The linear model is based on Prager's linear hardening relation between hardening stress and accumulated plastic strain, whereas the nonlinear model is based on the Armstrong-Frederick or Chaboche nonlinear kinematic hardening relation between hardening stress and accumulated plastic strain. The original Prager or Chaboche model and other related models suggest that the related kinematic hardening parameters can be estimated by using the stress-strain data for either the first quarter cycle or a stabilized cycle. That means the kinematic hardening parameters will remain the same over the entire fatigue cycles. However, in reality, these parameters may not remain constant but change over time. Based on this assumption, we have modified the linear and nonlinear hardening mapping relation, according to which the incremental back stress at the j^{th} instance in the i^{th} fatigue cycle can be expressed as:

$$\mathbf{d\alpha}_i^j = \frac{2}{3} C1_i^{av}(p) d\varepsilon^{pl} \quad \leftarrow \textit{Linear kinematic hardening} \tag{2.3}$$

$$\mathbf{d\alpha}_\mathbf{i}^\mathbf{j} = \frac{2}{3} C1_i^{av}(p) d\varepsilon^{pl} - \gamma 1_i^{av}(p) \alpha_i^j \, \bar{p} \quad \leftarrow \textit{Nonlinear kinematic hardening} \tag{2.4}$$

where $\bar{p} = \int_0^{d\varepsilon^{pl}} d\varepsilon^{pl'}$ represents the accumulated plastic strain within a cycle, and $C1_i^{av}(p)$ and $\gamma 1_i^{av}(p)$ are average kinematic hardening material constants that are dependent on fatigue cycle and inter-cycle accumulated plastic strain (p). The inter-cycle accumulated plastic strain (p) can be expressed as:

$$p_i = \int_{i=1}^{i=n} dp' \tag{2.5}$$

For the multi-axial case, the effective plastic strain rate can be given as:

$$dp = \sqrt{\frac{2}{3} d\varepsilon^p : d\varepsilon^p} \tag{2.6}$$

However, for the uni-axial case, the effective plastic strain rate can be expressed in terms of the cyclic plastic strain range $\Delta\varepsilon_i^{pR}$ as follows:

$$dp = 2\Delta\varepsilon_i^{pR} \tag{2.7}$$

The plastic strain range in Eq. (2.7) can be estimated from

$$\Delta\boldsymbol{\varepsilon}_i^{pR} = (\boldsymbol{\varepsilon}_i^{\max} - \frac{\boldsymbol{\varepsilon}_i^{\max}}{E_i}) - (\boldsymbol{\varepsilon}_i^{\min} - \frac{\boldsymbol{\varepsilon}_i^{\min}}{E_i})$$

The parameter $C1_i^{av}$ (in Eqs. 2.3 and 2.4) is a proportional constant that gives a linear relation between back stress $\boldsymbol{\alpha}_i^j$ and intra-cycle accumulated plastic strain $\bar{p}$, whereas $\gamma 1_i^{av}$ is a relaxation term that describes the rate at which the back stress decreases with increase of intra-cycle accumulated plastic strain $\bar{p}$. These parameters are averaged from values estimated through the corresponding upward and downward portion of the symmetric cycle stress-strain curve. The average kinematic hardening parameters can then be expressed as

$$C1_i^{av}(p) = \frac{1}{2}[C1_i^{up}(p) + C1_i^{down}(p)] \tag{2.8}$$

and

$$\gamma 1_i^{av}(p) = \frac{1}{2}[\gamma 1_i^{up}(p) + \gamma 1_i^{down}(p)] \tag{2.9}$$

Equations (2.3) and (2.4) give the incremental multi-axial representation for intra-cycle kinematic hardening stress or back stress. The equivalent uniaxial form can be integrated over a given cycle to estimate the corresponding cycle parameters ($C1_i^{up}$ and $\gamma 1_i^{up}$ or $C1_i^{down}$ and $\gamma 1_i^{down}$) by curve fitting the stress-strain data obtained through a fatigue test. For example, for the upward portion of the hysteresis curve, the integrated form of Eq. (2.3) and Eq. (2.4) can be written as:

$$\begin{aligned} \alpha_i^j = \int_0^{\bar{p}} d\,\alpha_i^j &= \int_0^{\bar{p}} \frac{2}{3} C1_i^{up}(p) d\boldsymbol{\varepsilon}^{pl} \\ &= \frac{2}{3} C1_i^{up}(p)\bar{p} \qquad \leftarrow \textit{Linear kinematic hardening} \end{aligned} \tag{2.10}$$

$$\begin{aligned} \alpha_i^j = \int_0^{\bar{p}} d\,\alpha_i^j &= \int_0^{\bar{p}} [\frac{2}{3} C1_i^{up}(p) - \gamma 1_i^{up}(p)\alpha_i^j] d\boldsymbol{\varepsilon}^{pl} \\ &= \frac{C1_i^{up}(p)}{\gamma 1_i^{up}(p)} [1 - \exp(-\gamma 1_i^{up}(p)\bar{p})] \quad \leftarrow \textit{Nonlinear kinematic hardening} \end{aligned} \tag{2.11}$$

Similarly, the bottom half of the cyclic stress-strain curve can be modeled in terms of $C1_i^{down}(p)$, $\gamma 1_i^{down}(p)$, and $\bar{p}$. By using the upward and downward portions of cyclic stress-strain curves and a nonlinear optimization technique such as the Gauss-Newton approach, we estimated all the above-mentioned hardening parameters. The steps for estimating the parameters by using Gauss-Newton approach for cycle *i* are as follows:

Step 1: Estimate the kinematic hardening stress and corresponding accumulated intra-cycle plastic strain for *j* instances ($j = 1,2,\cdots m$) using

$$\alpha_i^{j=1,2,\cdots m} = \sigma_i^j - \sigma_i^y \tag{2.12}$$

$$\bar{p}_i^j = \varepsilon_i^j - \frac{\sigma_i^j}{E_i} \tag{2.13}$$

where subscript i represents the ith fatigue cycle, superscript j represents the jth data point in the stress-strain curve shifted and scaled in the ith fatigue cycle, and σ_i^y is the yield stress in the

i[th] fatigue cycle. In Eq. (2.13), E_i represents the elastic modulus for the i[th] fatigue cycle. Note that in our earlier work [15-17] for 316 SS base metal we assumed a fixed E_i while estimating cyclic evolution of yield stress σ_i^y, intra-cycle accumulated plastic strain $\bar{p}_i^j$ (refer to Eq. 2.13), and inter-cycle accumulated plastic strain p_i (refer to Eq. 2.5). This was for simplicity. However, in the present version of the work to improve accuracy in estimated material parameters, we assumed E_i to be cycle dependent and as estimated through the procedure discussed above.

Step 2: Assume initial values for $\mathbf{L} = [C_i \;\; \gamma_i]^T$.

Step 3: Estimate the residual function vector

$$\mathbf{r} = [r^{j=1} \;\; r^{j=2} \cdots r^{j=m}]^T \tag{2.14}$$

with the j[th] instance residual as

$$r^j = \frac{C_i}{\gamma_i}[1 - \exp(-\gamma_i \, \bar{p}_i^j)] - \alpha_i^j \tag{2.15}$$

Step 4: Estimate the Jacobian matrix J as follows:

$$\mathbf{J} = \begin{bmatrix} \dfrac{\partial r^{j=1}}{\partial C_i} & \dfrac{\partial r^{j=1}}{\partial \gamma_i} \\ \dfrac{\partial r^{j=2}}{\partial C_i} & \dfrac{\partial r^{j=1}}{\partial \gamma_i} \\ \vdots & \vdots \\ \dfrac{\partial r^{j=m}}{\partial C_i} & \dfrac{\partial r^{j=1}}{\partial \gamma_i} \end{bmatrix} \tag{2.16}$$

In Eq. (2.16), the j[th] instance expression for the partial derivatives is given below:

$$\frac{\partial r^j}{\partial C_i} = \frac{1}{\gamma_i}[1-\exp(-\gamma_i \bar{p}_i^j)]$$

and (2.17)

$$\frac{\partial r^j}{\partial \gamma_i} = -\frac{C_i}{\gamma_i{}^2}[1-\exp(-\gamma_i \bar{p}_i^j)] + \frac{\bar{p}_i^j}{\gamma_i}\exp(-\gamma_i \bar{p}_i^j)$$

Step 5: Estimate the incremental change in parameters:

$$\mathbf{\Delta L} = [\Delta C_i \quad \Delta\gamma_i]^T = -\left[(\mathbf{J}^T\mathbf{J})^{-1}\mathbf{J}^T\right]\mathbf{r} \tag{2.18}$$

Step 6: Update the parameters as:

$$\mathbf{L} = [C_i \quad \gamma_i]^T = \mathbf{L} + \mathbf{\Delta L} \tag{2.19}$$

Step 7: Repeat step 3 to step 6 unless the L_2 norm of the incremental parameters $\mathbf{\Delta L}$ is less than a tolerance value, i.e.,

$$\| \mathbf{\Delta L} \|_2 \le t_{tol} \tag{2.20}$$

While employing the optimization scheme for parameter optimization, for all the results discussed in this report, we used a tolerance value of $t_{tol} = 10^{-9}$ for the convergence limit. Also note in Eqs. 2.1-2.20 that the bold face symbols represent either vector or tensor.

3 Test Specimens and Experimental Setup

The major aim of the tensile and fatigue tests is to characterize material behavior under different test and environment conditions and then to estimate the related material properties, which can be used for FE based mechanistic modeling. The details of the material being tested, specimen geometry, and test setup are briefly described below.

3.1 Test Specimen Material and Geometry

As part of the LWRS program at ANL, we are conducting tensile and fatigue tests on laboratory-scale specimens that represent reactor coolant system (RCS) materials, such as SS, LAS, and their weld metals. In particular, we are testing 316 SS and 508 LAS base metals, which are commonly used in U.S. LWRs. In addition, we are testing pairs of similar metal welds (316 SS-316 SS) and dissimilar metal welds (316 SS-508 LAS), which represent the typical nozzle area of a reactor. For example, the reactor pressure vessel (typically made from LAS) is joined with reactor coolant system pipes, such as a hot leg or cold leg (typically made from SS) using both similar metal and dissimilar metal welds.

Figure 3.1 shows a computer modeling schematic of a PWR and the different materials associated with the reactor pressure vessel, coolant system piping, and their nozzles. Five material types are being tested under in-air and PWR coolant water conditions: (1) 316 SS base metal, (2) 508 LAS base metal, (3) 316 SS-316 SS similar metal weld, (4) 316 SS-508 LAS dissimilar metal filler weld, and (5) 316 SS-508 LAS dissimilar metal butter weld. However, in the present report, test data and material modeling results only related to 508 LAS base metal and 316 SS-316 SS weld are discussed. Regarding 508 LAS most of the results discussed in this report are related to specimens drawn from 508 LAS base metal plates; however, some of the results are also for specimens drawn from the heat-affected zone (HAZ) of 316 SS-508 LAS weld plates. Figure 3.2 shows a cross section of 316 SS-508 LAS weld plate, highlighting the location of the HAZ zone 508 LAS specimens. The 316 SS-316 SS weld specimens were drawn from a doubly V-weld plate and along the weld direction. Figure 3.3 shows the location of a specimen with respect to 316 SS-316 SS weld plates. All the tensile and fatigue tests were conducted with small hourglass type specimens, whose geometry is shown in Figure 3.4.

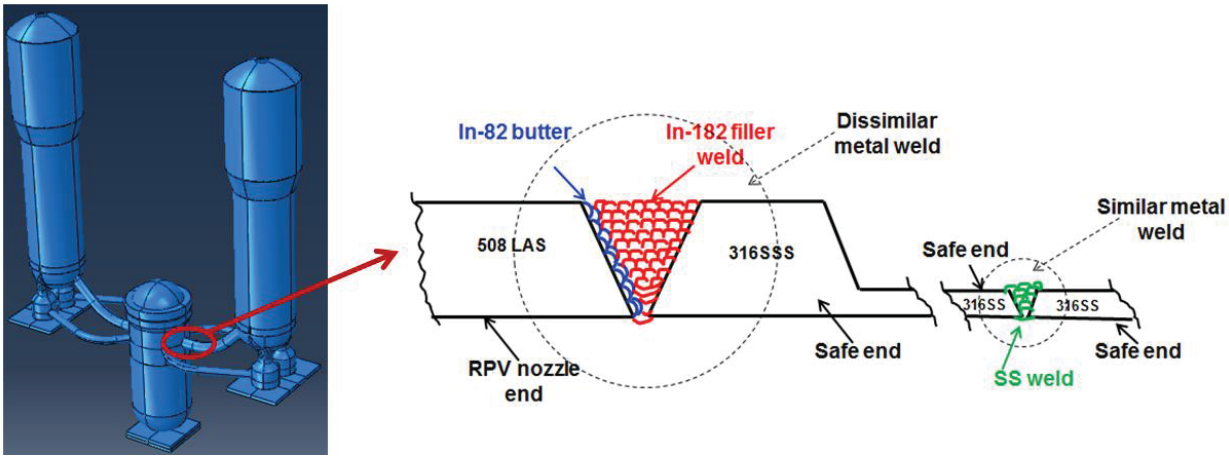

Figure 3. 1 Computer modeling schematic of a PWR showing different metals and welds used in the reactor pressure vessel, RCS pipe, and their joints.

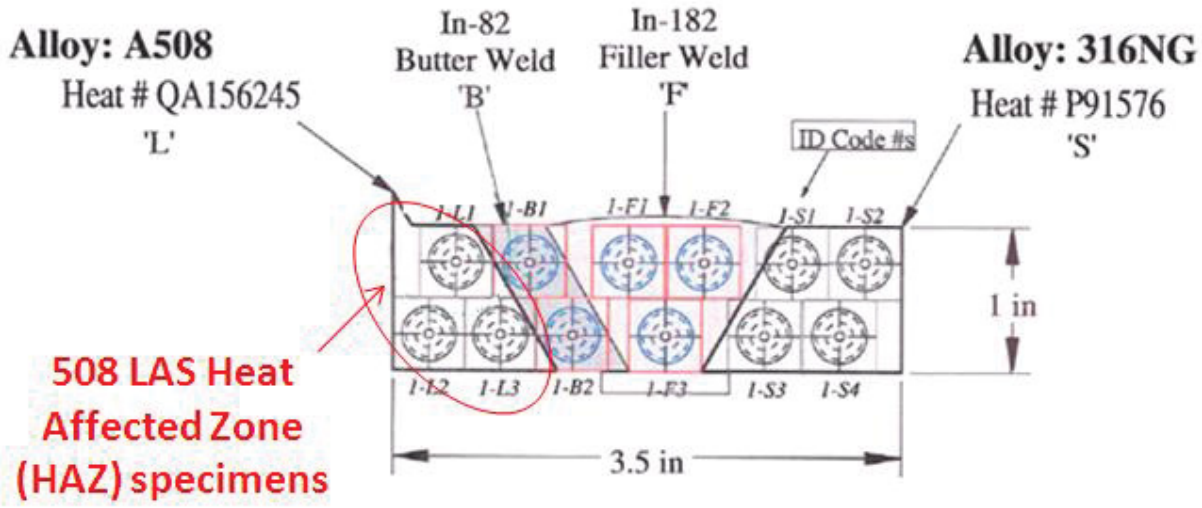

Figure 3. 2 Location of the 508 LAS (heat-affected zone) specimen.

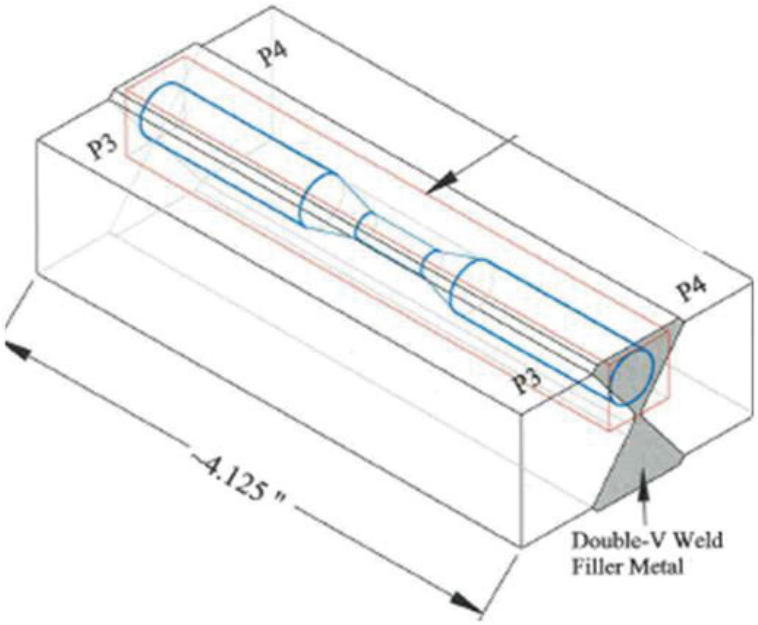

Figure 3. 3 Location of the 316 SS-316 SS similar weld specimen (with respect to 316 SS-316 SS similar metal weld plates).

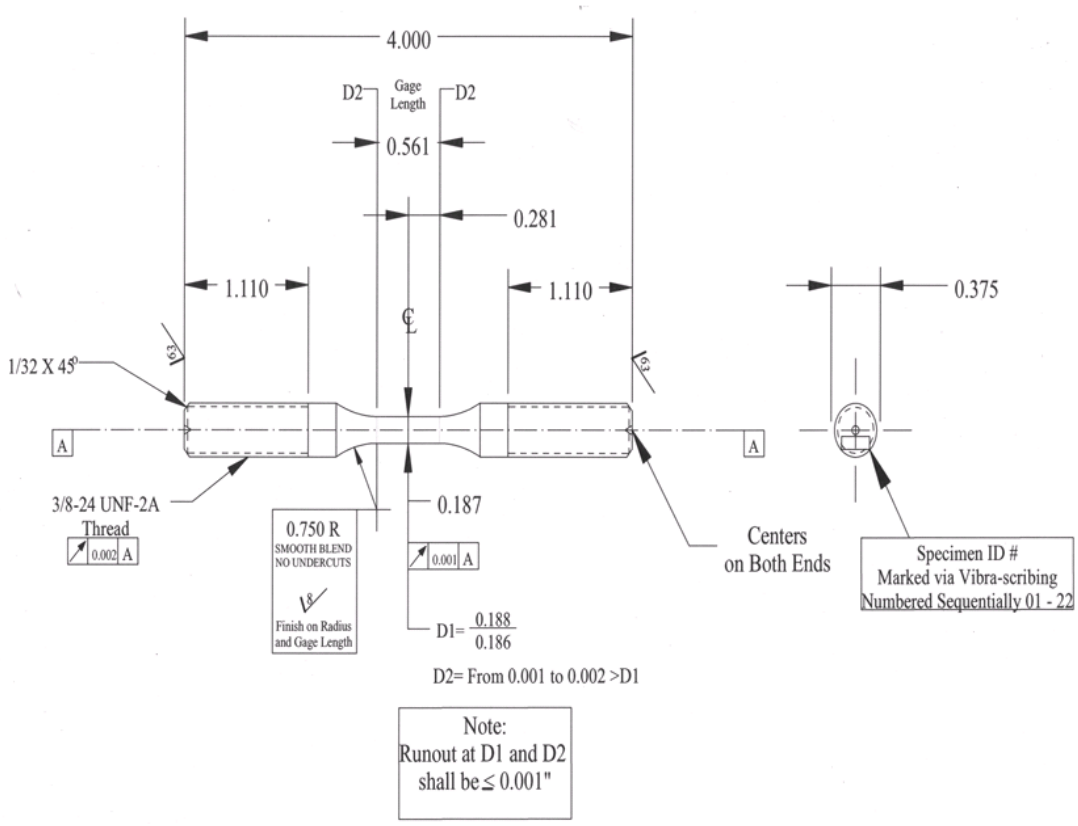

Figure 3. 4 Geometry of hourglass type specimens.

3.2 Experimental Setup

At ANL multiple custom-made material test systems are being used for different nuclear research programs. Two of these systems (one for in-air and the other for PWR water environment testing) have been dedicated to tensile/fatigue testing activities in the LWRS program. The in-air and PWR water environment testing systems are briefly discussed below.

3.2.1 In-air tensile/fatigue test setup

The in-air fatigue test setup is shown in Figure 3.5. This test setup was used for performing fatigue tests under in-air condition at both room temperature and elevated temperature. For elevated temperature tests, an induction-type heating source (Figure 3.5b) was used to locally heat the specimen. Specific coil shape (diameter and number of turn) was designed to achieve the required temperature in the test specimen. There were 15 thermocouples spot welded to the pull rod and specimen (9 on the specimen and 6 on the pull rod) to monitor and control the temperature. Note that, the elevated temperature isothermal fatigue tests were conducted in two steps. In the first step, under load control, the temperature was raised to the required test temperature in multiple steps and was allowed to stabilize for four to five hours. The induction heating process was controlled by appropriate design of the number of coils and coil configurations, such that the required temperature at the gauge area of the specimen can be achieved. In all the cases discussed in this paper the elevated temperature tests were conducted by keeping the gauge area temperature approximately at 300 ^{o}C. The PWR coolant system piping experience temperatures of a similar order, and our major aim is to study the fatigue performance of RCS piping materials. After the heatup and temperature stabilization, the main tensile/fatigue tests were conducted either under strain or stroke control condition.

Figure 3.6 shows an example temperature history as measured through the thermocouples during a typical heatup procedure. Figure 3.7 shows the temperature profile in a specimen and pull rod (with specimen gauge center at origin) at a particular instance during heatup procedures. For the strain control tests, the strain was measured using a precision high temperature extensometer mounted at the gauge area of the specimen (Figure 3.5c). While performing the strain control tests, along with strain measurements, the load, frame actuator displacement, and frame crosshead displacement (stroke) were acquired either through the INSTRON frame control and data acquisition software or through a stand-alone NI-LABVIEW data acquisition system. A sapphire-glass-based displacement sensor (Figure 3.5a) was used to measure the frame crosshead displacement (stroke).

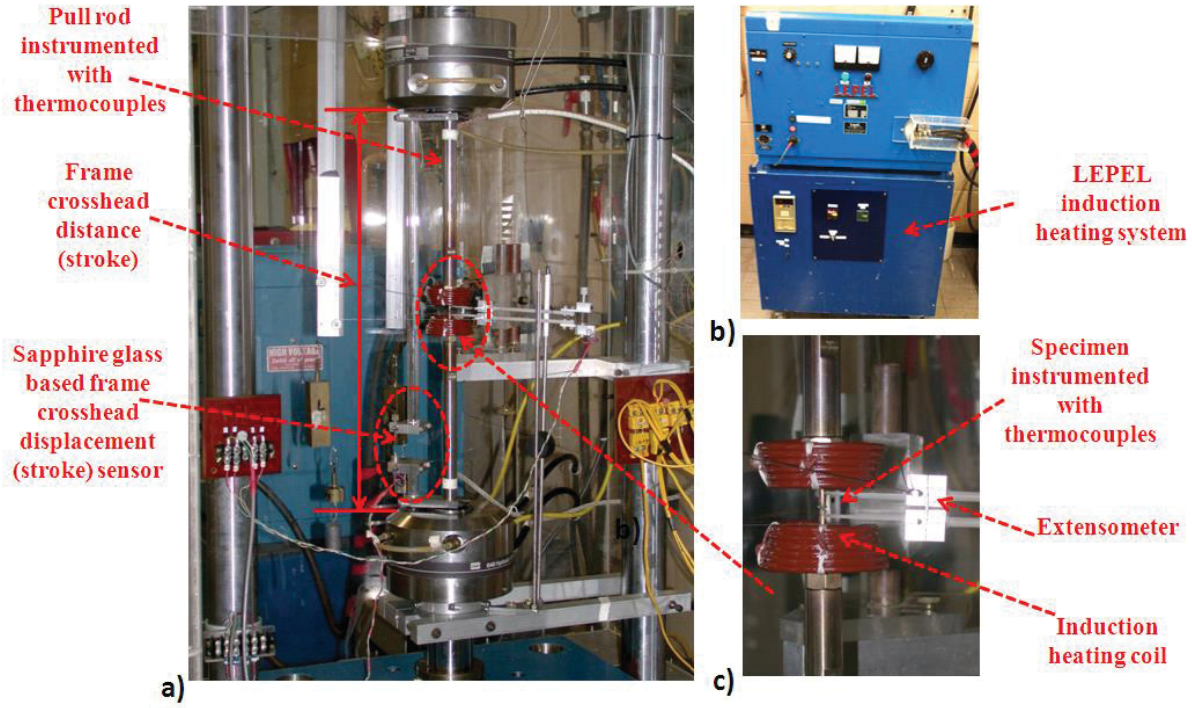

Figure 3. 5 a) Test section with induction heating coil, b) LEPEL induction heating system, and c) close view of induction heating coil and specimen and extensometer location.

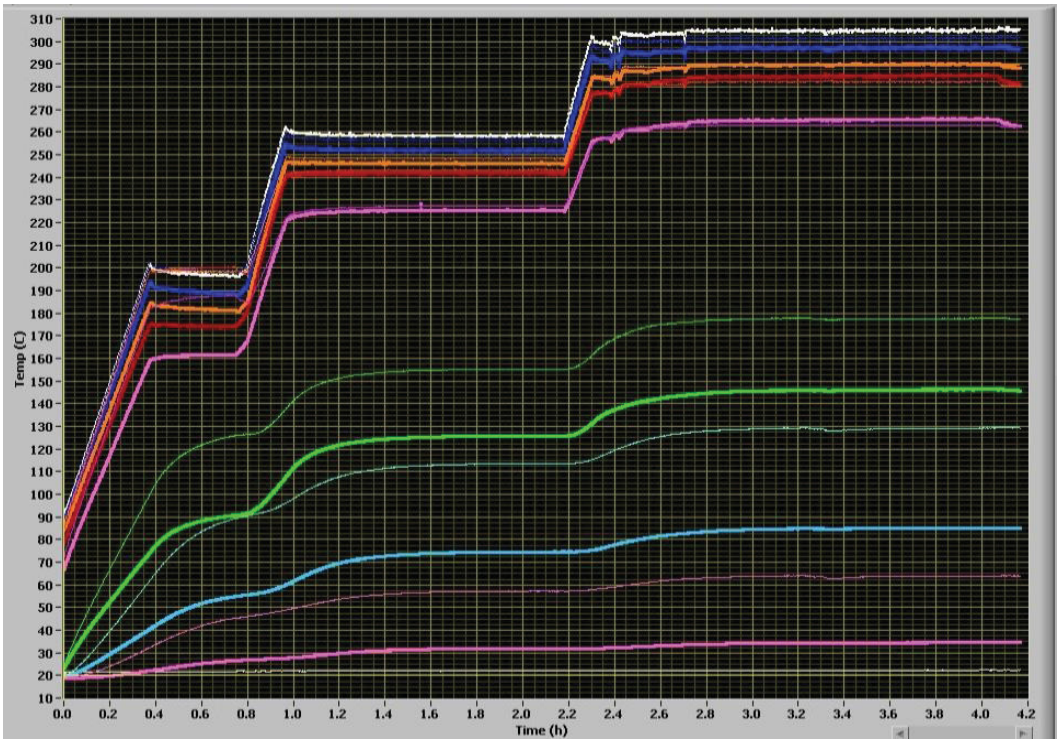

Figure 3. 6 LABVIEW screen shot showing examples of temperature history at different locations of a specimen and pull rod during the heatup and temperature stabilization procedures.

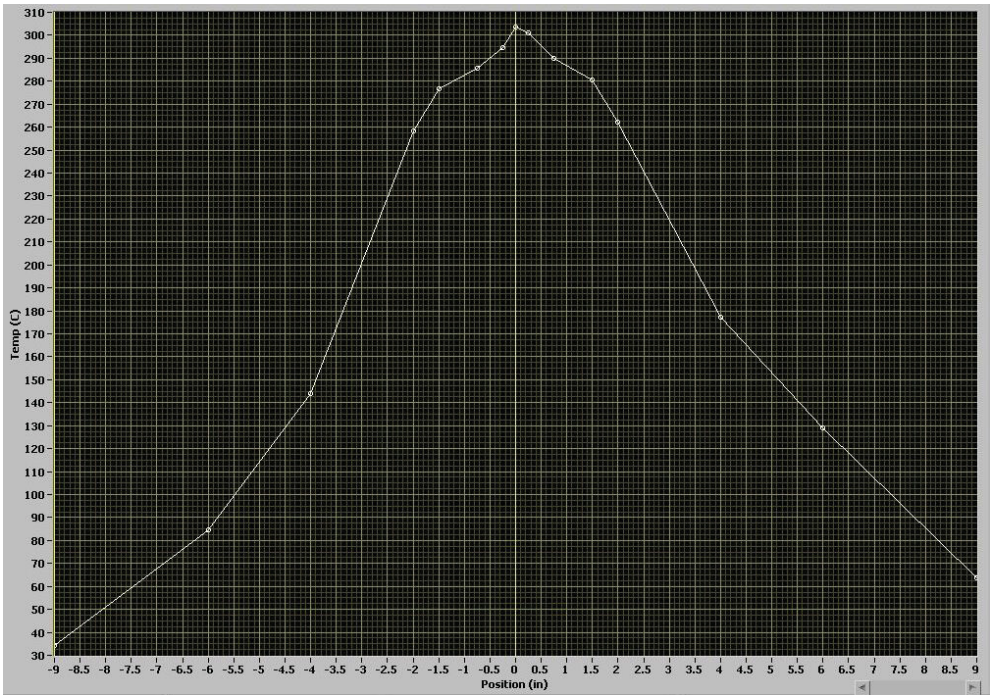

Figure 3. 7 LABVIEW screen shot showing examples of temperature profile along the length of specimen (specimen gauge center at origin) and pull rod during the heatup procedure.

3.2.2 PWR water loop fatigue test setup

A test loop specifically designed for performing fatigue tests under PWR coolant water conditions is used for the purpose. In addition to the regular fatigue test frame, the test loop consists of various subsystems such as autoclave, pre-heater, heat exchanger, hydrogen and other cover gas supply, re-circulating pump, feed water supply tank, etc. Figure 3.8 shows the MTS test frame and other subsystems used in the test loop. Thermocouples were instrumented on the outside of the autoclave to ascertain the temperature distribution along the length of the specimen. Before the start of the PWR environment fatigue test, a water solution was prepared with water chemistry similar as any typical PWR-type reactor RCS pipe. This solution was kept in the feed water supply tank shown in Figure 3.8. The feed water supply tank was also connected to the cover gas tank. For the PWR condition tests discussed in this report, the water chemistry of the feed water tank water was: 1000 ppm B as H_3BO_3, 2 ppm Li^+ as LiOH, 20% H_2/bal. N_2 cover gas, and dissolved oxygen (DO) < 5 ppb (pH=7). The temperature of the loop was adjusted such that the specimen gauge area temperature would be approximately at 300 ^oC (572 ^oF), which is typical for a PWR reactor coolant system pipe. The gauge area heating of water is conducted in two stages: by a pre-heater and through resistance coils warped around the autoclave (Figure 3.8).

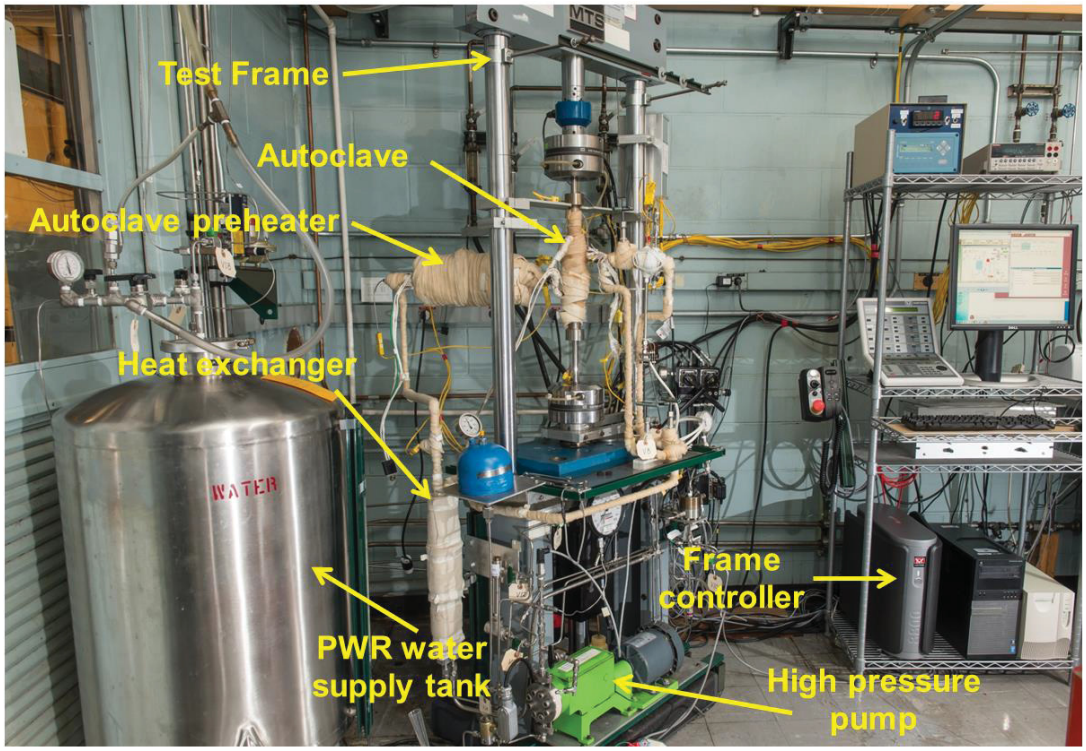

Figure 3.8 Environmental test loop showing different subsystems.

To prevent the 300 °C (572 °F) water from steaming out, the water was pressurized with a high pressure pump with maintaining a water pressure of 10.4 to 10.5 MPa (approximately 1510-1530 psi). The overall fatigue test was conducted following four steps:

- Step 1: Pressurization of the loop water to the predetermined pressure of 10.4-10.5 MPa (1510-1530 psi) at room temperature (RT), while keeping the specimen and frame under stroke or frame crosshead displacement control.
- Step 2: Heating up the gauge area water in several steps to 300 °C through the pre-heater and through resistance coils warped around the autoclave while keeping the specimen and frame under load control.
- Step 3: The main stroke control fatigue test under isothermal condition.
- Step 4: Cooling down and unloading.

Step 3 was started approximately 1 day after step 2. A sufficient time gap was maintained between step 1 and step 2 and between step 2 and step 3 to allow stabilization of the loop temperature and/or pressure and to check for any leaks from autoclave and other joints. Figure 3.9 shows example water pressure history measured during the heatup procedures for a PWR environment fatigue testing of a 508 LAS specimen (Test no. EN-F20). Figures 3.10 and 3.11, respectively, show the water flow rate and various temperature-time histories measured with the thermocouples. Figure 3.12 shows example temperature profiles along the length of a 508 LAS specimen and pull rod just before the start of the main fatigue test. This figure indicates that the temperature in the gauge area and part of the specimen shoulder was

approximately maintained at the intended value of 300 ^{o}C. This is over a length of approximately ±1 in. from the gauge center. Note that the length of the gauge section is approximately 0.561 in.

In addition to other test parameters, the conductivity of the loop was also measured during the test procedures. Figure 3.13 shows an example of the loop water conductivity [measured through an electrochemical potential (ECP) sensor channel with a multiplication factor of 10^{-2}] during initial loop pressurization, heatup, and main fatigue testing. The main fatigue test was conducted by controlling the crosshead displacement or stroke. Since it was not possible to use an extensometer for gauge area strain measurement due to a water-tight autoclave in the experimental assembly, the frame was controlled by measurements of the crosshead stroke. However, the stroke amplitude was based on a known stroke versus strain curve obtained through earlier conducted strain control tests in air and/or through FE models. While estimating strain-dependent material properties, we first estimated the unknown gauge area strain at a given instant by using stroke-strain mapping functions and the stroke input at that instant. The parameters of the mapping polynomials were estimated from known stroke versus strain data obtained through an in-air fatigue test (under stroke control and similar test conditions of temperature, stroke amplitude, and stroke rate). The detailed procedure regarding the stroke-to strain-mapping can be found in our earlier work [15].

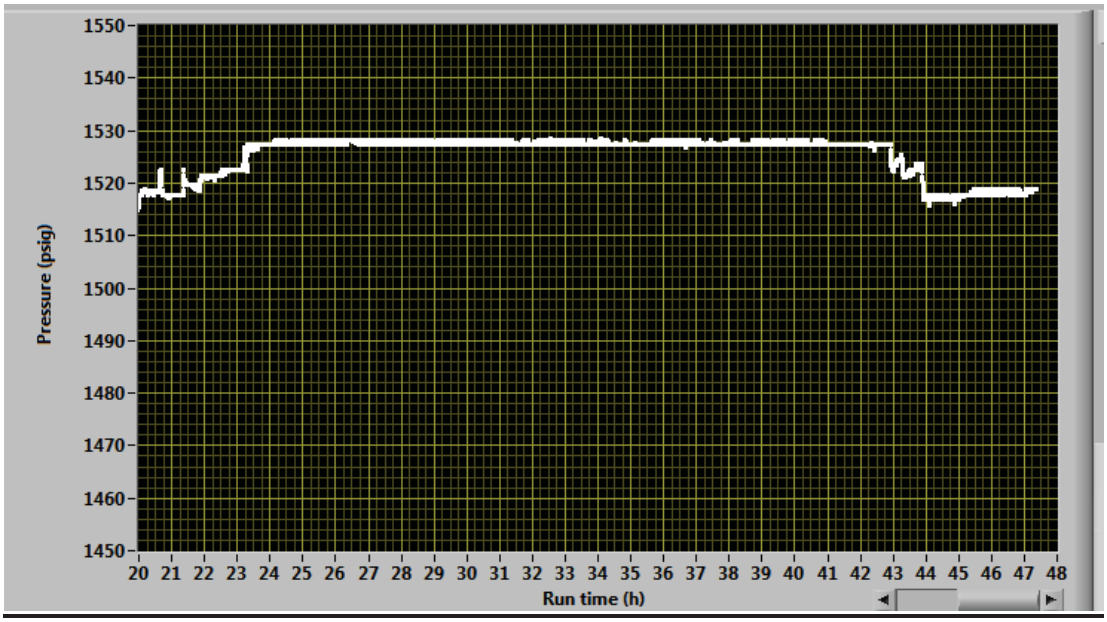

Figure 3. 9 Water pressure history measured during heatup for a PWR environment fatigue test of a 508 LAS specimen (Test EN-F20).

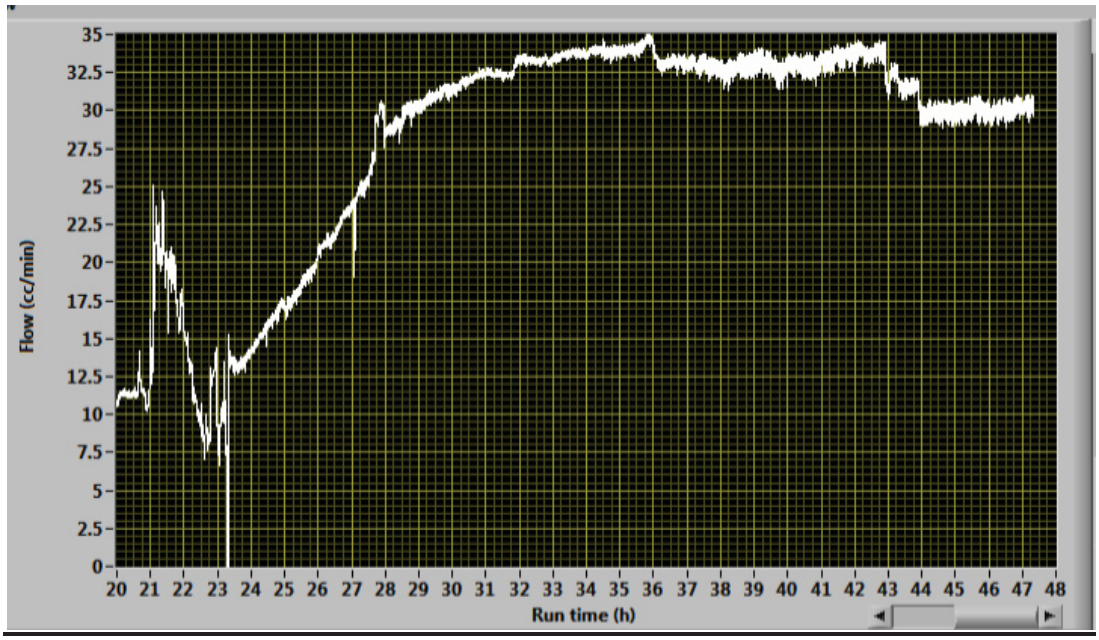

Figure 3. 10 Example water flow rate measured during heatup and temperature stabilization for a PWR environment fatigue test of a 508 LAS specimen (Test EN-F20).

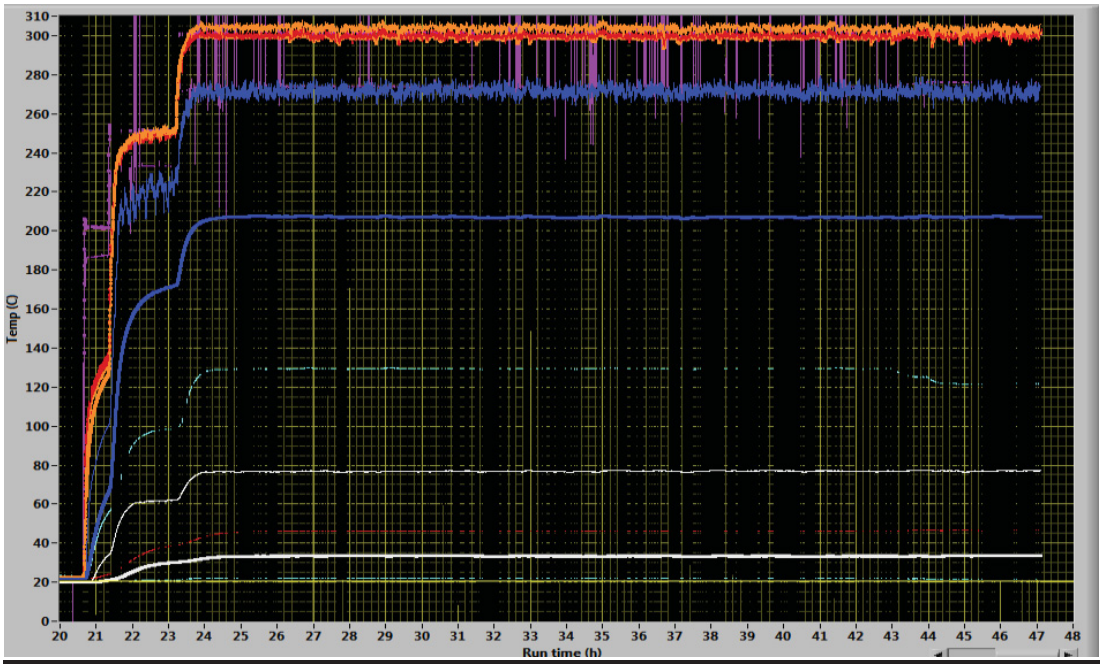

Figure 3. 11 Example temperature histories measured during heatup and temperature stabilization for a PWR environment fatigue test of a 508 LAS specimen (Test EN-F20).

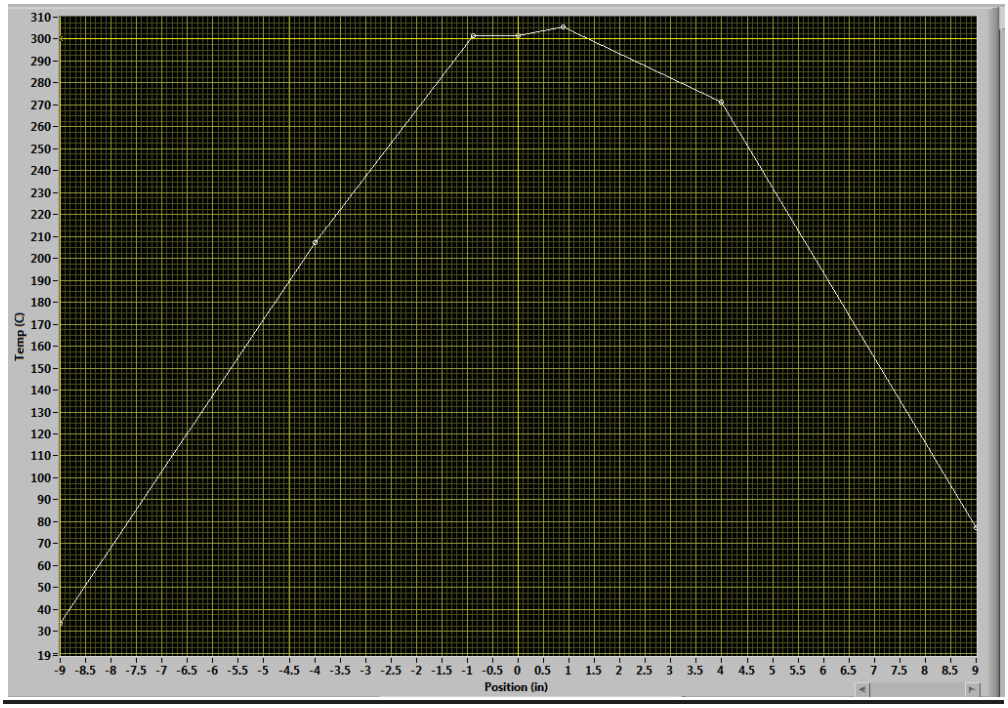

Figure 3. 12 Example temperature profile along the length of 508 LAS specimen and pull rod during a PWR environment fatigue test (Test EN-F20).

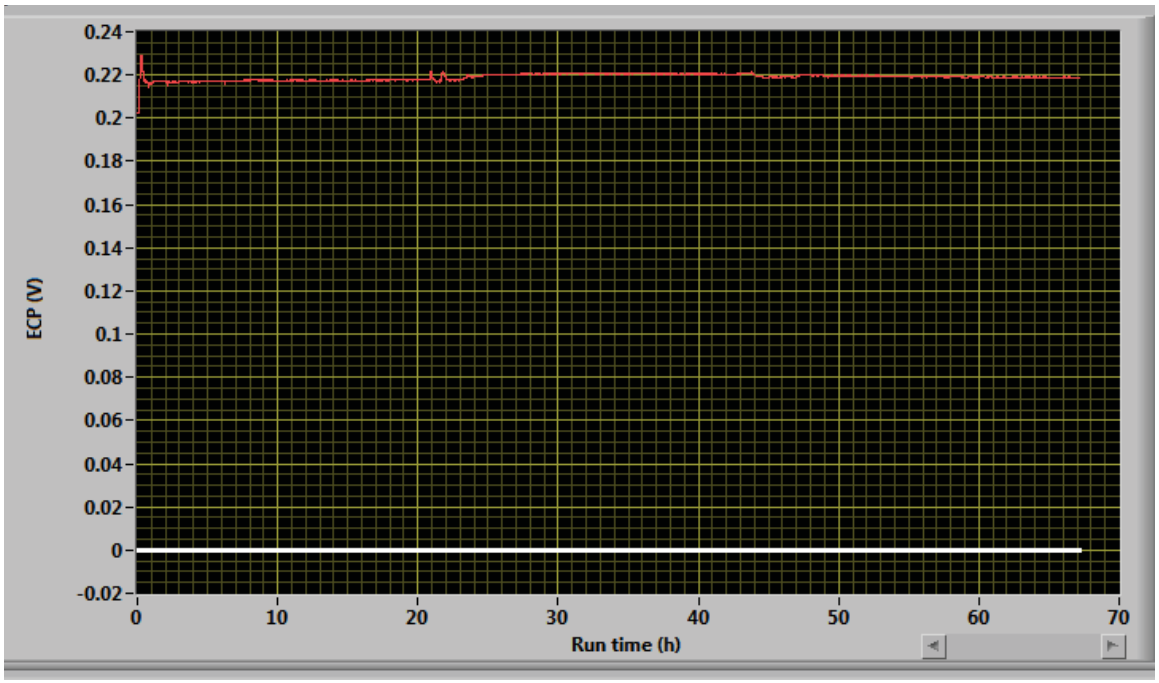

Figure 3. 13 Example loop water conductivity (measured through ECP sensor channel with a multiplication factor of 10^{-2}) time history during initial loop pressurization, heatup, temperature stabilization, and main fatigue test.

4 Results from 508 LAS Base and HAZ Metal Tensile Test and Material Model

The major aim of the project discussed in this report is to model the time-dependent cyclic plasticity behavior of various reactor steel materials under in-air and PWR coolant environments. To that end, we are conducting various fatigue tests using specimens made from different reactor steels. However, before conducting fatigue tests for a particular base/weld metals, we performed a series of tensile tests for the following reasons. First, based on the tensile test results, parameters for fatigue tests (e.g., frame stroke displacement for in-air or PWR water fatigue test) were selected. Second, the tensile test parameters (such as elastic modulus, yield stress, and kinematic hardening parameters) along with the corresponding cyclic test parameters can be used in FE model to perform parametric study. Note that, to restrict the effect of data scatter due to material micro-structural variability, both the tensile and fatigue test specimens were fabricated from the same base or weld metal plates. In this chapter we will summarize the test and material parameter results estimated through tensile tests of 508 LAS base and HAZ metal specimens. The associated test conditions, stress-strain results, and kinematic hardening model results are summarized below.

4.1 Test Conditions for 508 LAS Base and HAZ Metal Tensile Tests

Five tensile tests were conducted using specimens fabricated either from 508 LAS base metal plates or from HAZ (see Figure 3.2) of 508 LAS-316 SS weld plates. All the tests were conducted in air at either room temperature (22 ^{o}C) or 300 ^{o}C. Table 4.1 shows the test conditions for the five tensile tests. All these tests were conducted under an isothermal condition. For the 300 ^{o}C tensile tests, the specimens were heated in multiple steps to reach the desired gauge area temperature of 300 ^{o}C. Once the temperature stabilized, the main tensile test was conducted.

Figure 4.1 shows example temperature histories measured through all the thermocouples (attached to the specimen and pull rods) during heatup, the main tensile test, and cooldown of a 508 LAS HAZ specimen. Figure 4.2 is a magnified version of Figure 4.1 for the thermocouple measurements in the gauge area only. During heatup the specimens were held at stress control conditions with approximately negligible stress but allowed to expand freely due to the temperature increase. Figure 4.3 shows example stress readings during the entire test. As shown by the corresponding gauge-area strain history from Figure 4.4, the specimen experienced substantial strain of approximately 0.43% during heatup from room temperature to 300 ^{o}C. Since during heatup the specimens were held in a stress free and load control condition, the heatup procedure did not create any stress. However, in an actual reactor condition depending on the component geometry and boundary condition, substantial stress might be created during heatup and cooldown. Hence, this strain buildup during heatup is worth noting, although this information is irrelevant for a typical isothermal tensile test.

Table 4. 1 Test conditions for 508 LAS base and HAZ metal tensile tests.

Test ID	Material Type	Test Condition
T06	508 LAS base	In air, 22 °C, strain control, strain rate=0.1%/s
T07	508 LAS HAZ	In air, 22 °C, strain control, strain rate=0.1%/s
T08	508 LAS base	In air, 300 °C, strain control, strain rate=0.1%/s
T09	508 LAS HAZ	In air, 300 °C, strain control, strain rate=0.1%/s
T10	508 LAS base	In air, 300 °C, strain control, strain rate=0.01%/s

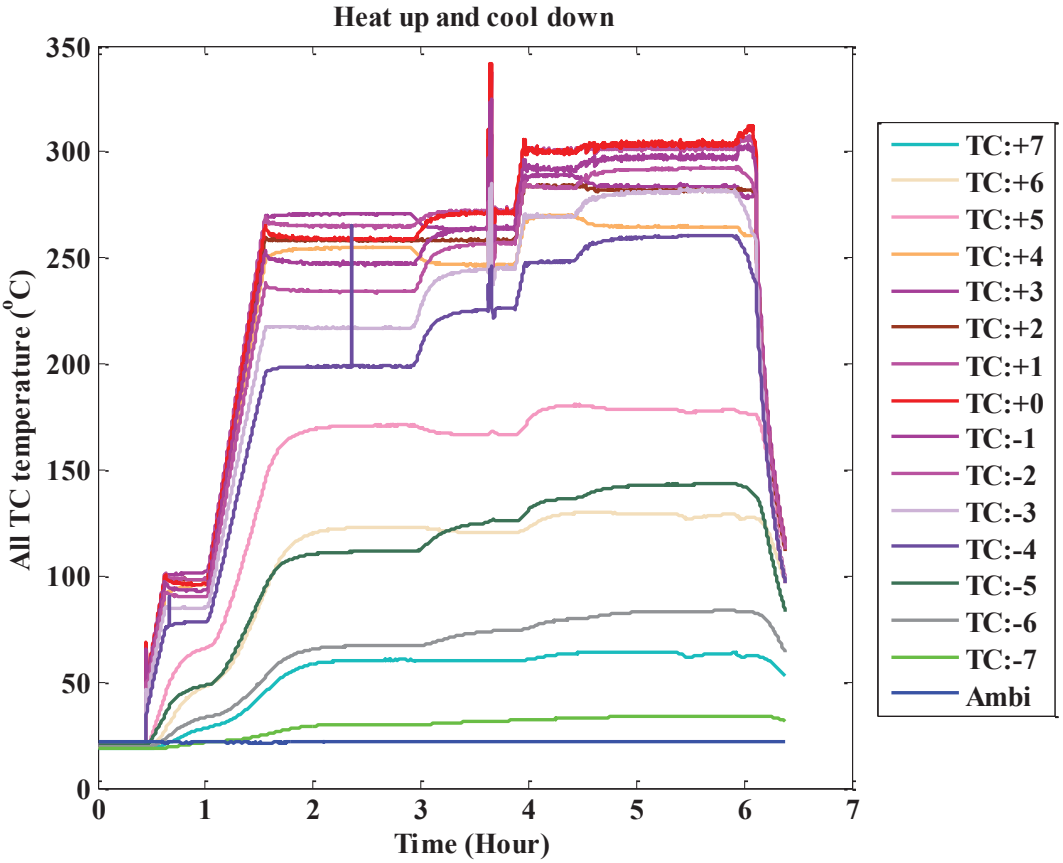

Figure 4. 1 Example temperature histories (measured through different thermocouples) during heatup, temperature stabilization, main tensile test, and cooldown for a 508 LAS HAZ specimen (Test T09).

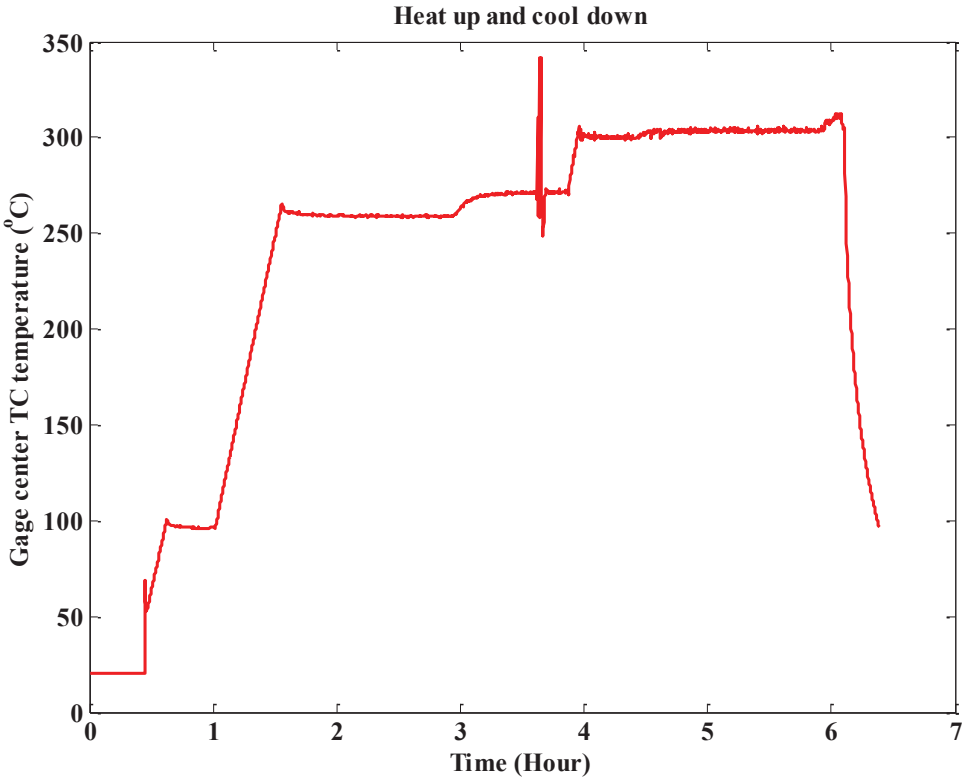

Figure 4. 2 Magnified version of Figure 4.1 showing temperature measured at gauge center thermocouple.

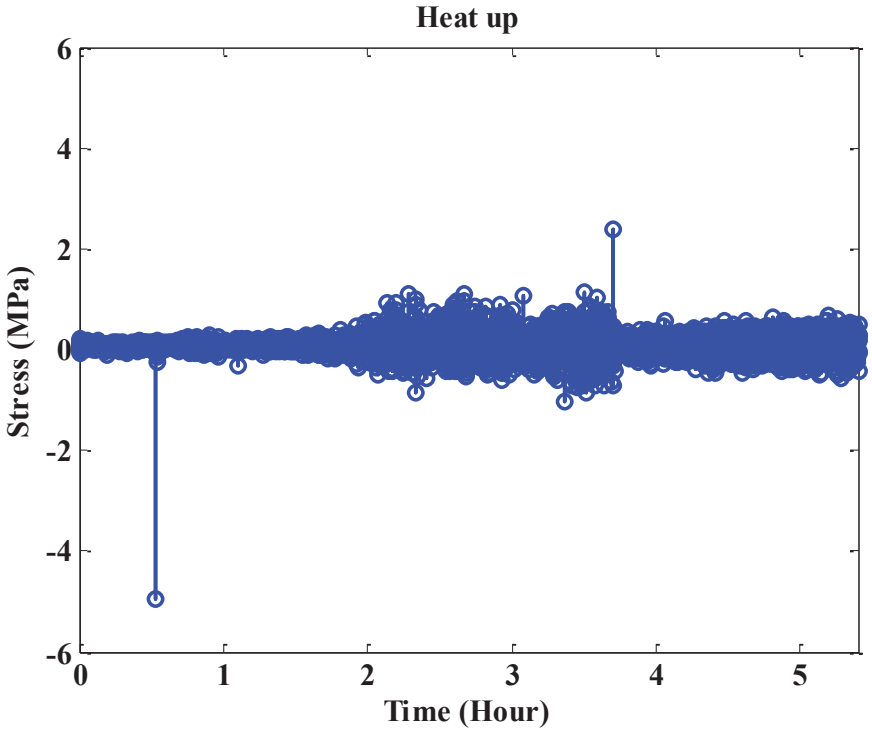

Figure 4. 3 Example stress readings during only heatup and temperature stabilization for a 508 LAS HAZ specimen (Test T09).

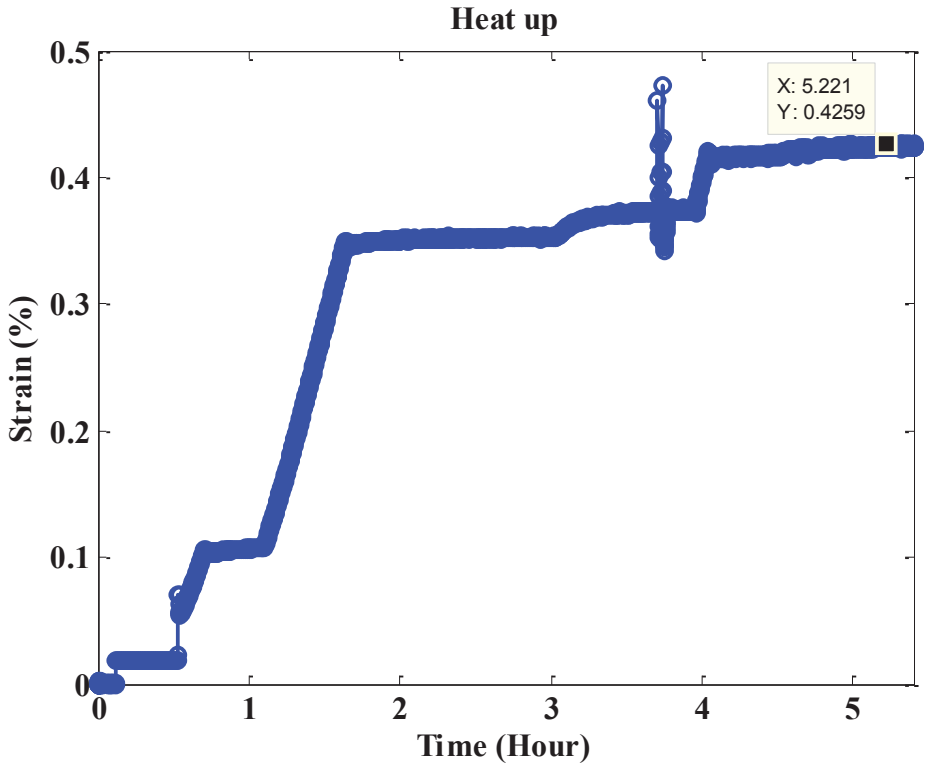

Figure 4. 4 Example strain history during only heatup and temperature stabilization for a 508 LAS HAZ specimen (Test T09).

4.2 Estimated Stress-Strain Curves for 508 LAS Base and HAZ Metal

Stress-strain curves were estimated from the tensile test data. Full stress-strain curves were estimated by combining different sensor measurements, such as those from the gauge area extensometer and frame actuator position. Note that a high-precision and high-temperature extensometer was used for the tensile and fatigue tests, which had a strain measurement limit of only 2%. (The details of the strain extrapolation procedure beyond 2% strain can be found from our earlier work reported in Ref. [18].) The resulting engineering stress-strain curves for all the mentioned tensile tests (in Table 4.1) are shown in Figure 4.5. The corresponding true stress-strain curves (up to ultimate strain) are shown in Figure 4.6. As evident from Figures 4.5 and 4.6, at room temperature the stress-strain curve for the base metal is significantly different from that of the HAZ metal specimen. However, at 300 ^{o}C the base and HAZ metal stress-strain curves look similar. Figures 4.5 and 4.6 also indicate that the strain rate has no significant effect on the stress-strain curve derived from the tensile test.

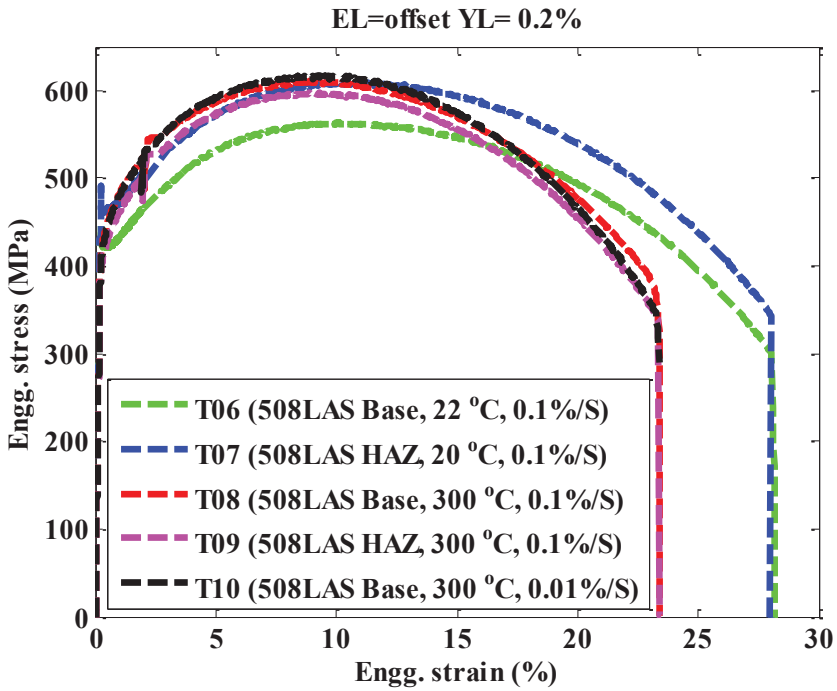

Figure 4. 5 Engineering stress-strain curves estimated from tensile test data of 508 LAS base and HAZ metal specimens under different conditions.

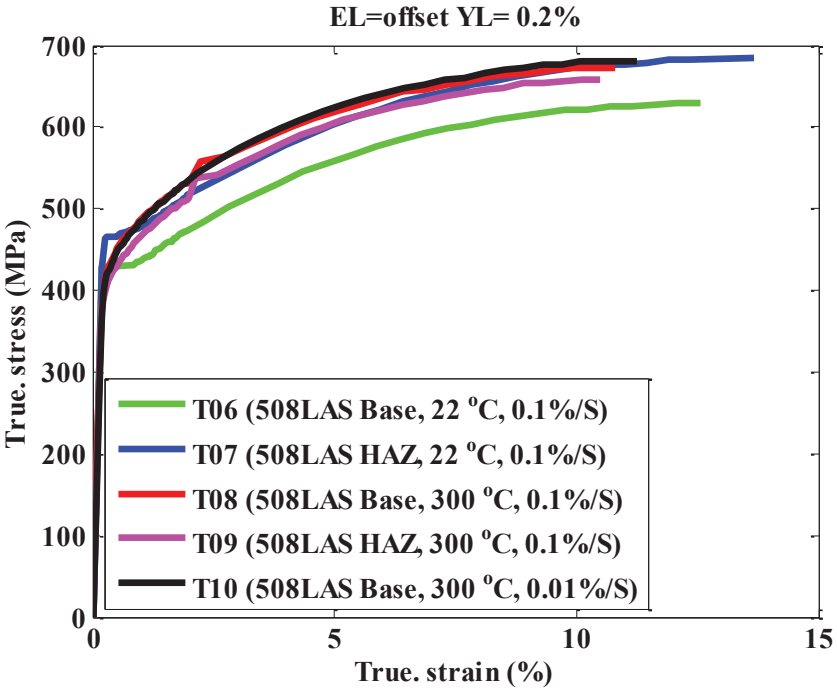

Figure 4. 6 True stress-strain curves (up to ultimate strain) estimated from tensile test data of 508 LAS base and HAZ metal specimens under different conditions.

4.3 Estimated Tensile Test and Kinematic Hardening Properties for 508 LAS Base and HAZ Metal

Using the stress-strain data discussed above, we estimated important tensile properties such as the elastic modulus, reduction in gauge area, elastic limit stress, yield, ultimate and fracture stress/strain for the test conditions shown in Table 4.1. These estimated properties are reported in Tables 4.2 to 4.6. In addition, the kinematic hardening parameters (both linear and nonlinear) were estimated from the corresponding stress-strain curves and the procedure discussed in Section 2.3 (Eqs. 2.3 to 2.20). However, unlike the procedure discussed in Section 2.3 for cyclic stress-strain curves, for particular test conditions, the tensile test produced a fixed stress-strain curve. Hence, each tensile test has a fixed set of kinematic hardening parameters that can be estimated based on a given yield condition.

In this work, we estimated kinematic hardening parameters from the tensile tests, assuming four yield stress conditions: 1) elastic limit stress, 2) 0.05% offset strain yield stress, 3) 0.1% offset strain yield stress, and 4) 0.2% offset strain yield stress. The resulting kinematic hardening parameters (both linear and nonlinear model parameters) are reported in Tables 4.3 to 4.6. Note that due to convergence issues associated with the parameter optimization scheme, we limited the stress-strain curves to 2% when considering condition 1 as the yield stress and to 5% when considering conditions 2-4 as the yield stress. According to ASME code Section III, a vessel design is considered acceptable if the maximum accumulated local strain does not exceed 5% [2, 10]. Also, while estimating the reported parameters, we considered the true stress-strain curves since a typical FE code requires that the stress-strain or equivalent parameters be represented in true stress-strain form. The reported results in this section can be used for developing simplified FE models of reactor components with time-independent models for kinematic hardening. Also, these tensile parameters can be compared with corresponding cyclic test parameters to determine how any differences affect the FE-based stress analysis results and associated fatigue life evaluation.

Table 4. 2 Estimated tensile test material properties for 508 LAS base and HAZ metal specimens tensile tested under different conditions.

Tensile test properties		**T06 (508 LAS Base, 22 ^{o}C, 0.1%/s)**	**T07 (508 LAS HAZ, 22 ^{o}C, 0.1%/s)**	**T08 (508 LAS Base, 300 ^{o}C, 0.1%/s)**	**T09 (508 LAS HAZ, 300 ^{o}C, 0.1%/s)**	**T10 (508 LAS Base, 300 ^{o}C, 0.1%/s)**
Elastic modulus (GPa)		209.19	208.4	197.57	194.95	194.1
Reduction in gauge area (%)		73.997	76.217	69.729	73.246	74.329
Ultimate	Stress (MPa)	563.18	609.13	610.28	597.41	617.37
	Strain (%)	10.581	11.102	9.0422	9.3115	9.1744
Fracture	Stress (MPa)	294.6	341.7	325.5	338.7	345.1
	Strain (%)	28.05	28.06	23.38	23.31	23.25

Table 4. 3 Estimated (or assumed) elastic limit and associated kinematic hardening properties for 508 LAS base and HAZ metal specimens tensile tested under different conditions.

Elastic limit and kinematic hardening properties (up to 2% true total strain)		**T06 (508 LAS Base, 22 °C, 0.1%/s)**	**T07 (508 LAS HAZ, 22 °C, 0.1%/s)**	**T08 (508 LAS Base, 300 °C, 0.1%/s)**	**T09 (508 LAS HAZ, 300 °C, 0.1%/s)**	**T10 (508 LAS Base, 300 °C, 0.1%/s)**
Assumed elastic limit	Stress (MPa)	424.45	460.47	391.01	381.99	379.82
	Strain (%)	0.2044	0.2218	0.2072	0.2072	0.2072
Lin./nonlin. kinematic hardening parameter	Lin. C1 (MPa)	2357.5	2762.7	9319	8553.1	10288
	Nonlin. C1 (MPa)	1065.6	1671.5	20090	16166	23961
	Nonlin. γ1	-102.91	-67.385	131.34	108.02	154.98

Table 4. 4 Estimated 0.05% offset yield limit and associated kinematic hardening properties for 508 LAS base and HAZ metal specimens tensile tested under different conditions.

0.05% offset yield limit and kinematic hardening properties (up to 5% true total strain)		**T06 (508 LAS Base, 22 °C, 0.1%/s)**	**T07 (508 LAS HAZ, 22 °C, 0.1%/s)**	**T08 (508 LAS Base, 300 °C, 0.1%/s)**	**T09 (508 LAS HAZ, 300 °C, 0.1%/s)**	**T10 (508 LAS Base, 300 °C, 0.1%/s)**
Estimated yield limit	Stress (MPa)	427.31	464.97	415.15	399.41	406.93
	Strain (%)	0.25545	0.27541	0.26176	0.25728	0.26138
Lin./nonlin. kinematic hardening parameter	Lin. C1 (MPa)	2642.2	2793.8	5607.2	5627.2	6096.2
	Nonlin. C1 (MPa)	2150.4	2353.7	10699	9779.2	11670
	Nonlin. γ1	-13.087	-10.62	49.624	43.019	51.785

Table 4. 5 Estimated 0.1% offset yield limit and associated kinematic hardening properties for 508 LAS base and HAZ metal specimens tensile tested under different conditions.

0.1% offset yield limit and kinematic hardening properties (up to 5% true total strain)		**T06 (508 LAS Base, 22 °C, 0.1%/s)**	**T07 (508 LAS HAZ, 22 °C, 0.1%/s)**	**T08 (508 LAS Base, 300 °C, 0.1%/s)**	**T09 (508 LAS HAZ, 300 °C, 0.1%/s)**	**T10 (508 LAS Base, 300 °C, 0.1%/s)**
Estimated yield limit	Stress (MPa)	422.6	462.57	426.4	407.61	419.61
	Strain (%)	0.30215	0.32285	0.31887	0.3099	0.31796
Lin./nonlin. kinematic hardening parameter	Lin. C1 (MPa)	2898.1	2959.6	5228.7	5351.8	5634
	Nonlin. C1 (MPa)	2644.3	2699.7	9379.1	8957.6	10078
	Nonlin. γ1	-6.0632	-5.8444	43.968	39.549	45.111

Table 4. 6 Estimated 0.2% offset yield limit and associated kinematic hardening properties for 508 LAS base and HAZ metal specimens tensile tested under different conditions.

0.2% offset yield limit and kinematic hardening properties (up to 5% true total strain)		**T06 (508 LAS Base, 22 °C, 0.1%/s)**	**T07 (508 LAS HAZ, 22 °C, 0.1%/s)**	**T08 (508 LAS Base, 300 °C, 0.1%/s)**	**T09 (508 LAS HAZ, 300 °C, 0.1%/s)**	**T10 (508 LAS Base, 300 °C, 0.1%/s)**
Estimated yield limit	Stress (MPa)	422.11	462.73	439.98	420.21	434.93
	Strain (%)	0.40218	0.42317	0.42399	0.41654	0.42525
Lin/nonlin. kinematic hardening parameter	Lin. C1 (MPa)	3045.2	3078.3	4817.5	4962.6	5131
	Nonlin. C1 (MPa)	2968.5	2970.6	8126.8	7906.6	8574.3
	Nonlin. γ1	-1.737	-2.3115	38.728	35.178	38.837

5 Results of 508 LAS Base Metal Fatigue Test and Material Model

Multiple fatigue tests were conducted using 508 LAS base metal to develop time-dependent models for isotropic and kinematic hardening and to estimate associated material parameters. The related fatigue test and material model results are summarized below.

5.1 Test Conditions for 508 LAS Base Metal Fatigue Tests

Six 508 LAS base metal specimens were fatigue tested under different conditions. Out of these six tests, only three were found completely successful. Results related to these successful tests are presented in this section.

Table 5.1 shows the conditions of these successful tests. The stroke (or frame crosshead displacement) amplitudes for the fatigue tests were selected based on the results of the FE models developed to model the earlier reported tensile tests: T06 (508 LAS base metal at room temperature) and T08 (508 LAS base metal at 300 ^{o}C). These two tests were conducted under strain control. However, the fatigue tests were conducted under stroke control. Using the stress-strain data of T06 and T08 tests, we developed FE models to estimate the equivalent stroke input for a gauge-area strain amplitude of approximately 0.5%. Since the extensometer cannot be used for gauge-area strain measurements in a PWR environment tests (because the specimen is inside the watertight autoclave), the fatigue tests had to be controlled either by using crosshead stroke (Figures 3.5 and 3.8), frame actuator position measurements, or frame load cell measurements (as in case of a typical stress control test). Since our intention was to mimic a typical gauge-area strain control test, we used the stroke measurements to control the frame and assumed that the effect of frame stiffness on stroke measurements is less than that for the frame actuator position measurements. The stroke amplitude for RT-F23 fatigue test was selected from the FE model results of T06 tensile test, whereas that for ET-F24 and EN-F20 fatigue tests was selected from the FE model results of T08 tensile test. Both the T06 and T08 FE models were simulated over 20 s, which is the time required to reach 2% gauge area strain in the corresponding tensile tests.

Figures 5.1 to 5.4 show example results obtained for the FE model of the T06 specimen and their comparison with experimental results. Similarly, Figures 5.5 to 5.8 show example model and experimental results for the T08 specimen.

Table 5. 1 Test conditions for 508 LAS base metal fatigue tests.

Test ID	Material type	Test Condition
RT-F23	508 LAS base	In air, 22 ^{o}C, stroke control, stroke amplitude=0.1671 mm, stroke rate = 0.03342 mm/s, cycle period = 20 s
ET-F24	508 LAS base	In air, 300 ^{o}C, stroke control, stroke amplitude=0.1813 mm, stroke rate = 0.0363 mm/s, cycle period = 20 s
EN-F20	508 LAS base	PWR water, 300 ^{o}C, stroke control, stroke amplitude=0.1813 mm, stroke rate = 0.0363 mm/s, cycle period = 20 s Water chemistry: 1000 ppm B as H_3BO_3, 2 ppm Li^+ as LIOH, 20% H_2/bal. N_2 cover gas, and DO < 5 ppb

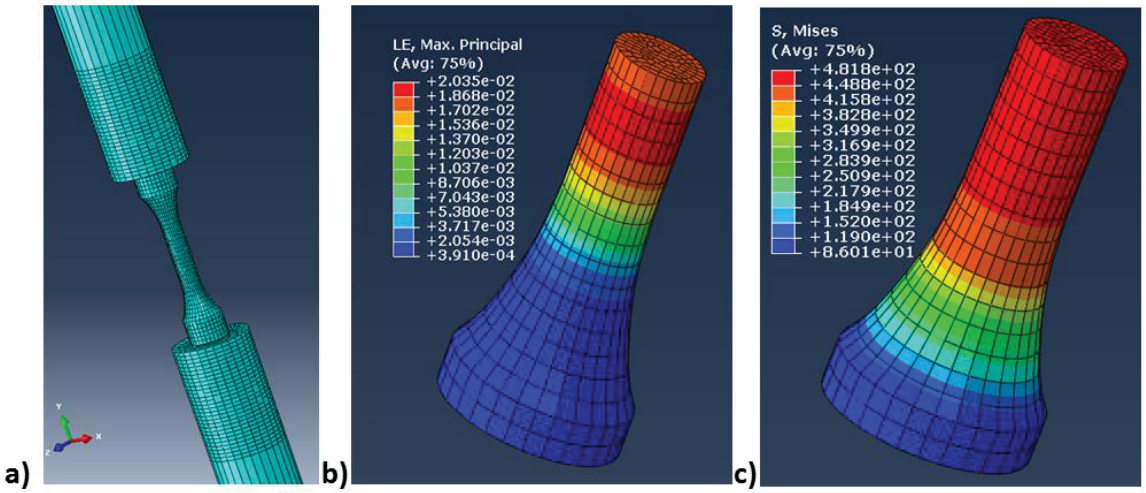

Figure 5. 1 a) FE mesh of tensile test specimen and pull rods, b) maximum principal strain distribution at the end of FE simulation of T06 tensile test, and c) Von Mises stress distribution at the end of FE simulation.

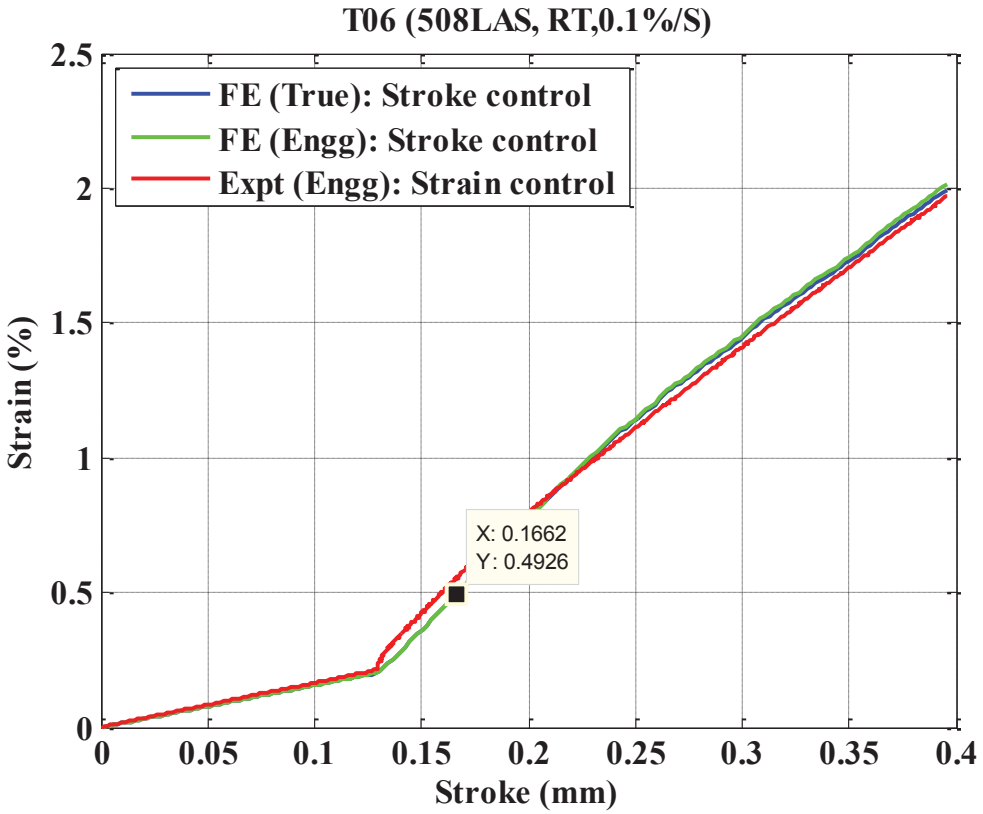

Figure 5. 2 Stroke versus strain data obtained from T06 FE model and comparison with experimental (T06 tensile test) results.

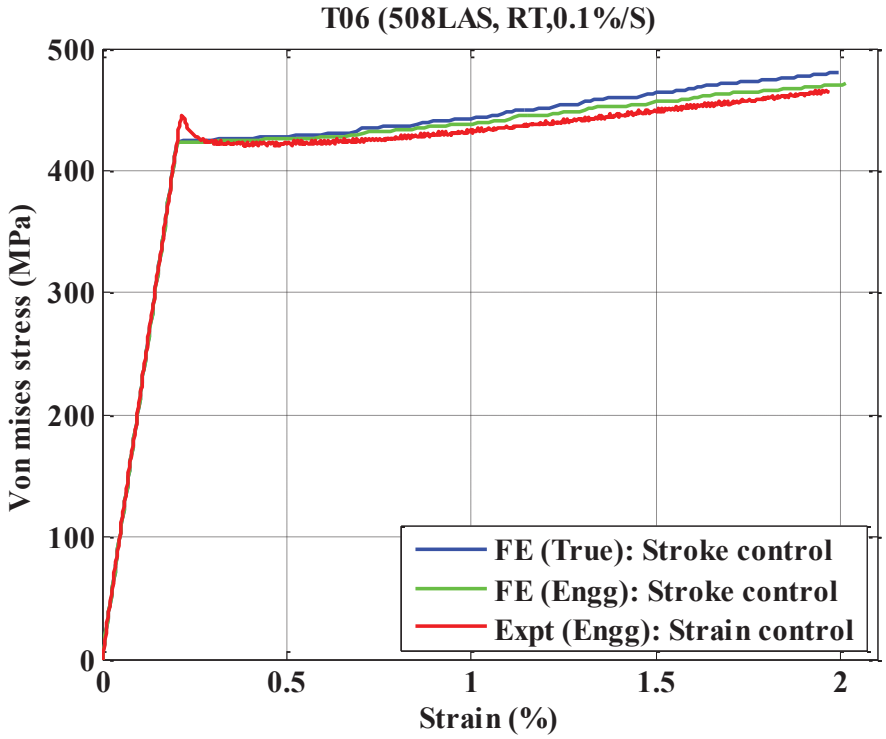

Figure 5. 3 Strain versus Von Mises stress data obtained from T06 FE model and comparison with experimental (T06 tensile test) results.

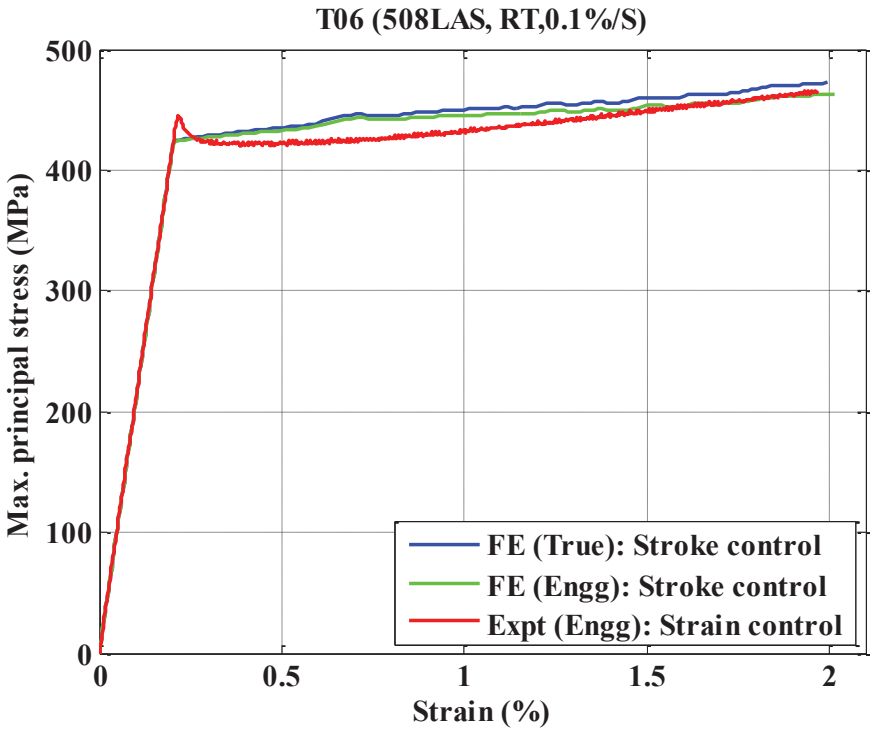

Figure 5. 4 Strain versus maximum principal stress data from T06 FE model and comparison with experimental (T06 tensile test) results.

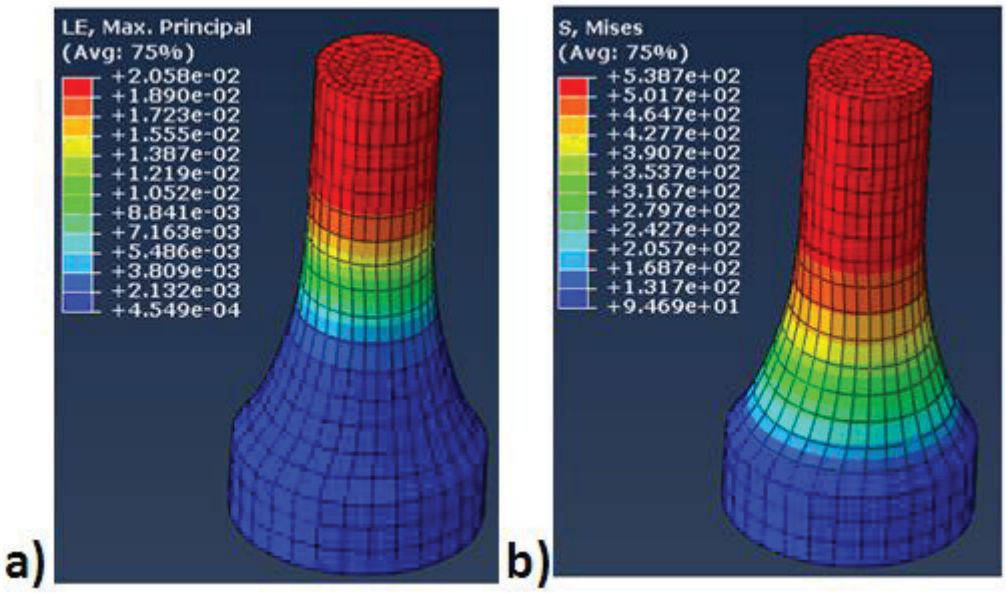

Figure 5. 5 a) Maximum principal strain distribution at the end of FE simulation of T08 tensile test and b) Von Mises stress distribution at the end of FE simulation.

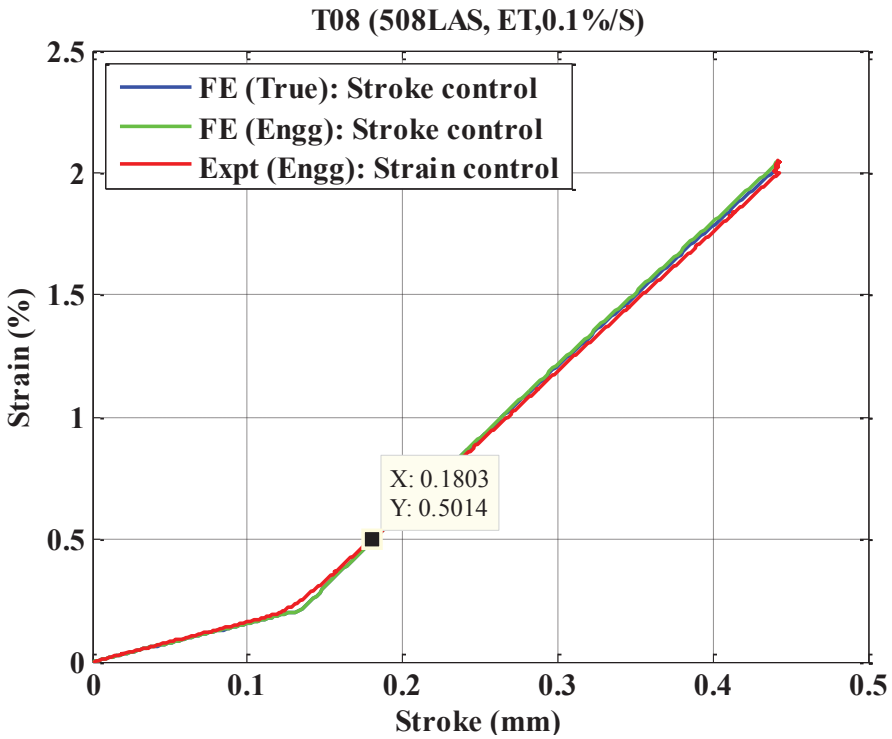

Figure 5. 6 Stroke versus strain data obtained from T08 FE model and comparison with experimental (T08 tensile test) results.

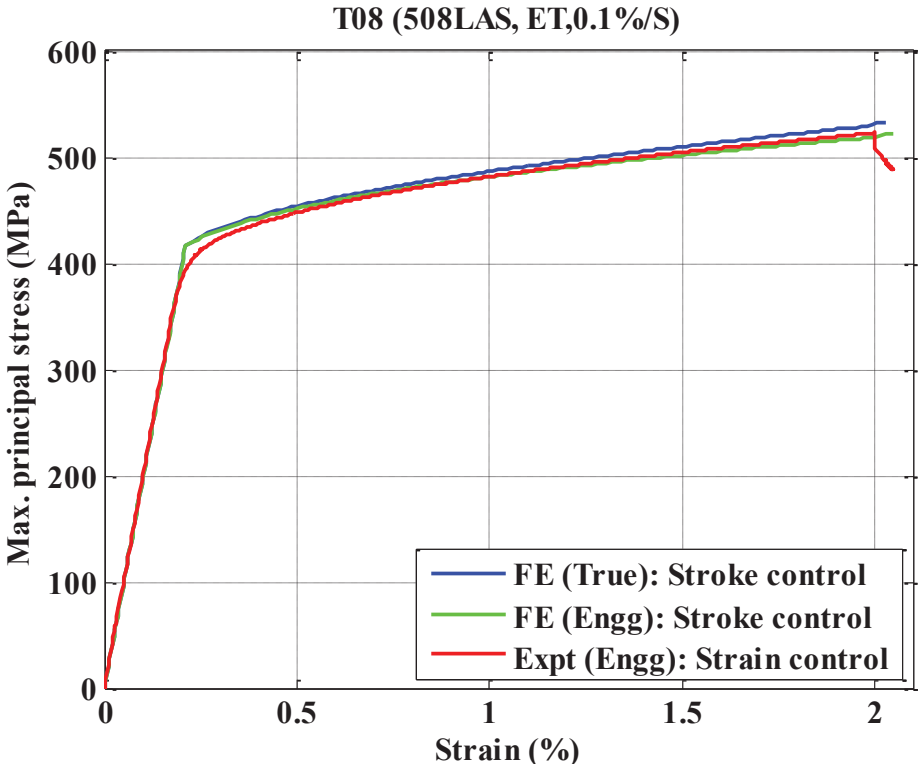

Figure 5. 7 Strain versus Von Mises stress data obtained from T08 FE model and comparison with experimental (T08 tensile test) results.

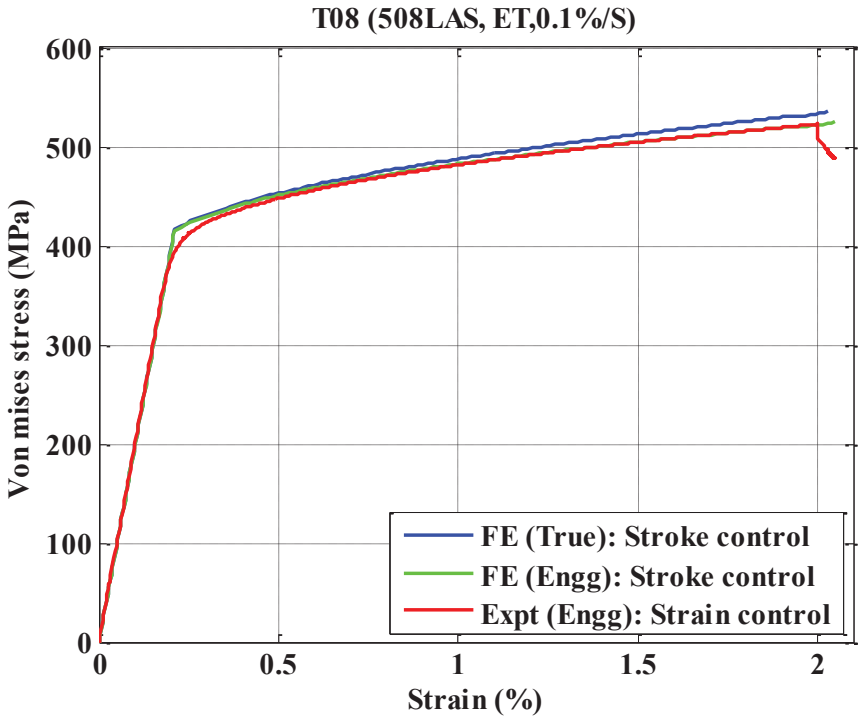

Figure 5. 8 Strain versus maximum principal stress data obtained from T08 FE model and comparison with experimental (T08 tensile test) results.

5.2 Bulk Fatigue Life and Maximum/Minimum Stress Time Histories for 508 LAS Base Metal Fatigue Tests

Test data were obtained from fatigue tests of 508 LAS base metal specimens under different test conditions (Table 5.1). Figure 5.9 shows the fatigue life under different conditions. The data indicate that under room temperature the specimen had fatigue life almost two times that in air at 300 ^{o}C and under PWR water conditions. The data also indicate little difference in fatigue lives between in-air and PWR water conditions at 300 ^{o}C. This possibly is either due to inherent scatter in the fatigue test results or the selection of the higher stroke rate (equivalent to 0.1%/s strain rate). At 0.1%/s equivalent strain rate, the effect of environment on the bulk fatigue life of 508 LAS base metal might not be significant. However, additional tests might be required to further verify this observation.

Figure 5.10 shows the maximum and minimum stress for 508 LAS base metal specimens fatigue tested under different conditions. A magnified version of Figure 5.10 is shown in Figure 5.11, which indicates substantial stress hardening during the first 100 cycles (approximately) at 300 ^{o}C in-air and PWR water conditions. However, at in-air room temperature, the specimen continuously softens over the entire fatigue life.

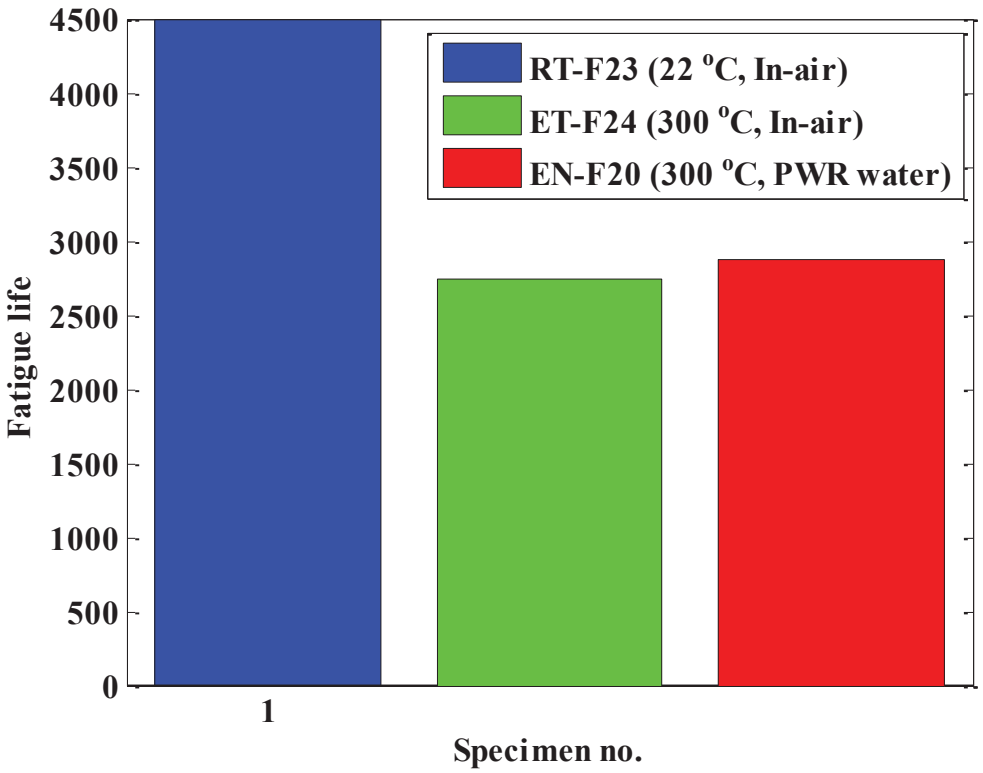

Figure 5. 9 Fatigue lives for 508 LAS base metal specimens fatigue tested under different conditions.

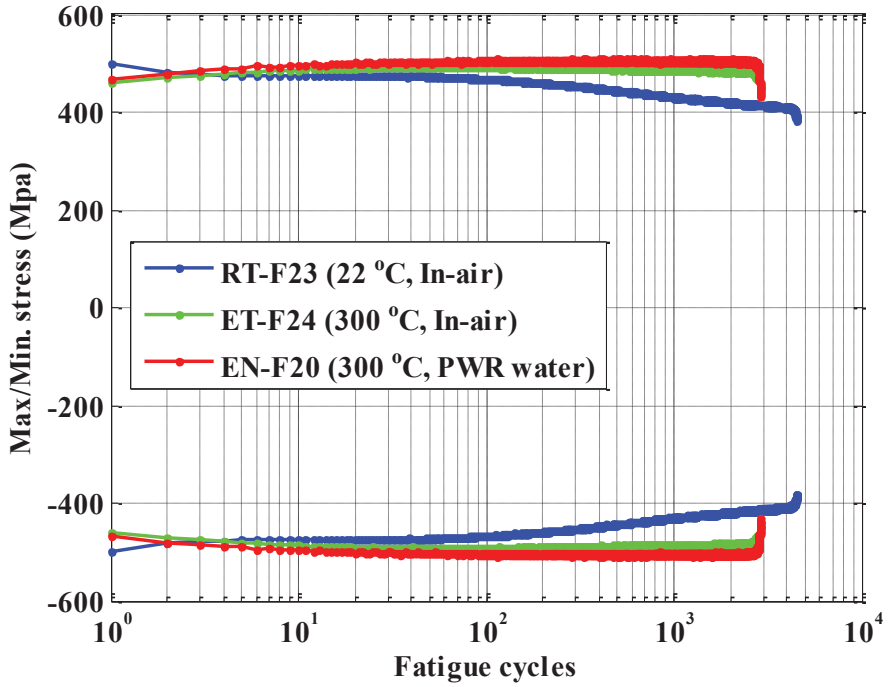

Figure 5. 10 Maximum and minimum stress for 508 LAS base metal specimens fatigue tested under different conditions.

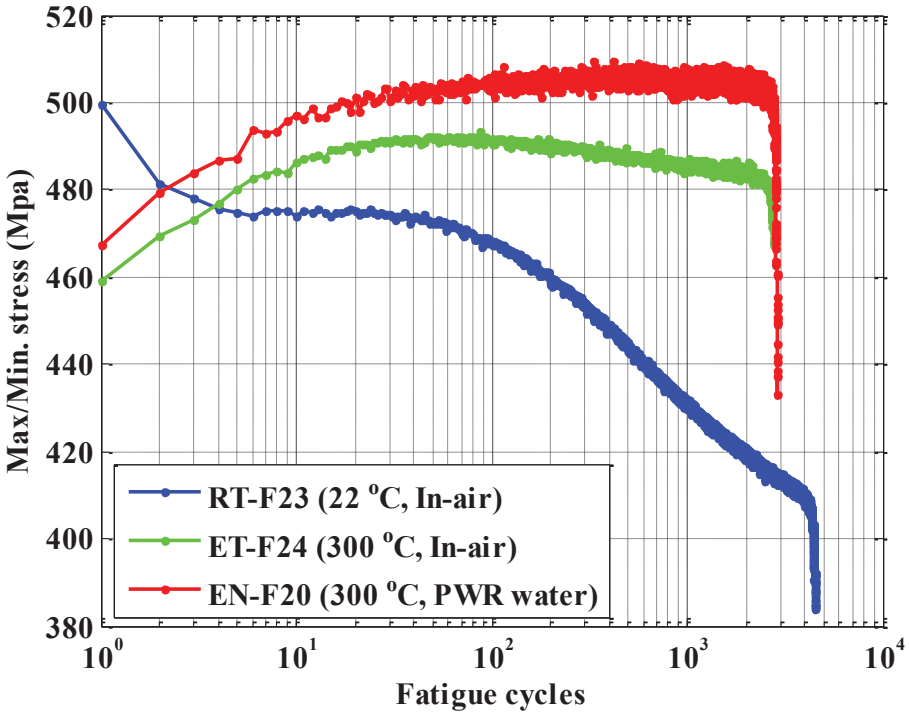

Figure 5. 11 Magnified version of Figure 5.10 showing the cyclic stress hardening/softening in 508 LAS base metal specimens under different conditions.

5.3 Elastic Modulus and Various Strain Range Time Histories for 508 LAS Base Metal Fatigue Tests

Using the cyclic stress-strain curve, we estimated the equivalent monotonic stress-strain curves under different test conditions (Table 5.1). Figures 5.12, 5.13, and 5.14 show the equivalent monotonic stress curves (first few cycles) for RT-F23, ET-F24, and EN-F20, respectively, as well as the corresponding tensile test results for T06 (room temperature) and T08 (300 ^{o}C). These figures also show the offset yield lines and corresponding elastic and yield limit stresses.

The equivalent monotonic curves were further processed with an ANL-developed material modeler code to automatically estimate the cyclic evolution of elastic modulus. Figure 5.15 shows the estimated elastic modulus under different test conditions. The data indicate that at room temperature the cyclic elastic modulus curve has a clear downward trend, but a slight upward trend for the 300 ^{o}C in-air and PWR condition. While more fatigue tests are required to confirm these trends, we did observe similar trends in our earlier work on 316 SS base metal [17].

Figures 5.16, 5.17, and 5.18 show the total, elastic, and plastic strain range histories under various test conditions. Finally, Figure 5.19 shows the accumulated plastic strain under different conditions. The accumulated plastic strain versus elastic limit or offset strain yield stress (discussed in the next section) data can be used in a FE code to model the isotropic component of the stress tensor.

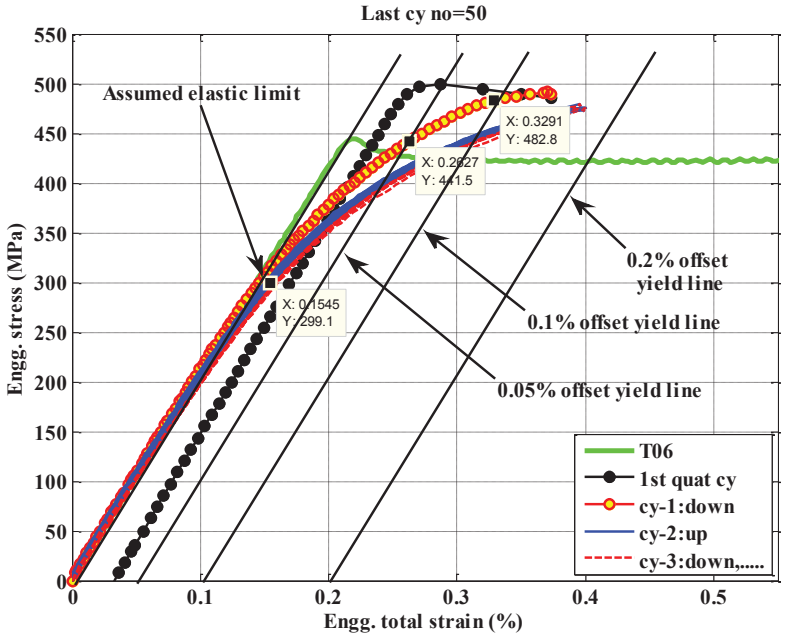

Figure 5. 12 Equivalent monotonic stress-strain curves estimated from upward/downward cycle (for first 50 cycles) stress-strain data of RT-F23 (22 ^{o}C, In-air condition) fatigue test and comparison with T06 (22 ^{o}C, in-air condition) tensile test data. Also the figure shows offset yield lines and corresponding elastic and yield limit stresses.

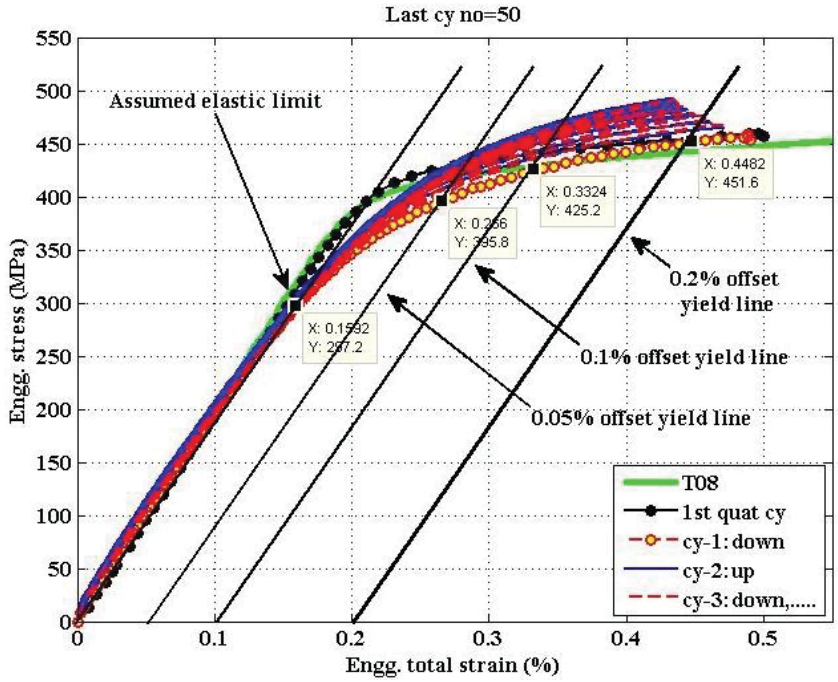

Figure 5. 13 Equivalent monotonic stress-strain curves estimated from upward/downward cycle (for first 50 cycles) stress-strain data for ET-F24 (300 °C, in air) fatigue test and comparison with T08 (300 °C, in air) tensile test data. Also given are the offset yield lines and corresponding elastic and yield limit stresses.

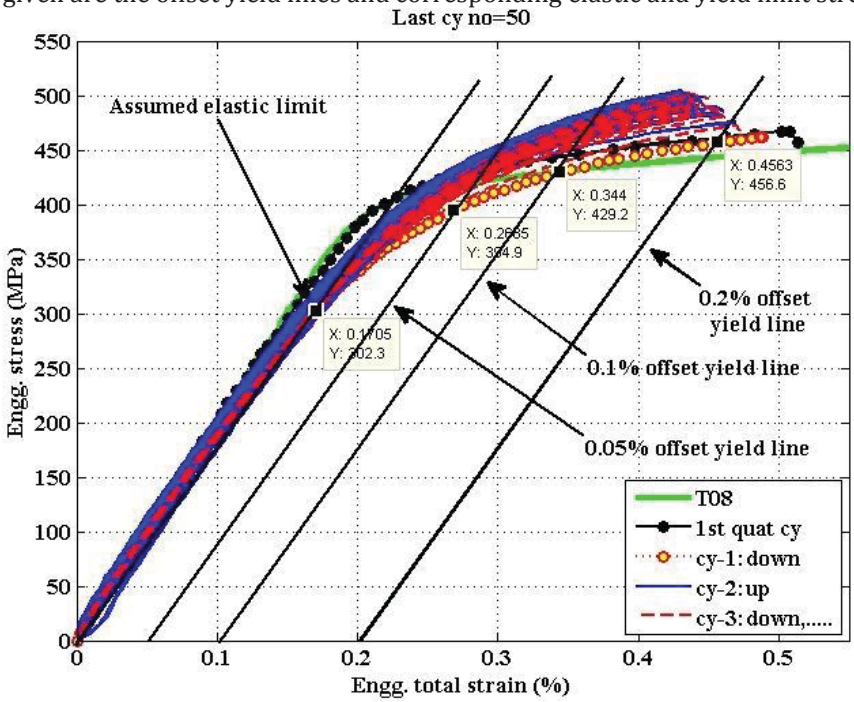

Figure 5. 14 Equivalent monotonic stress-strain curves estimated from upward/downward cycle (for first 50 cycles) stress-strain data for EN-F20 (300 °C, PWR Water) fatigue test and comparison with T08 (300 °C, in air) tensile test data. Also given are the offset yield lines and corresponding elastic and yield limit stresses.

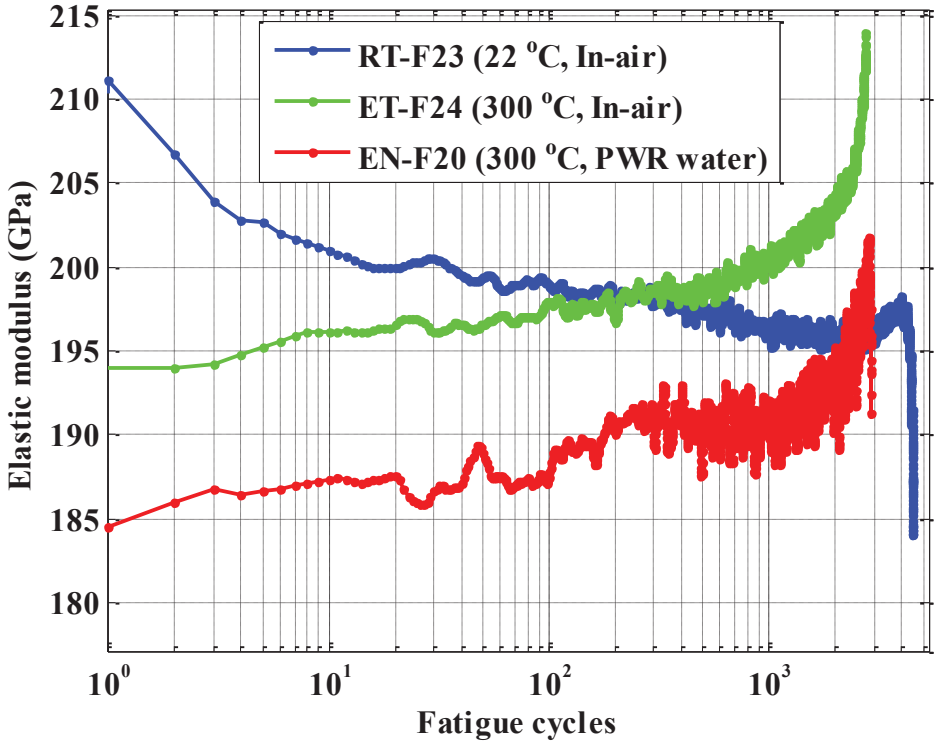

Figure 5. 15 Elastic modulus for 508 LAS base metal specimens fatigue tested under different conditions.

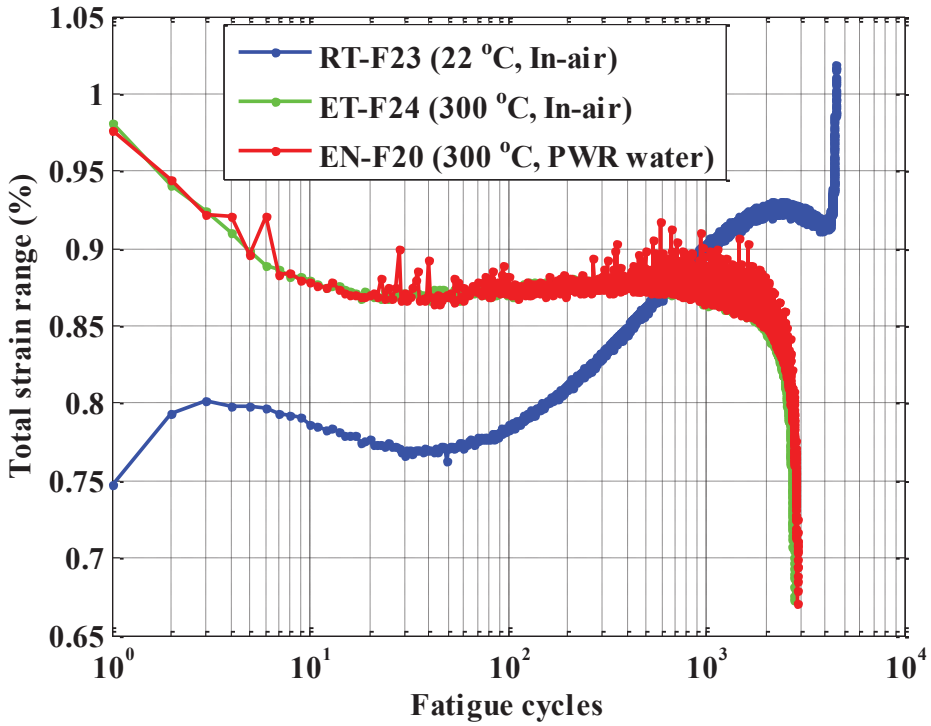

Figure 5. 16 Total strain range for 508 LAS base metal specimens fatigue tested under different conditions.

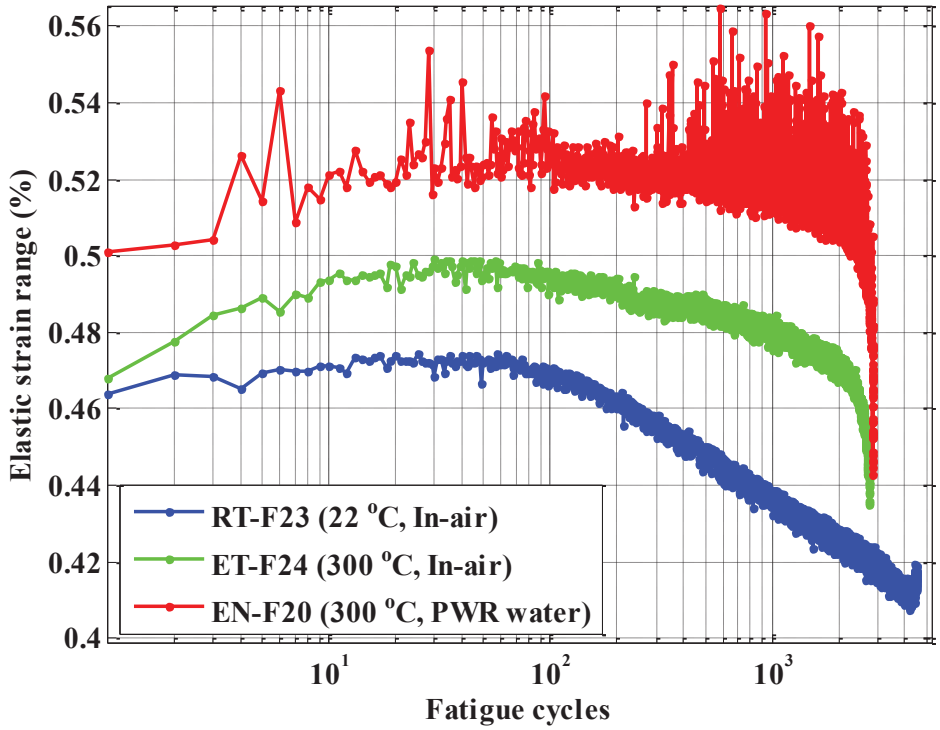

Figure 5. 17 Elastic strain range for 508 LAS base metal specimens fatigue tested under different conditions.

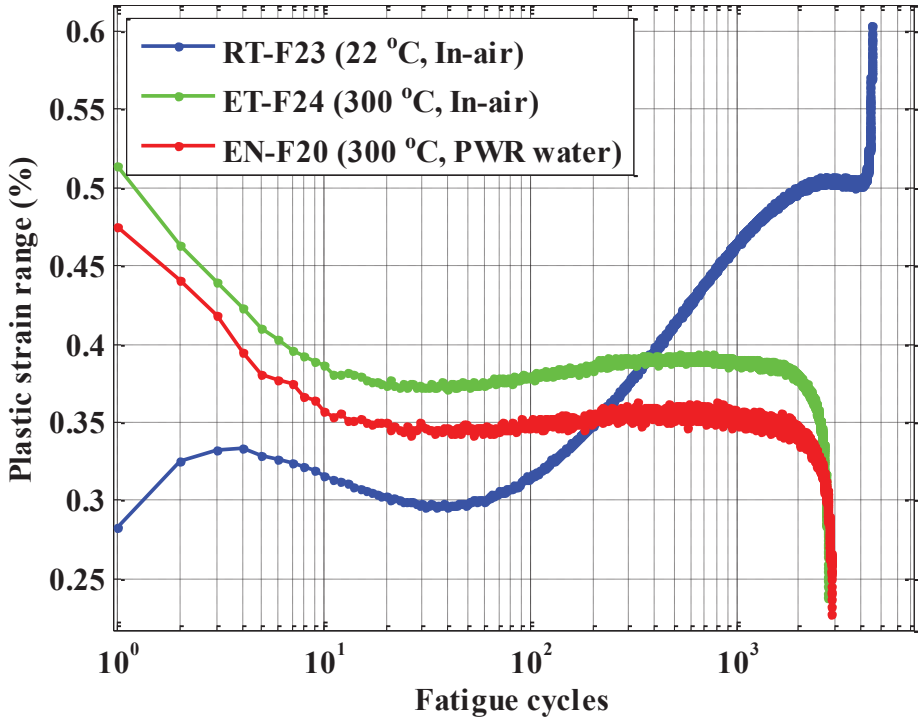

Figure 5. 18 Plastic strain range for 508 LAS base metal specimens fatigue tested under different conditions.

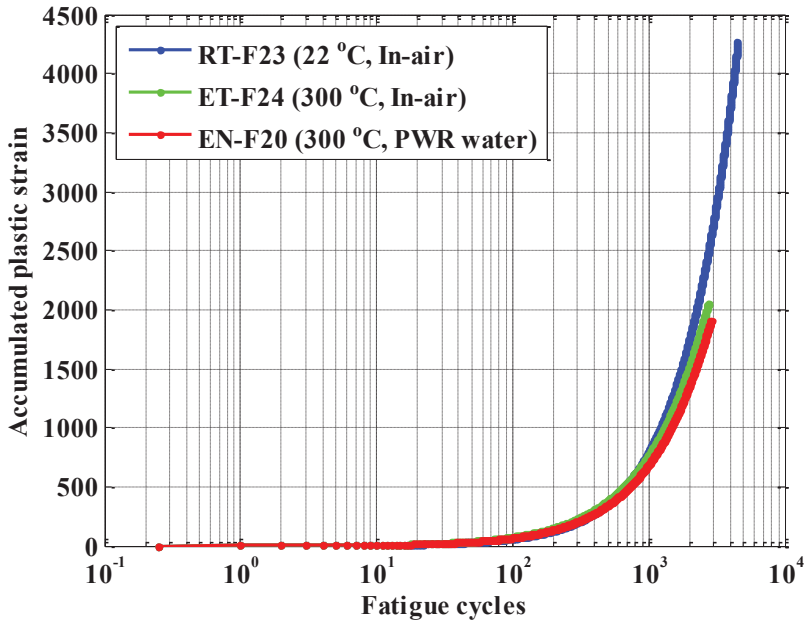

Figure 5. 19 Accumulated plastic strain for 508 LAS base metal specimens fatigue tested under different conditions.

5.4 Elastic Limit Stress and Kinematic Hardening Parameters for 508 LAS Base Metal Fatigue Tests

Based on the estimated equivalent monotonic stress-strain curve, we estimated the cyclic evolution of elastic limit stress for different test conditions (Table 5.1). These elastic limit stresses can be used as the yield stress in a FE code to model the isotropic hardening stress. However, the corresponding kinematic hardening parameters have to be used to model the kinematic hardening stress. Using the cyclic elastic limit stress, we estimated the corresponding cycle kinematic hardening parameters from the procedure discussed in Section 2.3. Both linear and nonlinear kinematic hardening parameters were estimated for individual fatigue cycles. Figure 5.20 shows the elastic limit stress curves under different test conditions. The curves show a substantial cyclic variation of elastic limit stress in the room temperature fatigue tests compared to the 300 °C in-air and PWR fatigue tests. Figure 5.21 shows the time history of the linear kinematic parameter (C1) based on the elastic limit stress line under different test conditions, and Figures 5.22 and 5.23 show the time histories of the nonlinear kinematic parameters (C1 and γ1) under different test conditions, respectively. Table 5.2 shows the material model parameters (elastic limit stress used as yield limit stress) for selected fatigue cycles and their comparison with tensile test parameters.

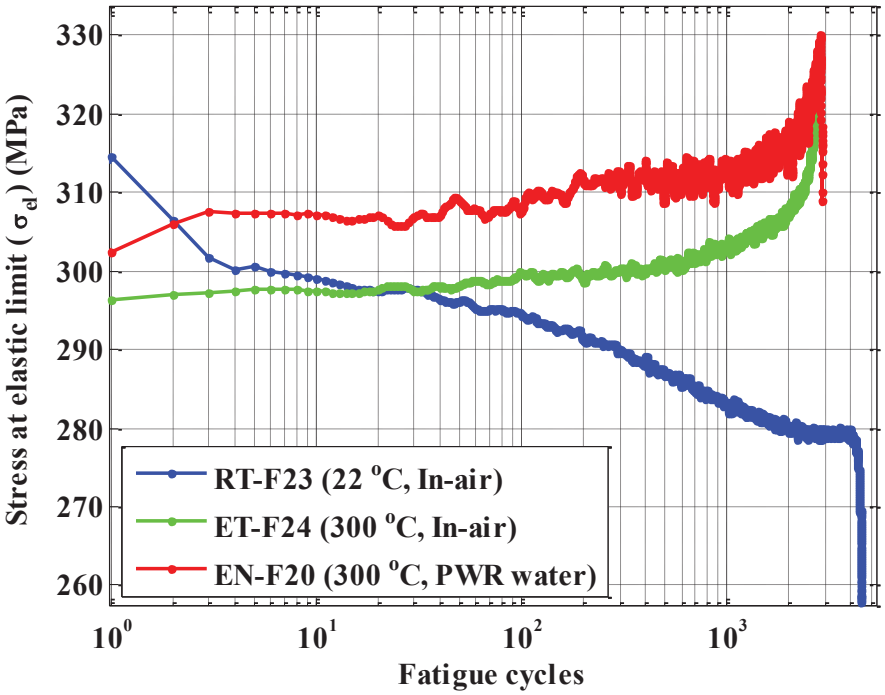

Figure 5. 20 Elastic limit stress for 508 LAS base metal specimens fatigue tested under different conditions.

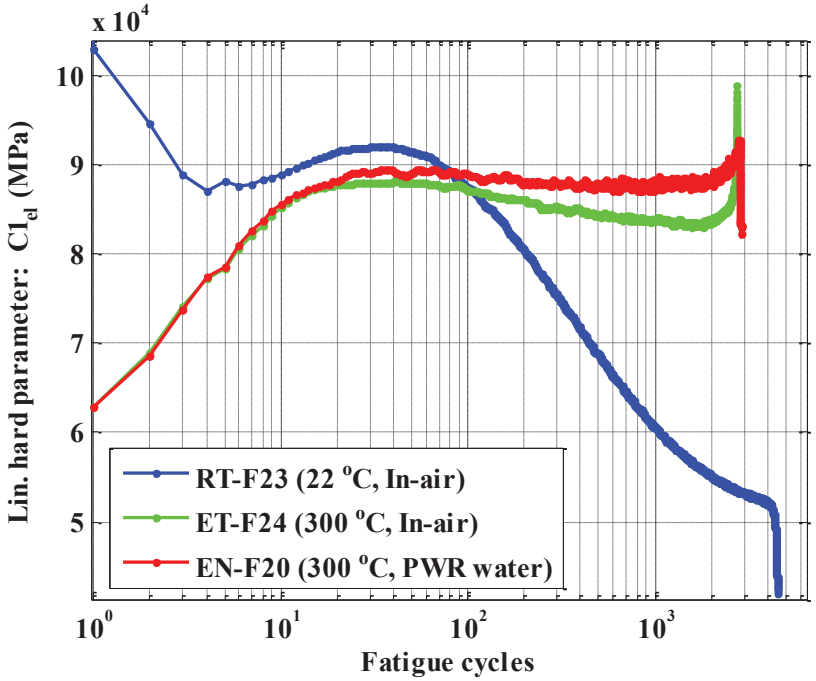

Figure 5. 21 Linear kinematic hardening parameter C1 (elastic limit stress used as yield stress) for 508 LAS base metal specimens fatigue tested under different conditions.

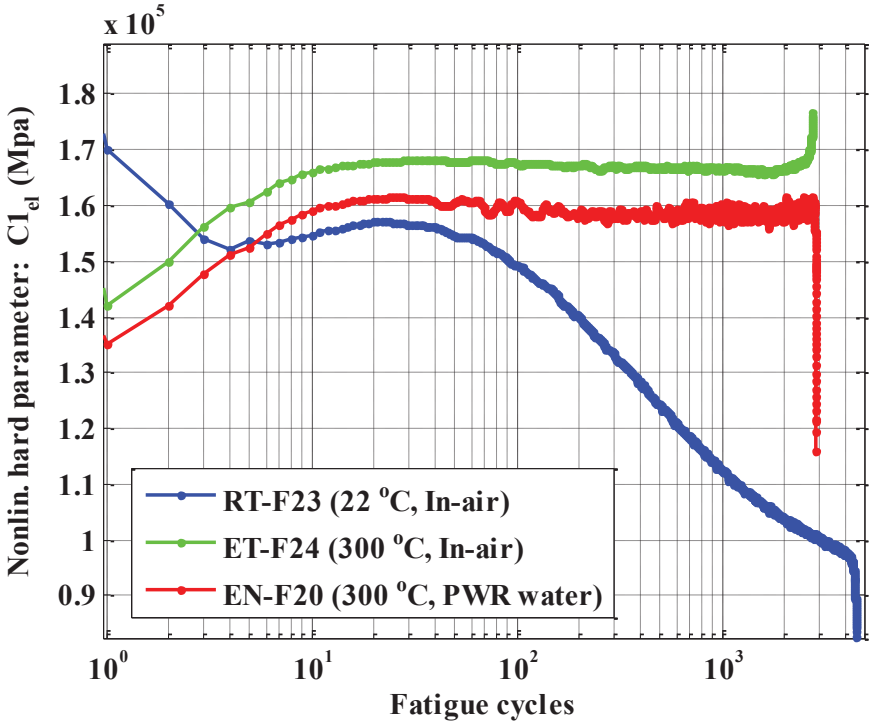

Figure 5. 22 Nonlinear kinematic hardening parameter C1 (elastic limit stress used as yield stress) for 508 LAS base metal specimens fatigue tested under different conditions.

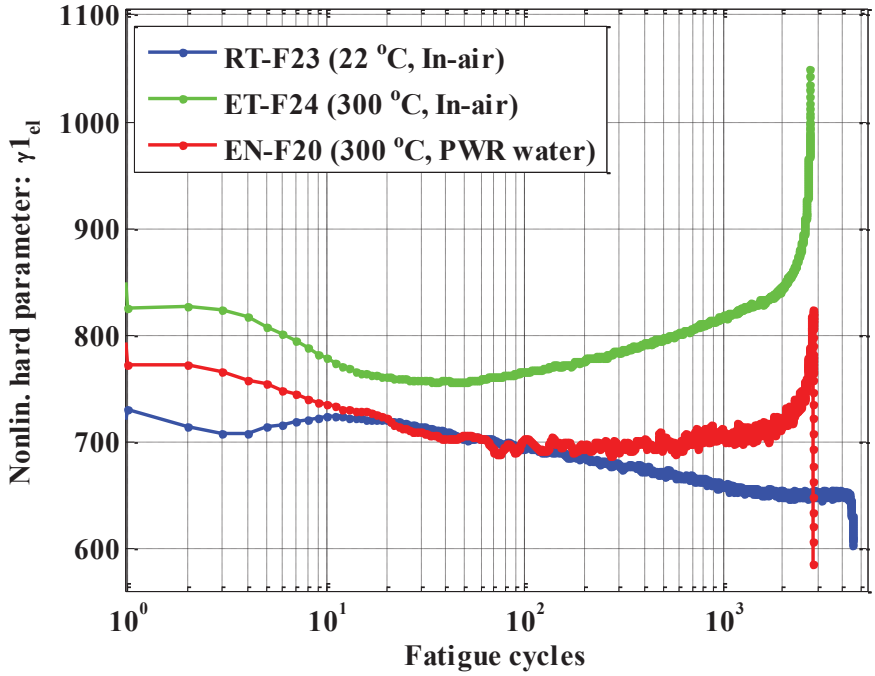

Figure 5. 23 Nonlinear kinematic hardening parameter γ1 (elastic limit stress used as yield stress) for 508 LAS base metal specimens fatigue tested under different conditions.

Table 5. 2 Material model parameters (elastic limit stress as yield limit stress) for 508 LAS base metal specimens, at selected fatigue cycles and comparison with tensile test parameters.

Tensile test or fatigue test cycle no.		Env. type	E (GPa)	σ_{EL} (MPa)	Lin. Model C_1 (MPa)	Nonlin. Model C_1 (MPa)	Nonlin. Model γ_1 (MPa)
Tensile tests (T06, and T08 data)		RT	209.19	424.45	2357.5	1065.6	102.91
		ET	197.57	391.01	9319	20090	131.34
Selected fatigue cycles (RT-F23, ET-F24, and EN-F20)	Cy=1	RT	211.16	314.54	1.03e+05	1.7017e+05	731.18
		ET	193.99	296.21	62935	1.4201e+05	825.36
		EN	184.51	302.36	62835	1.3503e+05	772.36
	Cy=20	RT	199.94	297.44	91510	1.5706e+05	720.66
		ET	196.57	297.61	87732	1.6776e+05	760.99
		EN	187.61	307.07	88255	1.6115e+05	722.23
	Cy=40	RT	199.5	296.41	91982	1.5607e+05	709.93
		ET	196.54	297.95	88114	1.681e+05	757.31
		EN	187.07	307.04	89298	1.6067e+05	703.43
	Cy=N/4 for RT-F23=1123, ET-F24=688, and EN-F20=719	RT	195.98	282.35	59369	1.1058e+05	656.35
		ET	199.39	301.68	83909	1.6658e+05	804.9
		EN	190.82	311.95	87960	1.5928e+05	706.41
	Cy=N/2 for RT-F23= 2247, ET-F24= 1375, and F20= 1438	RT	196.25	279.99	54361	1.0276e+05	652.12
		ET	201.61	304.83	83549	1.6603e+05	828.18
		EN	190.18	311.93	88560	1.5932e+05	705.69
	Cy=3N/4 for RT-F23= 3370, ET-F24= 2063, and EN-F20= 2156	RT	197.08	279.27	52893	99119	651.29
		ET	203.76	307.88	84006	1.669e+05	849.14
		EN	194.95	318.61	88643	1.5877e+05	726.76

* RT, ET, and EN symbolize room temperature, elevated temperature, and PWR environment, respectively.

5.5 Comparison of 0.05% Offset Yield Limit Stress and Kinematic Hardening Parameters for 508 LAS Base Metal Fatigue Tests

In addition to time histories for the elastic limit stress time-histories, curves for the 0.05% offset yield limit stress were estimated for different test conditions (Table 5.1). The results are shown in Figure 5.24. Figure 5.25 shows the time histories for the linear kinematic hardening parameter (C1), and Figures 5.26 and 5.27, those for the nonlinear kinematic hardening parameter (C1 and γ1) under different conditions. In addition, Table 5.3 shows material model parameters (0.05% offset strain stress used as yield limit stress) at selected fatigue cycles. For comparison, the tensile test parameters are also displayed.

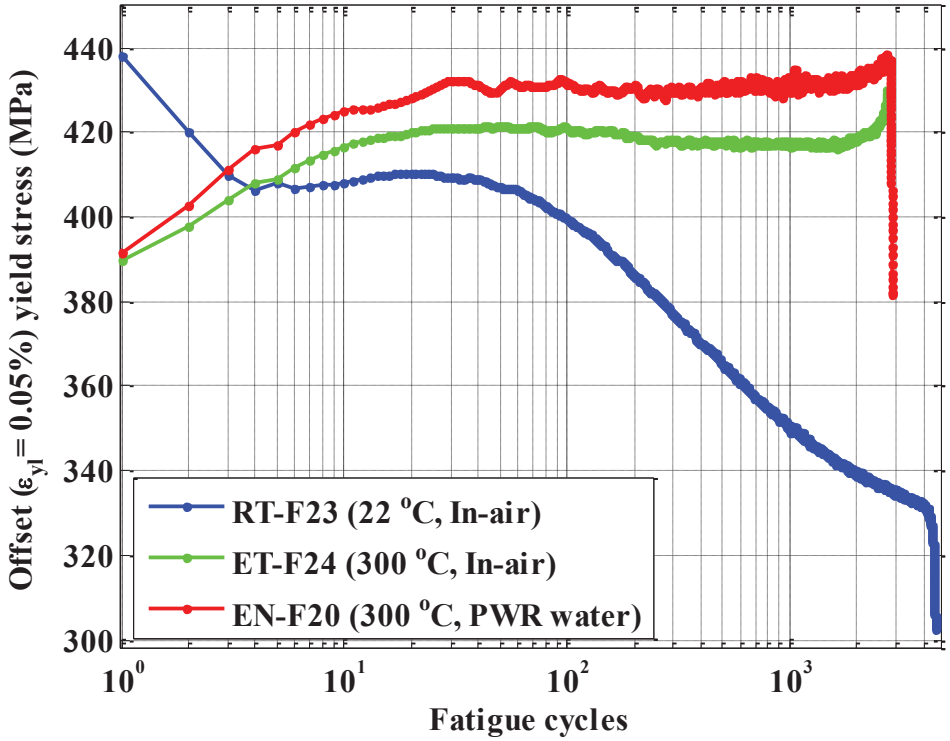

Figure 5. 24 Offset-strain (0.05%) yield limit stress for 508 LAS base metal specimens fatigue tested under different conditions.

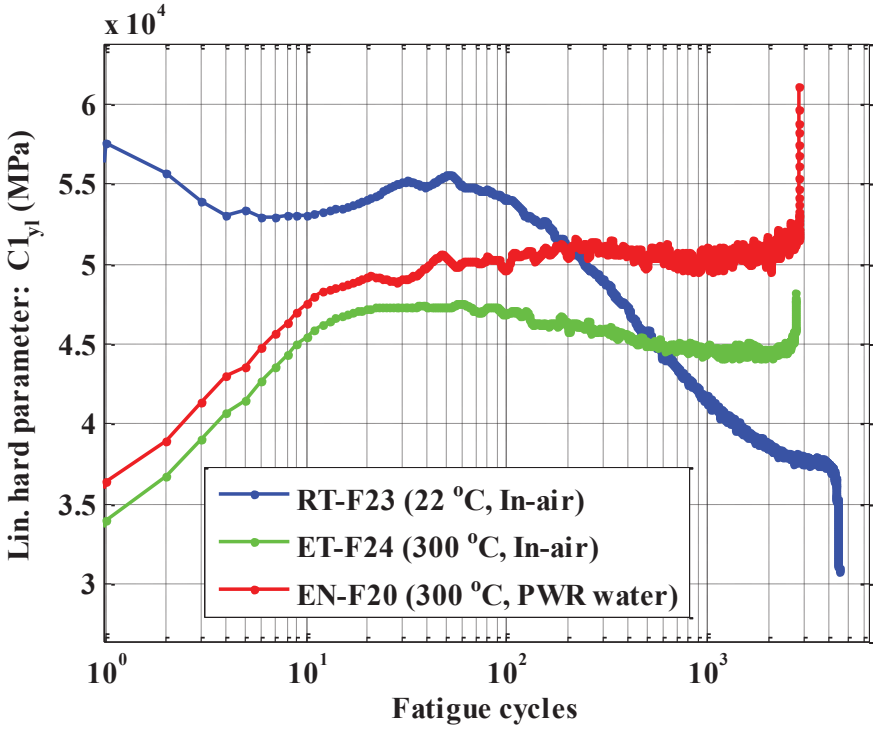

Figure 5. 25 Linear kinematic hardening parameter C1 (0.05% offset strain stress used as yield stress) for 508 LAS base metal specimens fatigue tested under different conditions.

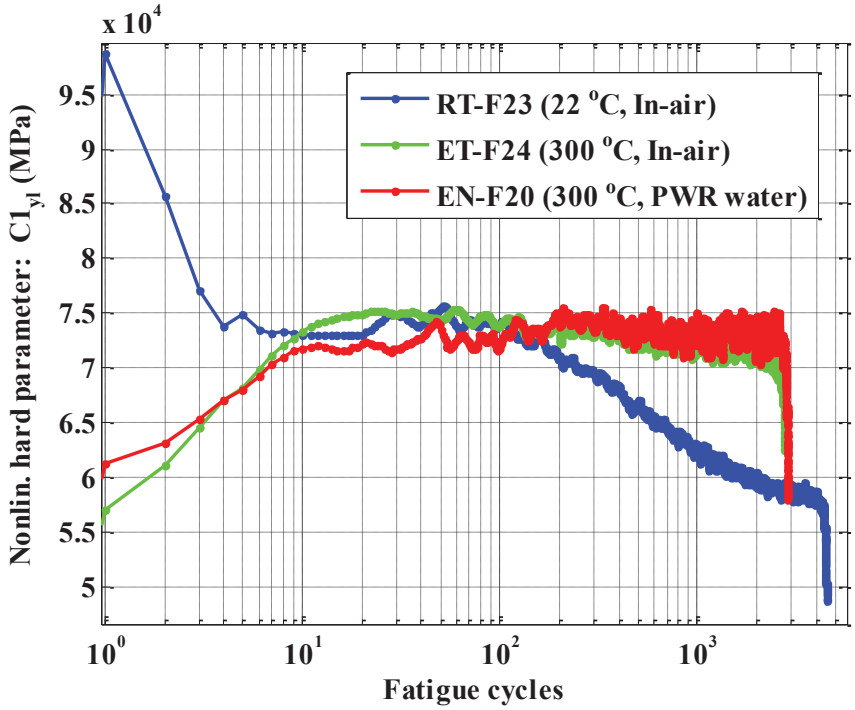

Figure 5. 26 Nonlinear kinematic hardening parameter C1 (0.05% offset strain stress used as yield stress) for 508 LAS base metal specimens fatigue tested under different conditions.

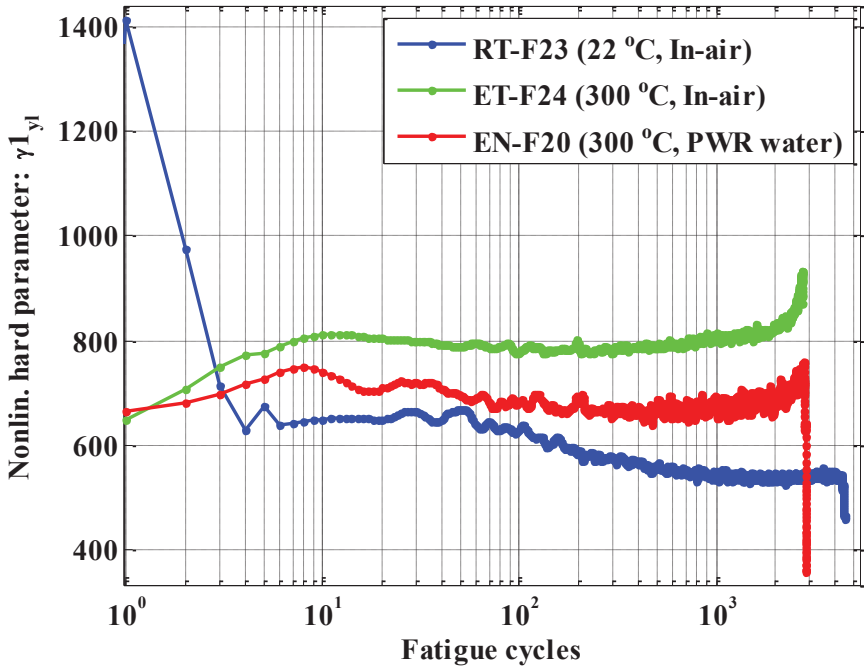

Figure 5. 27 Nonlinear kinematic hardening parameter γ 1 (0.05% offset strain stress used as yield stress) for 508 LAS base metal specimens fatigue tested under different conditions.

Table 5. 3 Material model parameters (0.05% offset strain stress used as yield limit stress) for 508 LAS base metal specimens, at selected fatigue cycles and comparison with tensile test parameters.

Tensile test or fatigue test cycle no.		**Env. type**	**E (GPa)**	**σ_{YL} (MPa)**	**Lin. Model C_1 (MPa)**	**Nonlin. Model C_1 (MPa)**	**Nonlin. Model γ_1 (MPa)**
Tensile tests (T06, and T08 data)		RT	209.19	427.31	2642.2	2150.4	-13.087
		ET	197.57	415.15	5607.2	10699	49.624
Selected fatigue cycles (RT-F23, ET-F24, and EN-F20)	Cy=1	RT	211.16	437.9	57637	98625	1411.5
		ET	193.99	389.88	34002	56965	649.24
		EN	184.51	391.55	36371	61236	666.75
	Cy=20	RT	199.94	410.48	54015	73064	649.53
		ET	196.57	419.99	47176	74922	804.33
		EN	187.61	428.29	49190	72211	709.58
	Cy=40	RT	199.5	408.97	54919	73951	649.12
		ET	196.54	421.19	47378	74752	792.61
		EN	187.07	431.11	49820	72676	708.44
	Cy=N/4 for RT-F23=1123, ET-F24=688, and EN-F20=719	RT	195.98	347.7	41076	62681	551.96
		ET	199.39	417.65	44622	71679	793.59
		EN	190.82	430.71	50559	73033	657.99
	Cy=N/2 for RT-F23= 2247, ET-F24= 1375, and F20= 1438	RT	196.25	338.37	38164	59082	537.76
		ET	201.61	416.82	44669	71618	809.75
		EN	190.18	432.1	50740	72998	675.49
	Cy=3N/4 for RT-F23= 3370, ET-F24= 2063, and EN-F20= 2156	RT	197.08	333.7	37676	58177	538.05
		ET	203.76	418.8	44547	70968	827.15
		EN	194.95	433.17	51357	74774	719.96

* RT, ET, and EN symbolize room temperature, elevated temperature, and PWR environment, respectively.

6 Results of 316 SS - 316 SS Similar Metal Tensile Test and Material Model

Tensile tests were earlier conducted using 316 SS-316 SS weld specimens and the related stress-strain curves and tensile properties were estimated [18]. Those tensile data have been further analyzed to estimate kinematic hardening parameters. These parameters can be used for developing FE component models with time-independent models of kinematic hardening. Also, these parameters can be compared with corresponding cyclic test parameters. The following sections summarize the test conditions, stress-strain data, tensile properties, and kinematic hardening material parameters.

6.1 Test Conditions for Tensile Test of 316 SS-316 SS Weld Specimens

Two 316 SS-316 SS weld specimens (T03 and T05) were tensile tested. Table 6.1 shows the test conditions. The main tensile test for T05 was conducted under isothermal conditions with gauge area temperature of 300 ^{o}C. Before starting the main tensile test under strain control, the specimen was heated up from room temperature to the gauge area temperature of 300 ^{o}C. Then, the temperature was allowed to stabilize for 2-3 hours before starting the main tensile test. After the main tensile test, the temperature was reduced back to room temperature.

Figure 6.1 shows example thermocouple (instrumented to specimen and pull rods) readings during the entire tensile test. Figure 6.2 is a magnified version of Figure 6.1, showing the gauge-center thermocouple readings. During heatup, the frame was operated under stress control with the aim of achieving approximately zero stress in the specimen. Figure 6.3 shows the nearly zero stress history during heatup. During heatup we also measured the gauge area strain to estimate the thermal strain under free thermal expansion (or zero stress). Figure 6.4 shows the free expansion thermal strain history during heatup and indicates that the thermal strain is approximately 0.53% at 300 ^{o}C. A reactor component (e.g., reactor internals) with 316 SS-316 SS weld could experience similar thermal strain unless it is restrained. If the component is restrained 0.53%, thermal strain can create substantial stress (beyond yield stress) in the component. Hence, this result is worth reporting, although it is irrelevant for the present isothermal condition tensile test.

Table 6. 1 Test conditions for 508 LAS base and HAZ metal tensile tests.

Test ID	Material type	Test Condition
T03	316 SS-316 SS similar metal weld	In air-22 ^{o}C, strain control, strain rate=0.1%/s
T05	316 SS-316 SS similar metal weld	In air-300 ^{o}C, strain control, strain rate=0.1%/s

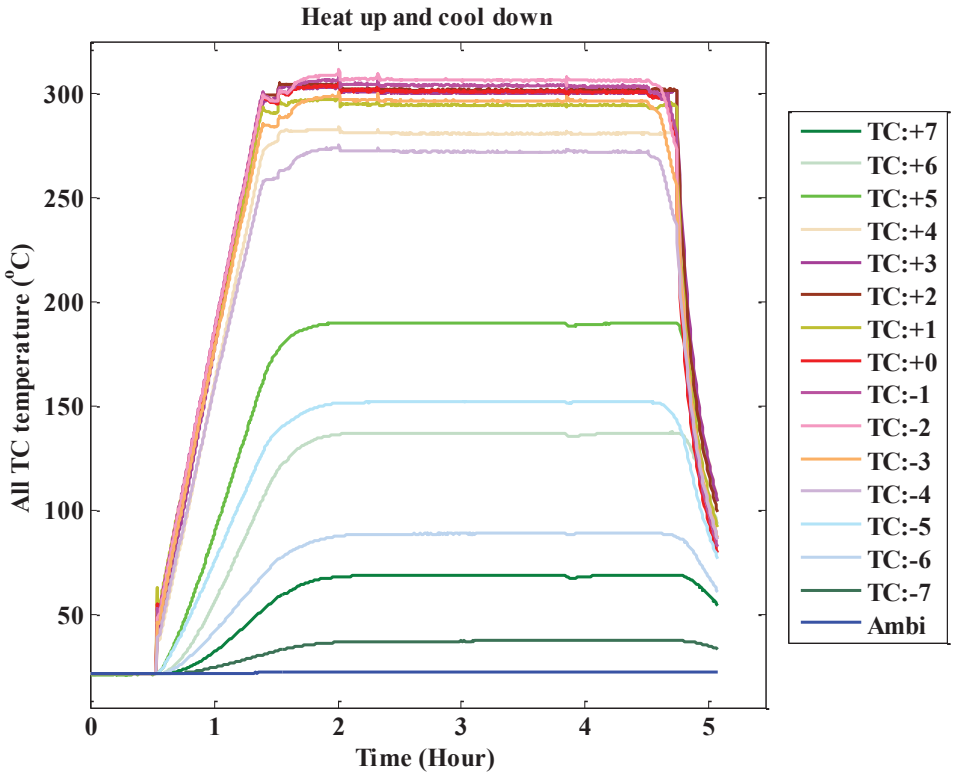

Figure 6. 1 Example temperature histories (measured through different thermocouples) during heatup, temperature stabilization, main tensile test, and cooldown for a 316 SS-316 SS weld specimen (Test T05).

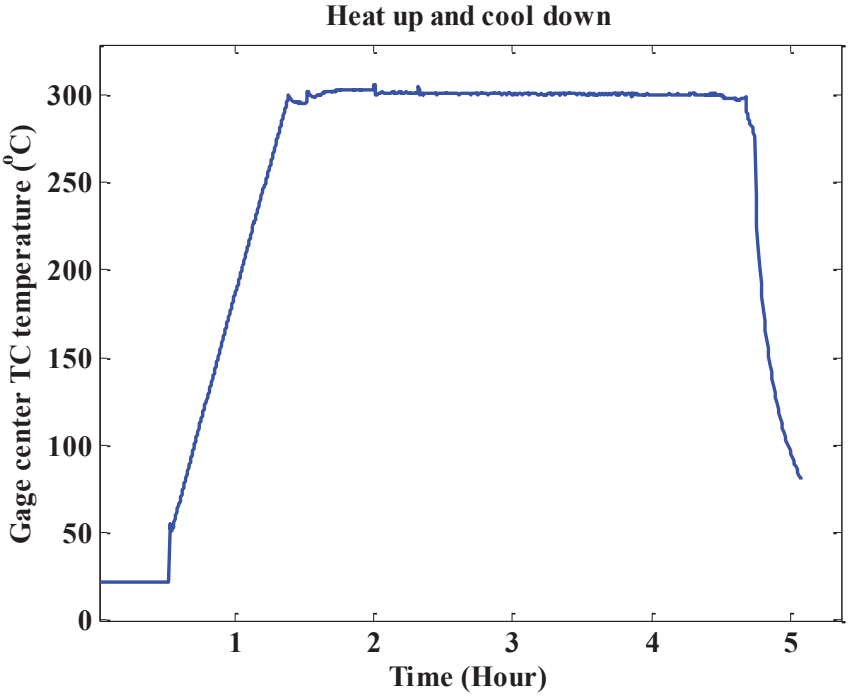

Figure 6. 2 Magnified version of Figure 6.1 showing temperature measured at gauge-center thermocouple.

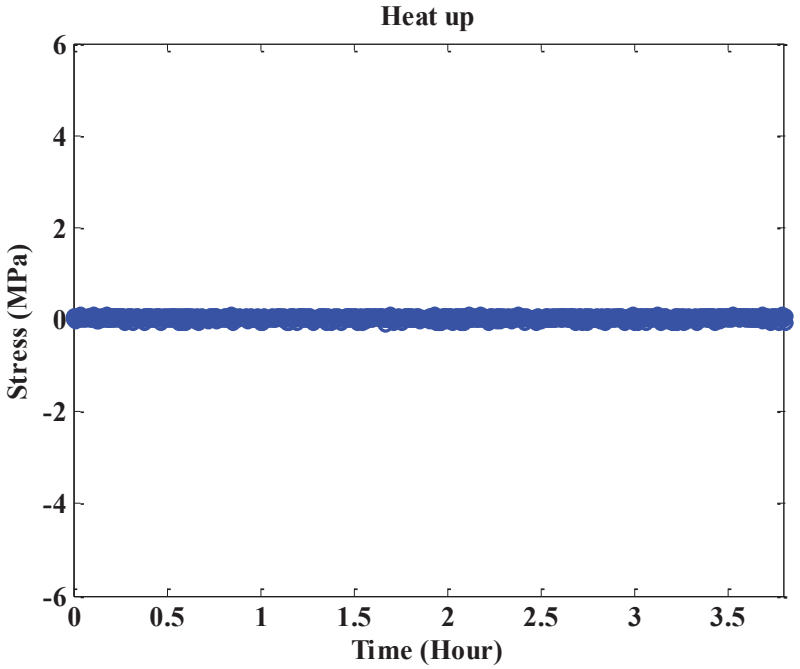

Figure 6. 3 Example stress history during only heatup and temperature stabilization for a 316 SS-316 SS weld specimen (Test T05).

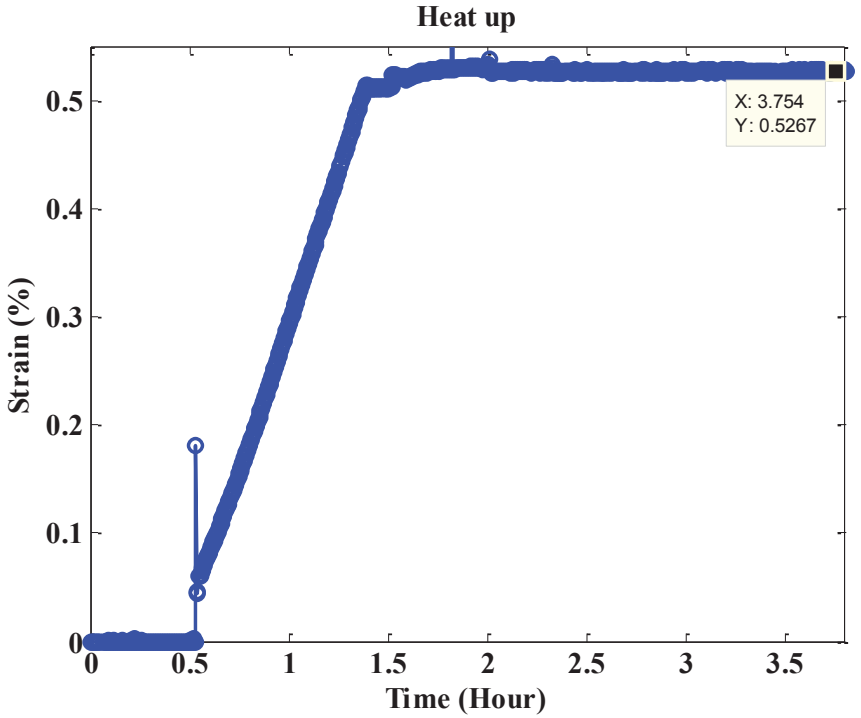

Figure 6. 4 Example strain history during only heatup and temperature stabilization for a 316 SS-316 SS weld specimen (Test T05).

6.2 Estimated Stress-Strain Curves for 316 SS-316 SS Similar Metal Welds

Engineering stress-strain curves at room temperature and at 300 °C are shown in Figure 6.5. The corresponding true stress-strain curves (up to ultimate strain) are shown Figure 6.6. Figure 6.5 shows that the ultimate and fracture strains of 316 SS-316 SS weld at 300 °C are almost half of their corresponding values at room temperature.

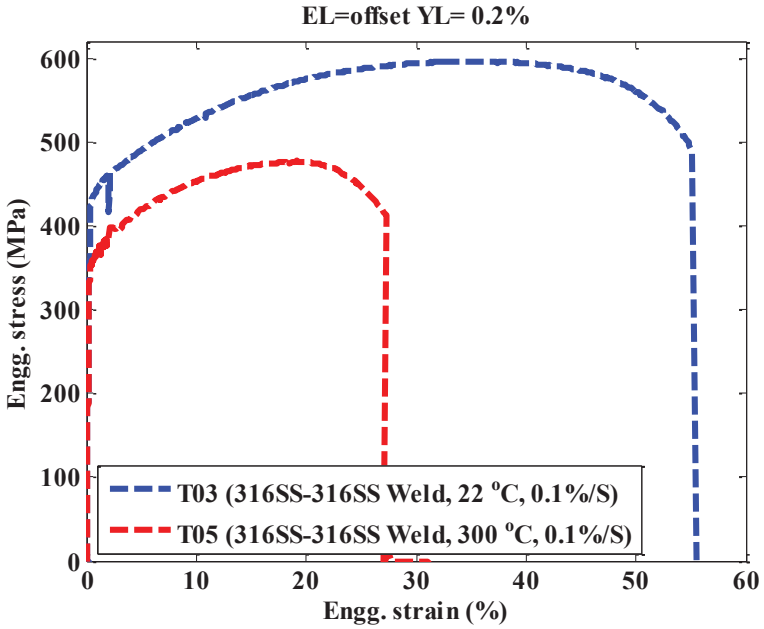

Figure 6. 5 Engineering stress-strain curves estimated from tensile test data of 316 SS-316 SS weld specimens, which were tensile tested at room temperature and 300 °C.

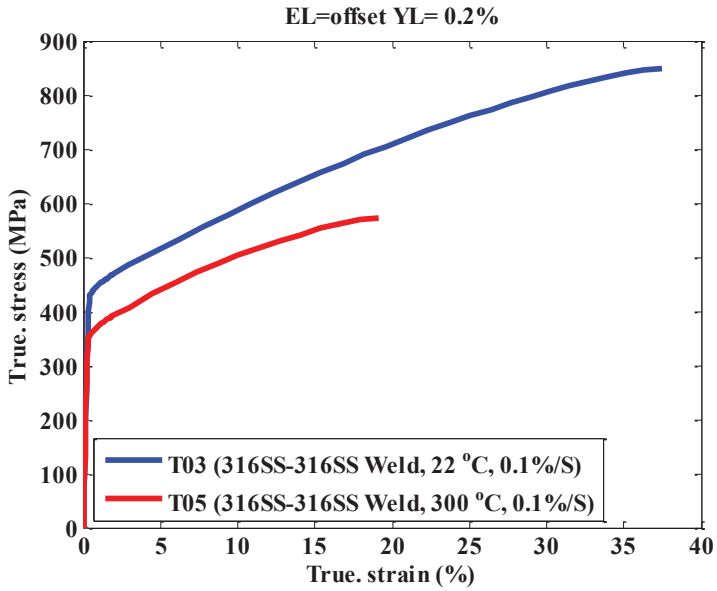

Figure 6. 6 True stress-strain curves (up to ultimate strain) estimated from tensile test data of 316 SS-316 SS weld specimens, which were tensile tested at room temperature and 300 °C.

6.3 Estimated Tensile Test and Kinematic Hardening Properties for 316 SS-316 SS Welds

Using the above stress-strain data, the tensile properties (e.g., elastic modulus, elastic and yield limit stress, ultimate and fracture stress/strain, and reduction in gauge area) were estimated for 316 SS-316 SS welds at room temperature and 300 ^{o}C. The related results are reported in Tables 6.2 to 6.6. In addition, based on the procedure discussed in Section 2.3 (Eqs. 2.3 to 2.20), the related kinematic hardening parameters were estimated for different yield limit stresses. Table 6.3 shows the linear and nonlinear kinematic hardening parameters, estimated by assuming that the elastic limit stress is the yield limit stress. Tables 6.4, 6.5, and 6.6 show the linear and nonlinear kinematic hardening parameters, estimated by assuming offset yield limit stresses of 0.05%, 0.1%, and 0.2%, respectively. These parameters can be used for developing simplified component-level FE models for elastic-plastic cyclic stress. In addition, these parameters can be compared with corresponding fatigue test parameters to perform a parametric study on component-level stress analysis and fatigue life evaluation.

Table 6. 2 Estimated tensile test material properties for 316 SS-316 SS weld specimens, which were tensile tested under different conditions.

Tensile test properties		**T03 (316 SS-316 SS Weld, 22 ^{o}C, 0.1%/s)**	**T05 (316 SS-316 SS Weld, 300 ^{o}C, 0.1%/s)**
Elastic modulus (GPa)		131.93	130.66
Reduction in gauge area (%)		62.207	44.693
Ultimate	Stress (MPa)	596.11	476.97
	Strain (%)	36.523	19.164
Fracture	Stress (MPa)	485.9	413.1
	Strain (%)	55.11	27.24

Table 6. 3 Estimated (or assumed) elastic limit and associated kinematic hardening properties for 316 SS-316 SS weld specimens, which were tensile tested under different conditions.

Elastic limit and kinematic hardening properties (up to 2% true total strain)		**T03 (316 SS-316 SS Weld, 22 ^{o}C, 0.1%/s)**	**T05 (316 SS-316 SS Weld, 300 ^{o}C, 0.1%/s)**
Assumed elastic limit	Stress (MPa)	371.08	320.85
	Strain (%)	0.2918	0.2572
Lin./Nonlin. kinematic hardening parameter	Lin. C1 (MPa)	7523	5531.6
	Nonlin. C1 (MPa)	43190	21913
	Nonlin. γ1	501.26	369.61

Table 6. 4 Estimated 0.05% offset yield limit and associated kinematic hardening properties for 316 SS-316 SS weld specimens, which were tensile tested under different conditions.

0.05% offset yield limit and kinematic hardening properties (up to 5% true total strain)		**T03 (316 SS-316 SS Weld, 22 °C, 0.1%/s)**	**T05 (316 SS-316 SS Weld, 300 °C, 0.1%/s)**
Estimated yield limit	Stress (MPa)	414.56	345.8
	Strain (%)	0.3649	0.31836
Lin./Nonlin. kinematic hardening parameter	Lin. C1 (MPa)	3223.3	2593.6
	Nonlin. C1 (MPa)	5749.7	4046.3
	Nonlin. γ1	65.753	40.831

Table 6. 5 Estimated 0.1% offset yield limit and associated kinematic hardening properties for 316 SS-316 SS similar weld specimens, which were tensile tested under different conditions.

0.1% offset yield limit and kinematic hardening properties (up to 5% true total strain)		**T03 (316 SS-316 SS Weld, 22 °C, 0.1%/s)**	**T05 (316 SS-316 SS Weld, 300 °C, 0.1%/s)**
Estimated yield limit	Stress (MPa)	424.39	350.43
	Strain (%)	0.4217	0.36878
Lin./nonlin. kinematic hardening parameter	Lin. C1 (MPa)	2653.2	2364.9
	Nonlin. C1 (MPa)	3937.5	3370
	Nonlin. γ1	40.737	31.039

Table 6. 6 Estimated 0.2% offset yield limit and associated kinematic hardening properties for 316 SS-316 SS weld specimens, which were tensile tested under different conditions.

0.2% offset yield limit and kinematic hardening properties (up to 5% true total strain)		**T03 (316 SS-316 SS Weld, 22 °C, 0.1%/s)**	**T05 (316 SS-316 SS Weld, 300 °C, 0.1%/s)**
Estimated yield limit	Stress (MPa)	431.2	355.96
	Strain (%)	0.5288	0.47395
Lin./nonlin. kinematic hardening parameter	Lin. C1 (MPa)	2320.5	2130.6
	Nonlin. C1 (MPa)	3127.1	2763.9
	Nonlin. γ1	29.278	21.711

7 Results of 316 SS-316 SS Similar Metal Fatigue Test and Material Model

We conducted fatigue tests using 316 SS-316 SS weld specimens under different test conditions. The resulting fatigue test data were analyzed to estimate the cyclic or time-dependent material parameters. The test conditions for the various tests and material parameter results are summarized below.

7.1 Test Conditions for 316 SS-316 SS Weld Fatigue Tests

Five fatigue tests were conducted using 316 SS-316 SS weld specimens (Figure 3.3). Out of the five fatigue tests, four were completely successful in terms of test data accuracy. Table 7.1 shows the associated test conditions for these fatigue experiments. Out of the four tests, two were strain controlled, and two were stroke controlled. For all the tests the aim was to maintain the gauge area strain amplitude equal to 0.5%. For the stroke control tests, the equivalent stroke input was selected based on the earlier tensile test results. For both the 300 ^{o}C in-air and PWR water conditions, we considered a stroke amplitude of 0.1944 mm. This value was selected based on the stroke versus strain data (Figure 7.1) estimated from test T05 (conducted at 300 ^{o}C and in-air condition).

Table 7. 1 Test conditions for 316 SS-316 SS weld fatigue tests.

Test ID	Material type	Test Condition
RT-F08	316 SS-316 SS weld	In air-22 ^{o}C, strain control, strain amplitude=0.5%, strain rate = 0.1%/s, cycle period = 20 s
ET-F07	316 SS-316 SS weld	In air-300 ^{o}C, strain control, strain amplitude=0.5%, strain rate = 0.1%/s, cycle period = 20 s
ET-F17	316 SS-316 SS weld	In air-300 ^{o}C, stroke control, stroke amplitude=0.1944 mm, stroke rate = 0.003888 mm/s, cycle period = 200 s
EN-F18	316 SS-316 SS weld	PWR water-300 ^{o}C, stroke control, stroke amplitude=0.1944 mm, stroke rate = 0.003888 mm/s, cycle period = 200 s Water chemistry: 1000 ppm B as H_3BO_3, 2 ppm Li^+ as LiOH, 20% H_2/bal. N_2 cover gas, and DO < 5 ppb

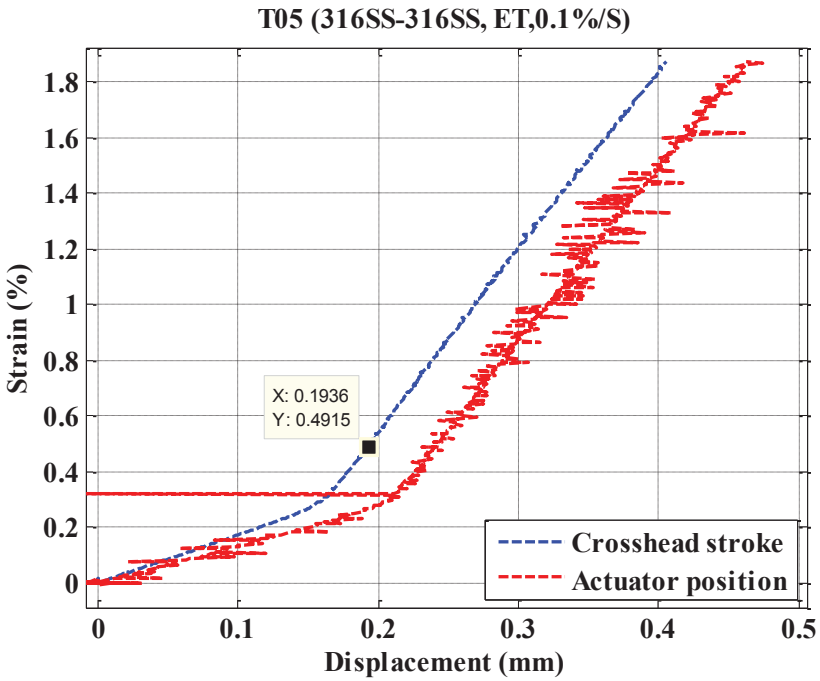

Figure 7. 1 Stroke versus strain data estimated from T05 (conducted at 300 °C and in-air condition for 316 SS-316 SS weld specimen) results.

7.2 Bulk Fatigue Life and Maximum/Minimum Stress Histories for 316 SS-316 SS Weld Specimens

The bulk fatigue lives under different test conditions are presented in Figure 7.2, which shows that the environment (both 300 °C in-air and PWR water) and test control method (stroke versus strain control) has a significant effect. The stroke-controlled ET-F17 specimen survived significantly fewer fatigue cycles compared to the strain-controlled ET-F07 specimen. This difference is due to the generation of a larger strain (in the ET-F17 specimen) compared to the intended strain amplitude of 0.5% (as in the ET-F07 specimen).

The ET-F07 test was conducted at 0.1%/s strain rate, whereas the ET-F17 test was conducted at 0.01%/s strain rate. However, we assume that, at the in-air condition, the strain rates do not have a significant effect on fatigue lives and other fatigue test parameters such as stress-strain behavior. Comparing the fatigue life of ET-F17 with that of EN-F18, although both tests were conducted under the same stroke amplitude and stroke rate and at 300 °C, we found that the life of the PWR water specimen (EN-F18) is almost half that of the in-air specimen (ET-F17). That means that the PWR environment has a significant effect on the bulk fatigue life of 316 SS-316 SS weld specimens, particularly at the chosen stroke rate of 0.003888 mm/s. Note that the equivalent approximate strain rate for both these test was 0.01%/s, with cyclic time period of 200 s.

The stress histories for all the above test cases were also compared. The corresponding maximum and minimum stress amplitudes are plotted in Figure 7.3. Figure 7.4 is a magnified version of Figure 7.3, showing only the maximum stress histories. This figure indicates that temperature has a more significant effect on stress amplitudes compared to test method, strain/stroke rate, and PWR water environment.

Figures 7.3 and 7.4 show that, for the initial 10-30 cycles, cyclic stress hardening and then softening are observed for all the test cases.

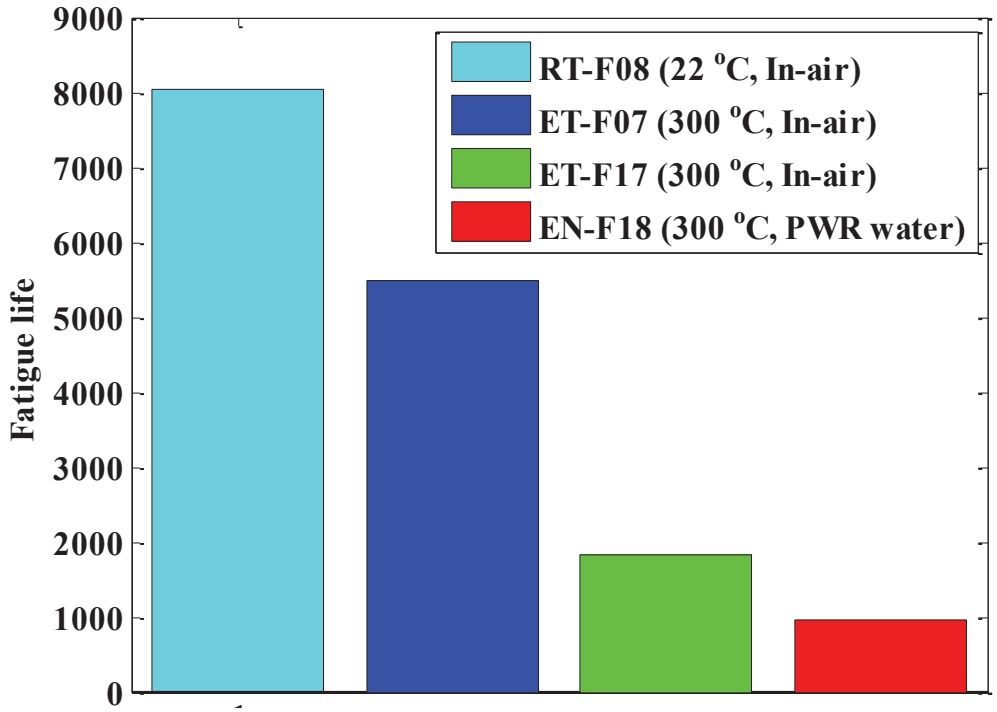

Figure 7. 2 Fatigue lives for 316SS-316SS weld specimens fatigue tested under different conditions.

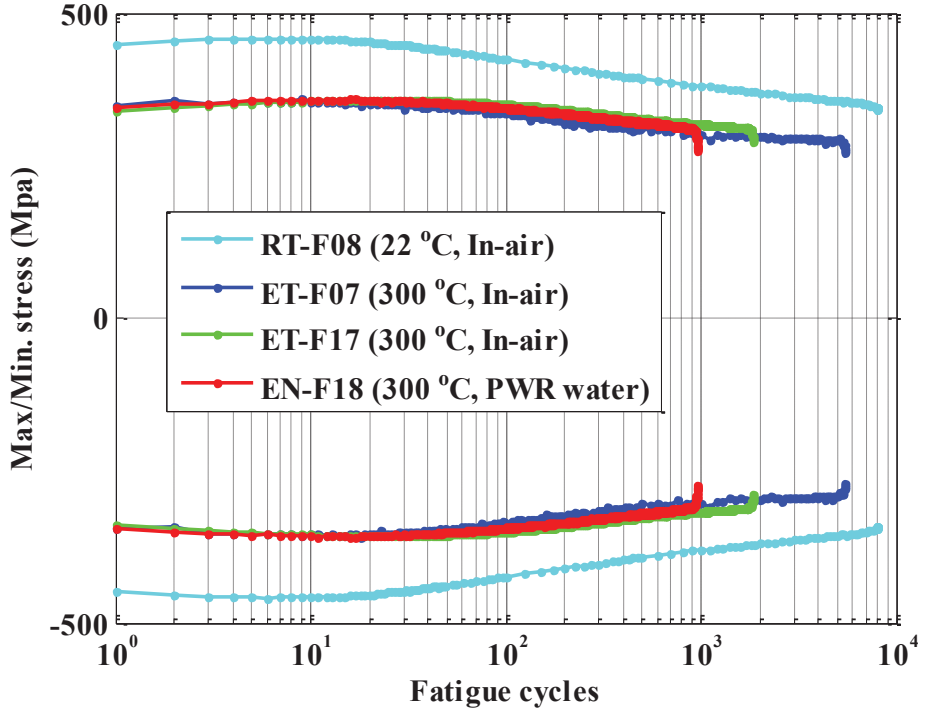

Figure 7. 3 Maximum and minimum stress for 316SS-316SS weld specimens fatigue tested under different conditions.

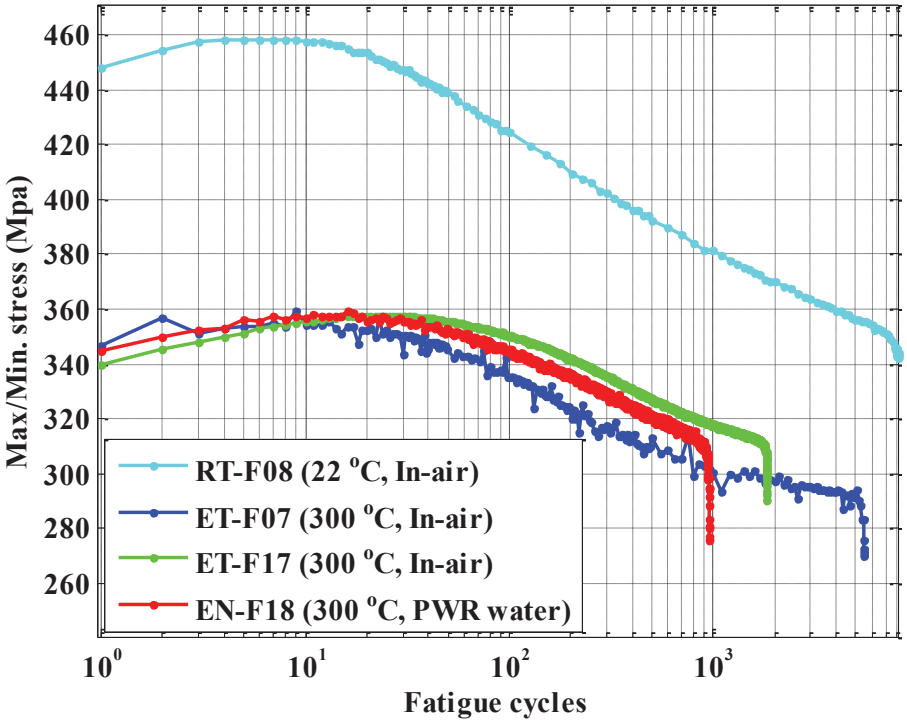

Figure 7. 4 Magnified version of Figure 7.3 showing level of cyclic stress hardening/softening in 316SS-316SS weld specimens under different conditions.

7.3 Elastic Modulus and Strain Range Histories for 316 SS-316 SS Welds

The cyclic stress-strain or hysteresis data generated through various test cases were converted to equivalent monotonic stress-strain curves for further data modeling. Figures 7.5 to 7.8, respectively, show the estimated equivalent monotonic stress-strain curves (first few cycles) for RT-F08, ET-F07, ET-F17, and EN-F18. In these figures, we have also plotted the tensile test stress-strain curves. These figures show the assumed elastic limit for various test cases. Based on the assumed elastic limit strain, the elastic portion of the equivalent monotonic stress-strain curves is selected to estimate the corresponding elastic moduli.

The elastic modulus time histories for the test cases can be seen in Figure 7.9, which indicates that temperature has a significant effect on the elastic modulus compared to other test variables such as test method (strain versus stroke control), environment (in-air versus PWR water), and stroke/strain rate. Using the cyclic stress-strain data and estimated elastic modulus, the cyclic elastic strain ranges were estimated from the cyclic total strain range. The corresponding cyclic plastic strain ranges were also estimated. Figures 7.10 to 7.12, respectively, show the total, elastic, and plastic strain range for all the test cases. Figure 7.13 shows the corresponding accumulated plastic strain for the test cases.

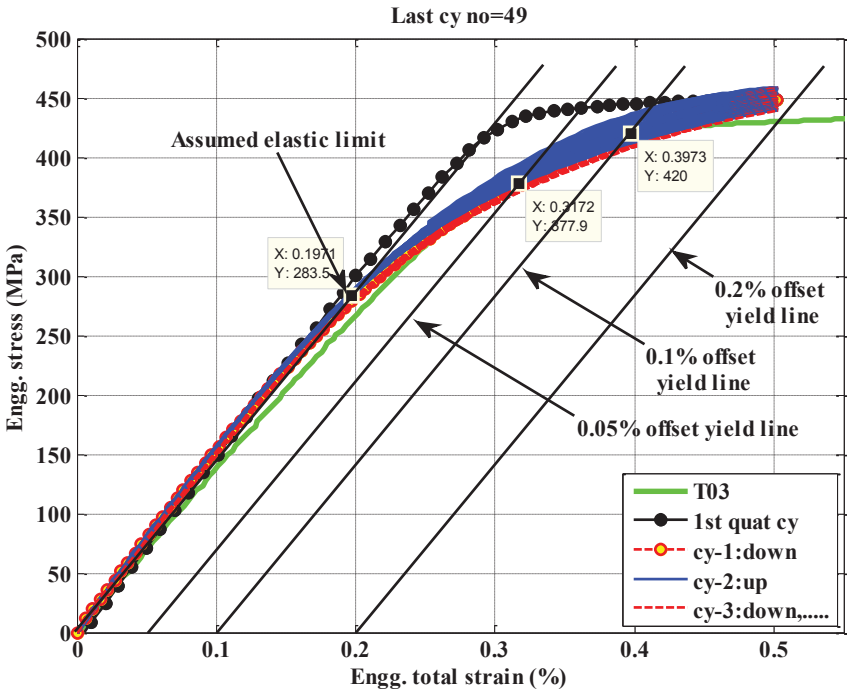

Figure 7. 5 Equivalent monotonic stress-strain curves estimated from upward/downward cycle (first 49 cycles) stress-strain data for ET-F08 fatigue test and T03 tensile test data. Also shown are the offset yield lines and elastic and yield limit stress.

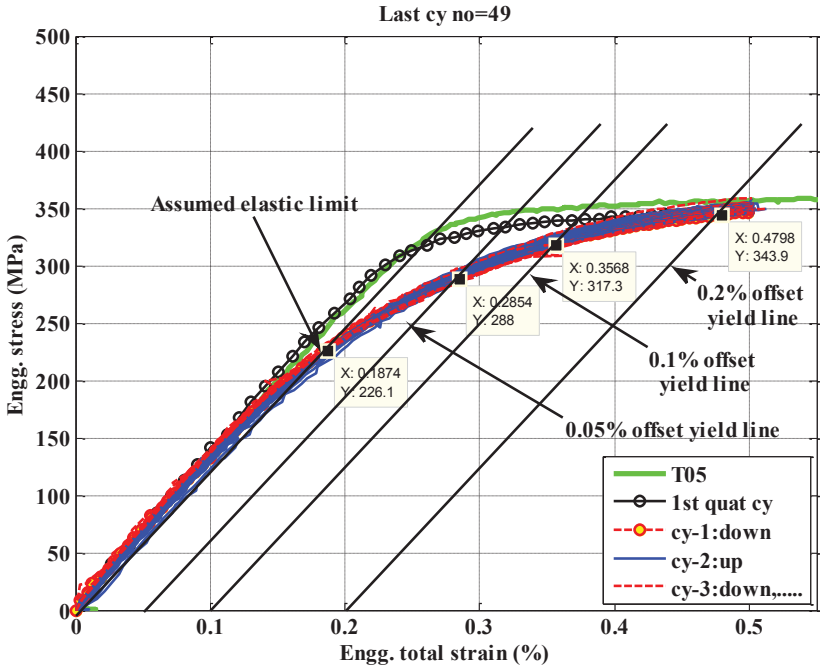

Figure 7. 6 Equivalent monotonic stress-strain curves estimated from upward/downward cycle (first 49 cycles) stress-strain data for ET-F07 fatigue test and T05 tensile test data. Also shown are various offset yield lines and the elastic and yield limit stress.

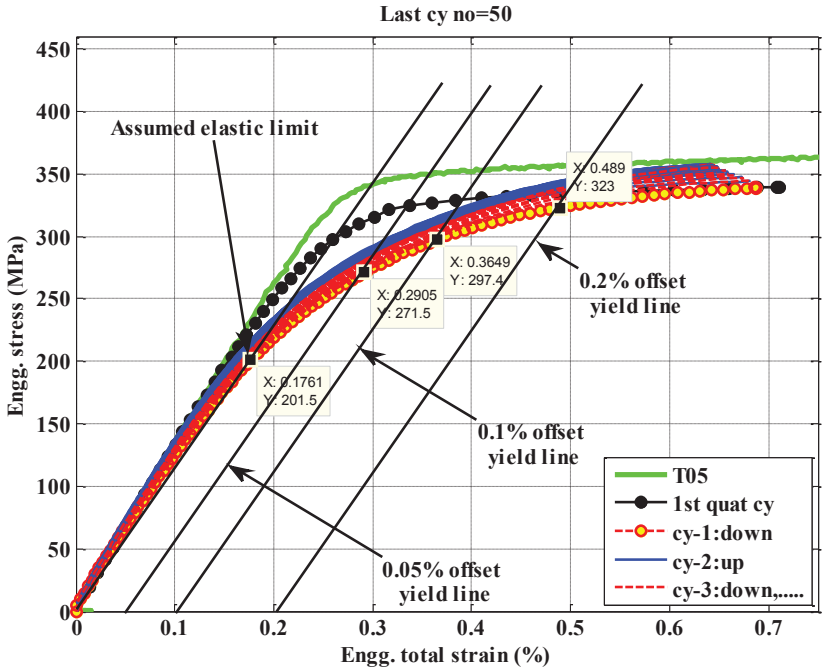

Figure 7. 7 Equivalent monotonic stress-strain curves estimated from upward/downward cycle (first 50 cycles) stress-strain data for ET-F17 fatigue test and T05 tensile test data. Also shown are various offset yield lines and the elastic and yield limit stress.

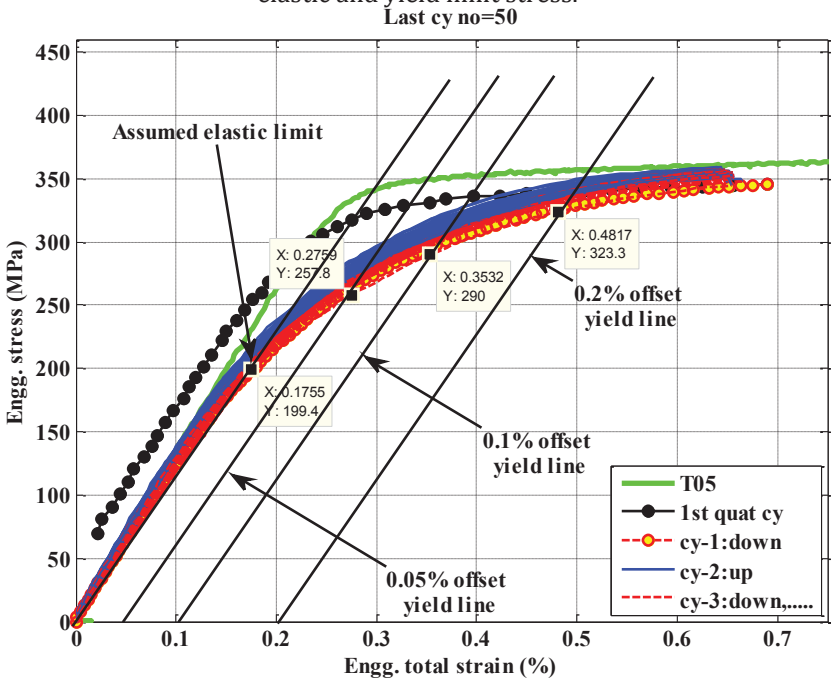

Figure 7. 8 Equivalent monotonic stress-strain curves estimated from upward/downward cycle (first 50 cycles) stress-strain data for EN-F18 fatigue test and T05 tensile test data. Also shown are various offset yield lines and elastic and yield limit stress.

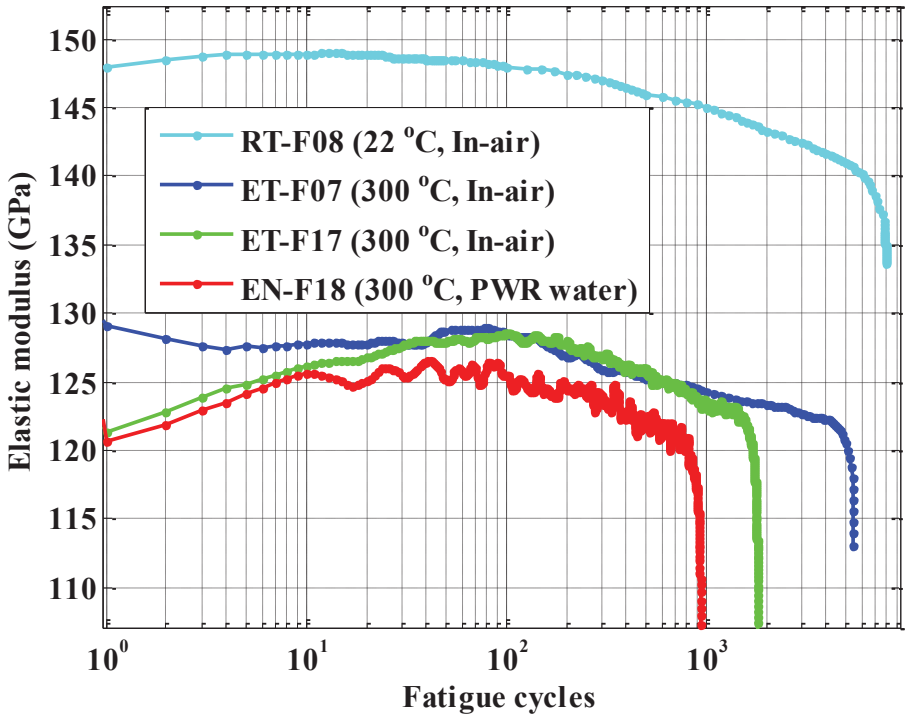

Figure 7. 9 Elastic modulus for 316SS-316SS weld specimens fatigue tested under different conditions.

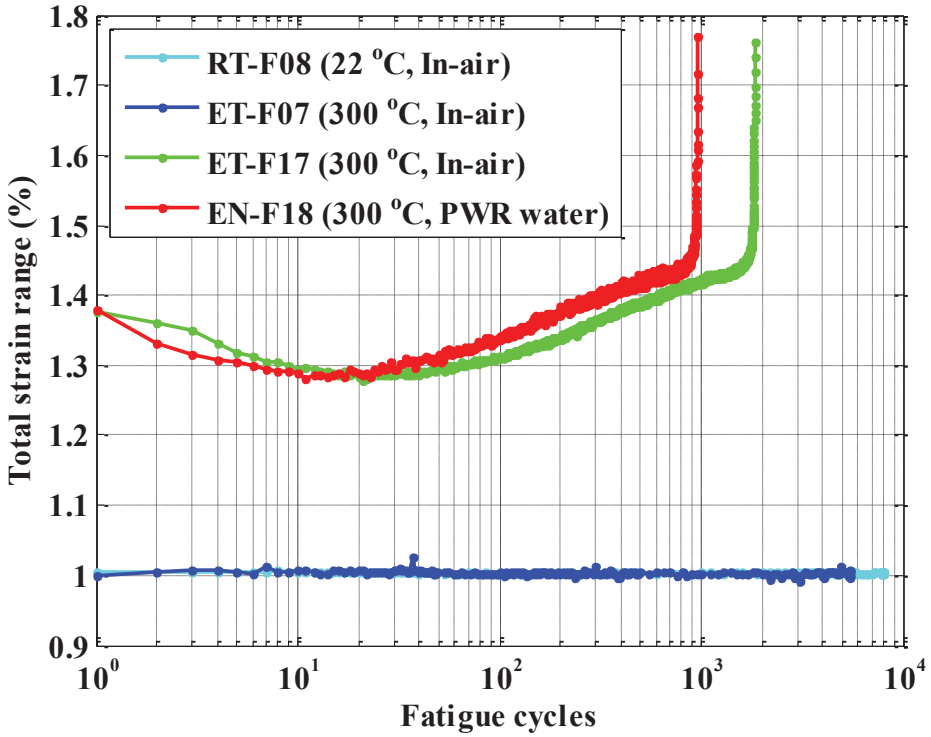

Figure 7. 10 Total strain range for 316SS-316SS weld specimens fatigue tested under different conditions.

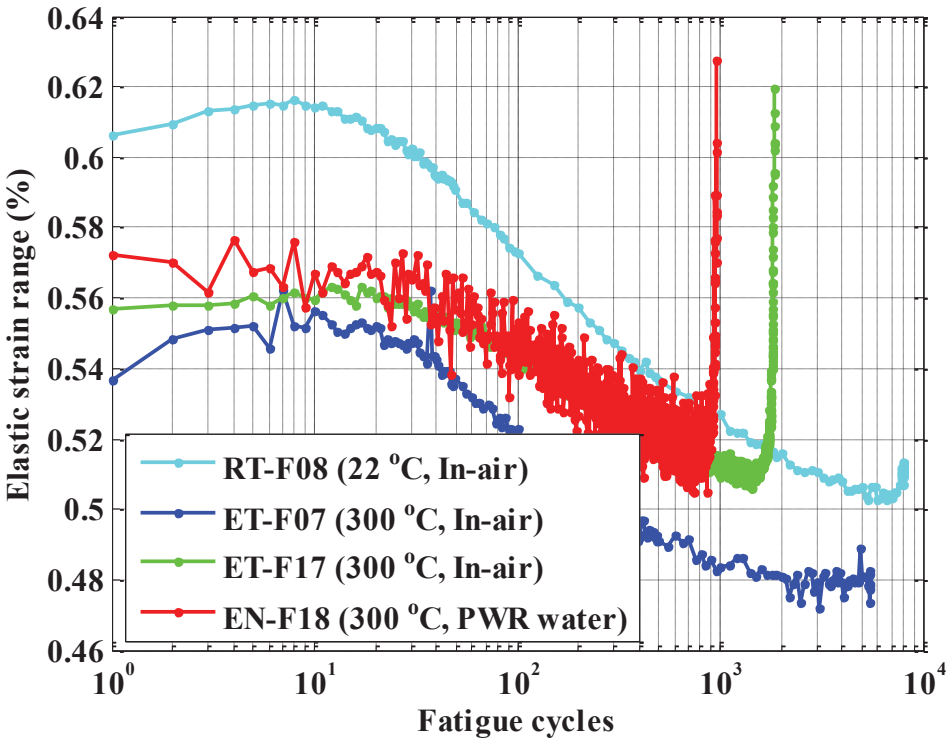

Figure 7. 11 Elastic strain range for 316SS-316SS weld specimens fatigue tested under different conditions.

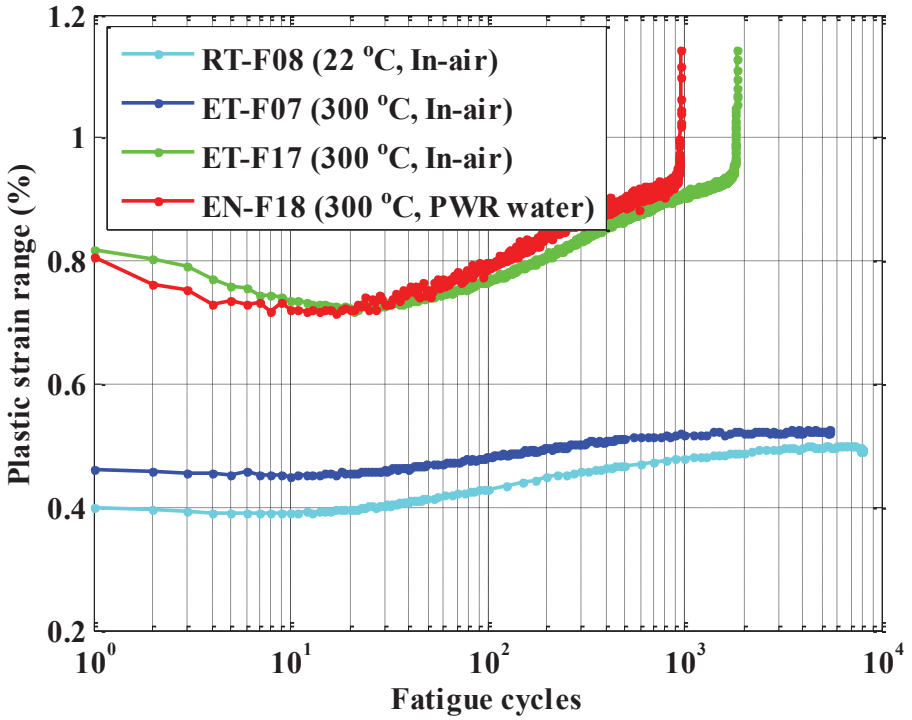

Figure 7. 12 Plastic strain range for 316SS-316SS weld specimens fatigue tested under different conditions.

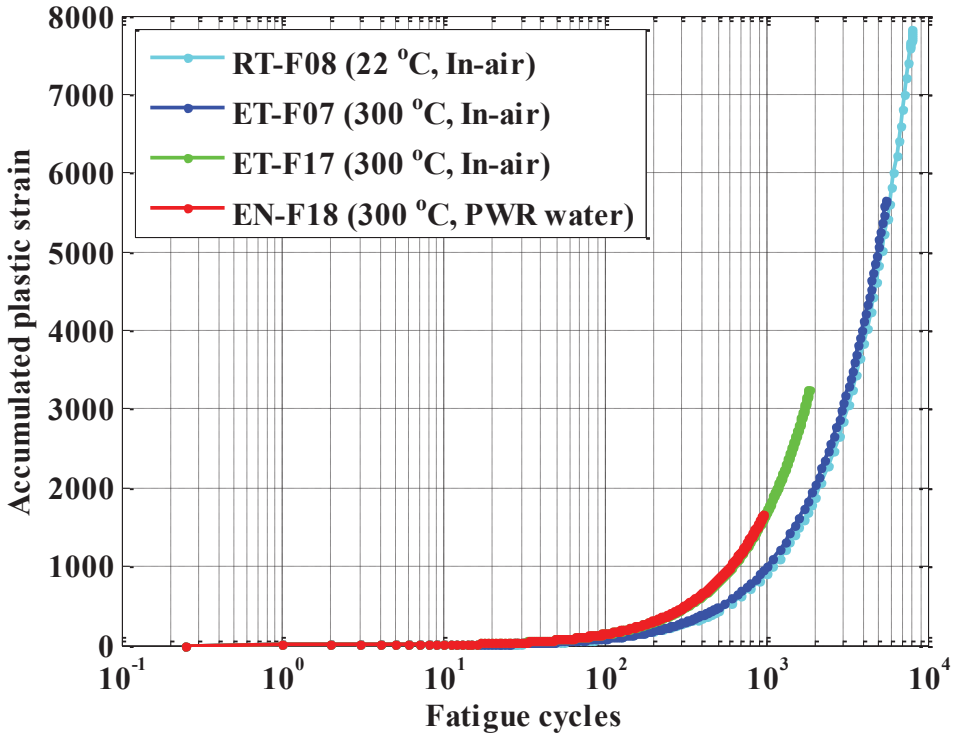

Figure 7. 13 Accumulated plastic strain for 316SS-316SS weld specimens fatigue tested under different conditions.

7.4 Elastic Limit Stress and Kinematic Hardening Parameters for 316 SS-316 SS Welds

Using the equivalent monotonic stress-strain curve, we estimated the stresses at an assumed elastic limit strain for different test cases (Table 7.1). As shown in Figure 7.14, the test method and temperature have a significant effect on the elastic limit stress histories. Following the procedure discussed in Section 2.3 and using the cyclic elastic limit stress as yield stress, we estimated the corresponding cyclic linear and nonlinear kinematic hardening parameters for the different test cases. Figure 7.15 shows the evolution of the linear kinematic hardening parameters (C1) for the different test cases. The curves indicate that the C1 is mostly sensitive to temperature and test method. In addition, we also estimated the cycle dependent nonlinear kinematic hardening parameters (C1 and $\gamma 1$) for the test cases (Figures 7.16 and 7.17, respectively). These figures indicate that C1 is mostly sensitive to temperature, whereas $\gamma 1$ is mostly sensitive to both temperature and test method (or stress/strain amplitude). Because of the cyclic strain hardening/softening in the stroke control test (EN-F18), increased/decreased strains are generated compared to the fixed strain amplitude in the case of the two strain control tests. Table 7.2 tabulates data elastic modulus, elastic limit stress, and the corresponding linear and nonlinear kinematic hardening parameters at selected fatigue cycles. This table also shows the corresponding tensile test parameters (elastic modulus, elastic limit, and kinematic hardening parameters) for comparison.

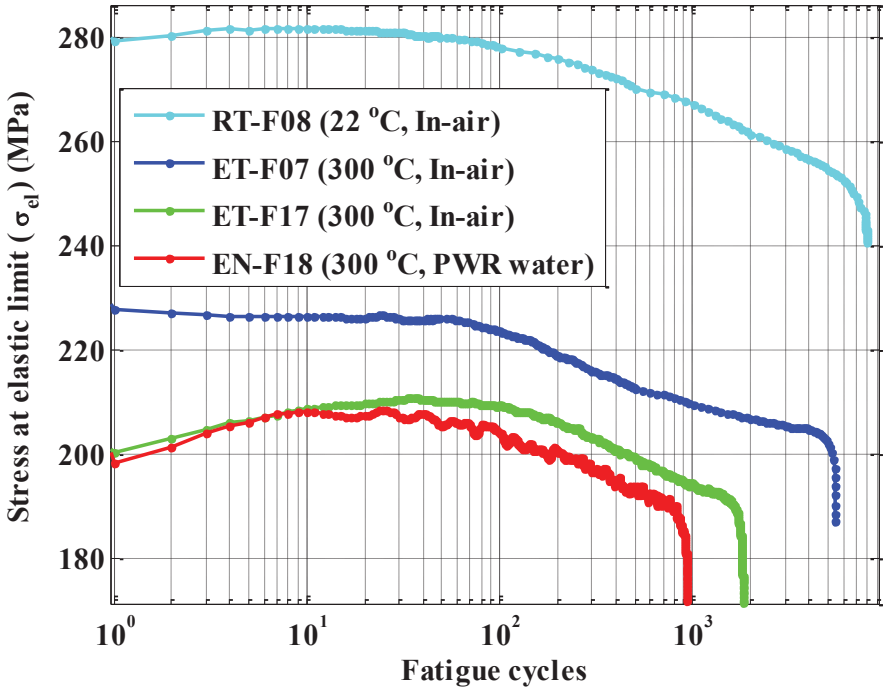

Figure 7. 14 Elastic limit stress for 316SS-316SS weld specimens fatigue tested under different conditions.

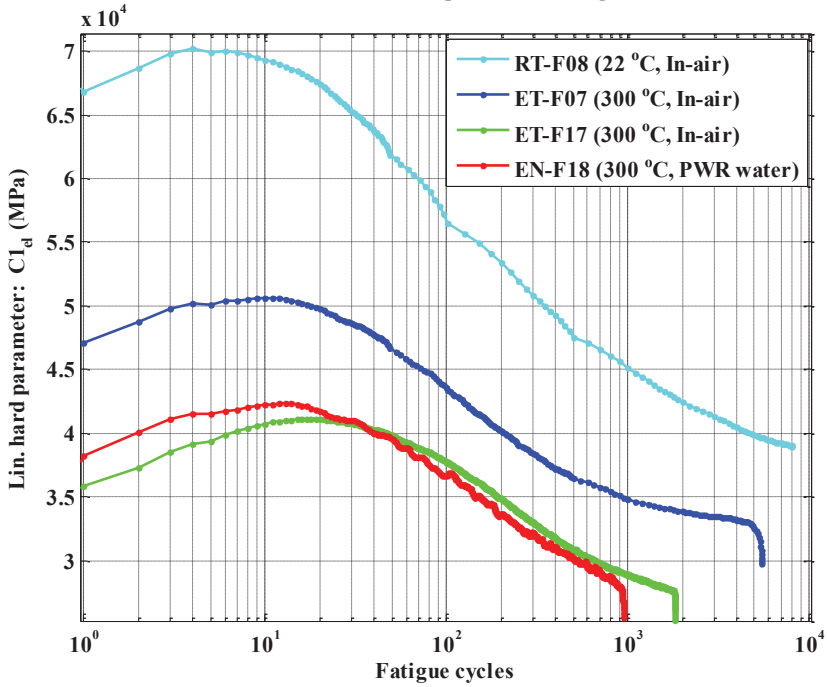

Figure 7. 15 Linear kinematic hardening parameter C1 (elastic limit stress used as yield stress) for 316SS-316SS weld specimens fatigue tested under different conditions.

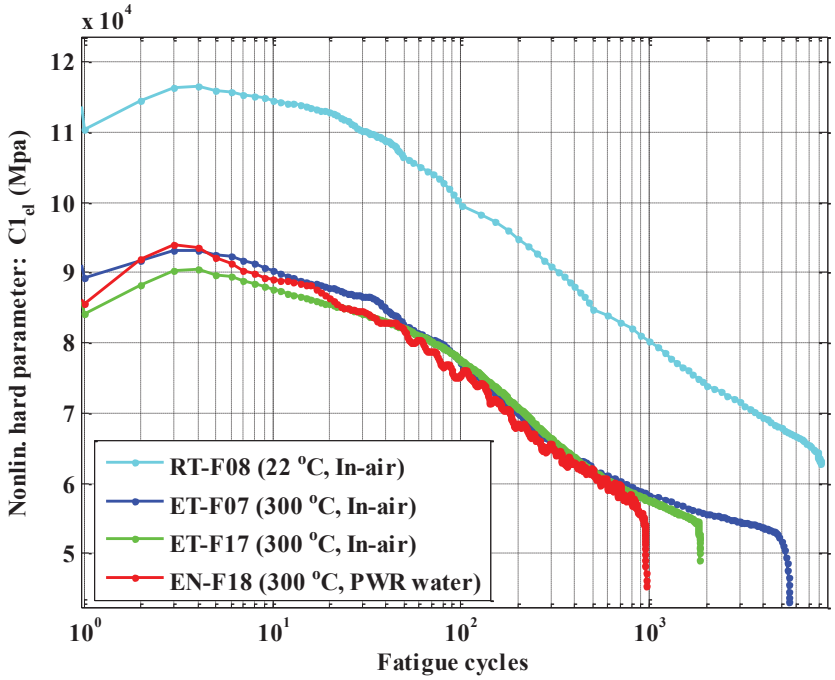

Figure 7. 16 Nonlinear kinematic hardening parameter C1 (elastic limit stress used as yield stress) for 316SS-316SS weld specimens fatigue tested under different conditions.

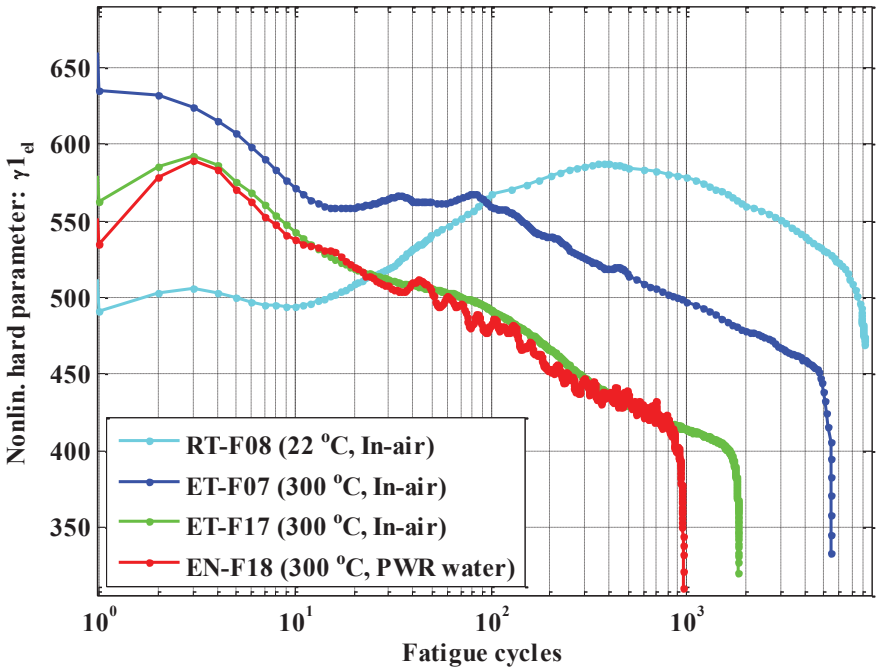

Figure 7. 17 Nonlinear kinematic hardening parameter γ1 (elastic limit stress used as yield stress) for 316SS-316SS weld specimens fatigue tested under different conditions.

Table 7. 2 Material model parameters (elastic limit stress used as yield limit stress) for 316 SS-316 SS weld specimens, at selected fatigue cycles and comparison with tensile test parameters.

Tensile test or fatigue test cycle no.		Env. type	E (GPa)	σ_{EL} (MPa)	Lin. Model C_1 (MPa)	Nonlin. Model C_1 (MPa)	Nonlin. Model γ_1 (MPa)
Tensile tests (RT→T03 and ET→T05 data)		RT	131.93	371.08	7523	43190	501.26
		ET	130.66	320.85	5531.6	21913	369.61
Selected fatigue cycles (RT-F08, ET-F17, and EN-F18)	Cy=1	RT	147.94	279.26	66863	1.1036e+05	491.14
		ET	121.39	200.2	35796	84228	562.64
		EN	120.66	198.44	38226	85532	535.05
	Cy=20	RT	148.91	281.22	67432	1.128e+05	508.55
		ET	126.78	209.73	41090	85524	519.12
		EN	125.06	207.41	41707	86367	520.05
	Cy=40	RT	148.54	280.18	63746	1.0885e+05	531.83
		ET	127.99	210.58	40293	83093	508.47
		EN	126.47	207.77	39974	82863	509.48
	Cy=N/4 for RT-F08=2001, ET-F17=460, and EN-F18=239	RT	143.29	261.38	42396	73972	559.93
		ET	125.87	199.92	31196	62403	432.68
		EN	124.55	198.91	32878	66817	448.1
	Cy=N/2 for RT-F08= 4001, ET-F17= 919, and EN-F18= 478	RT	141.67	256.63	40457	69407	539.64
		ET	123.58	194.37	29112	58045	416.3
		EN	122.21	193.4	30351	61796	434.94
	Cy=3N/4 RT-F08= 6001, ET-F17= 1379, and EN-F18= 717	RT	140.16	252.58	39480	66739	522.76
		ET	122.96	192.4	28133	55856	406.58
		EN	120.94	190.94	28854	58329	422.07

* RT, ET, and EN symbolize room temperature, elevated temperature, and PWR environment, respectively.

7.5 Comparison of 0.05% Offset Yield Limit Stress and Corresponding Kinematic Hardening Parameters for 316 SS-316 SS Weld

We estimated the cyclic evolution of 0.05% offset strain yield stress for the different test cases (Table 7.1). As evident from Figure 7.18, 0.05% offset strain stresses are broadly sensitive to test method (indirectly to stress/strain amplitude) and temperature. Based on the cyclic 0.05% offset strain yield stress, we estimated the corresponding cycle linear kinematic hardening parameters. As evident in Figure 7.19, the linear kinematic hardening parameters (C1) are broadly sensitive to both test method and test temperature. We also estimated the cyclic evolution of nonlinear kinematic hardening parameters C1 and γ1 with 0.05% offset strain yield stress (Figures 7.20 and 7.21, respectively). The curves indicate that C1 is mostly sensitive to temperature, whereas γ1 is sensitive to both temperature and test method. For numerical comparison, Table 7.3 tabulates the 0.05% offset-strain stress, elastic modulus, and linear and nonlinear kinematic hardening parameters at selected fatigue cycles. Also given are the corresponding tensile test parameters.

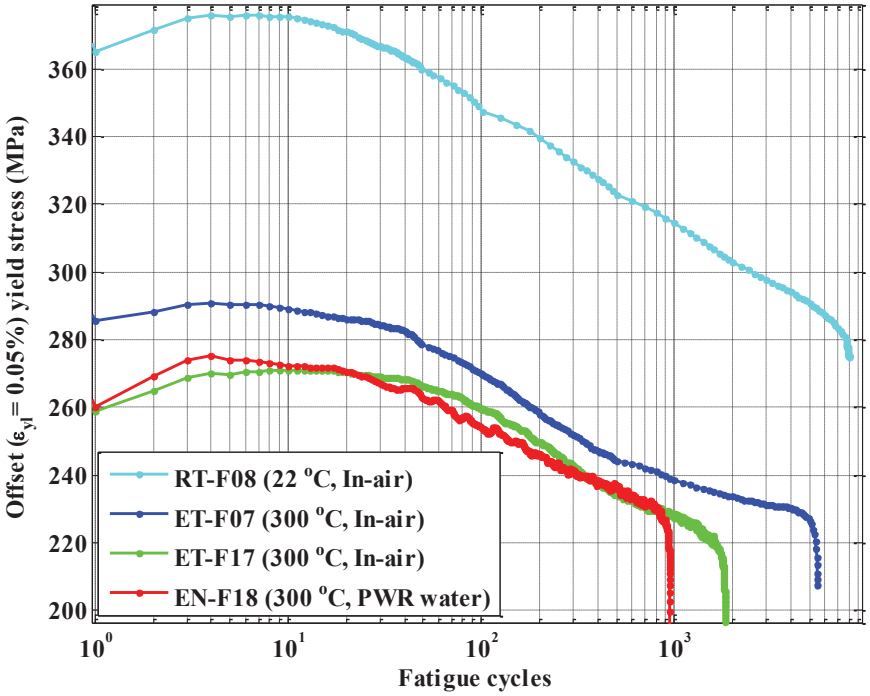

Figure 7. 18 Offset strain (0.05%) yield limit stress for 316SS-316SS weld specimens fatigue tested under different conditions.

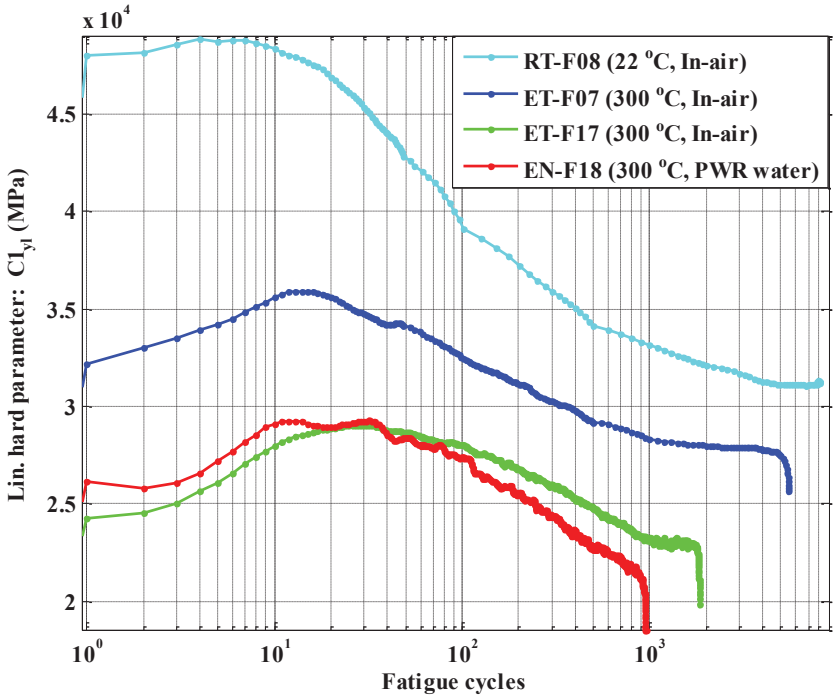

Figure 7. 19 Linear kinematic hardening parameter C1 (0.05% offset strain stress used as yield stress) for 316SS-316SS weld specimens fatigue tested under different conditions.

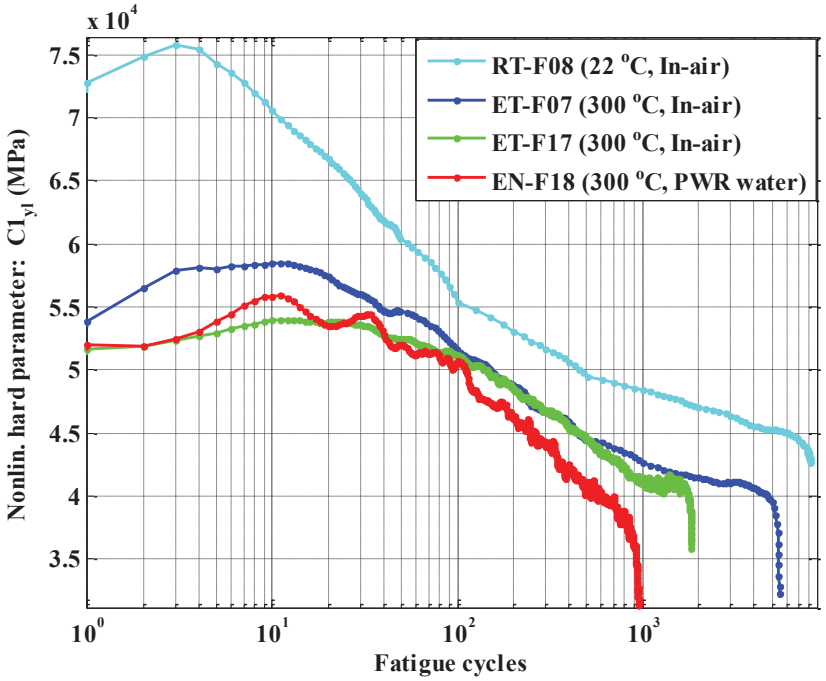

Figure 7. 20 Nonlinear kinematic hardening parameter C1 (0.05% offset strain stress used as yield stress) for 316SS-316SS weld specimens fatigue tested under different conditions.

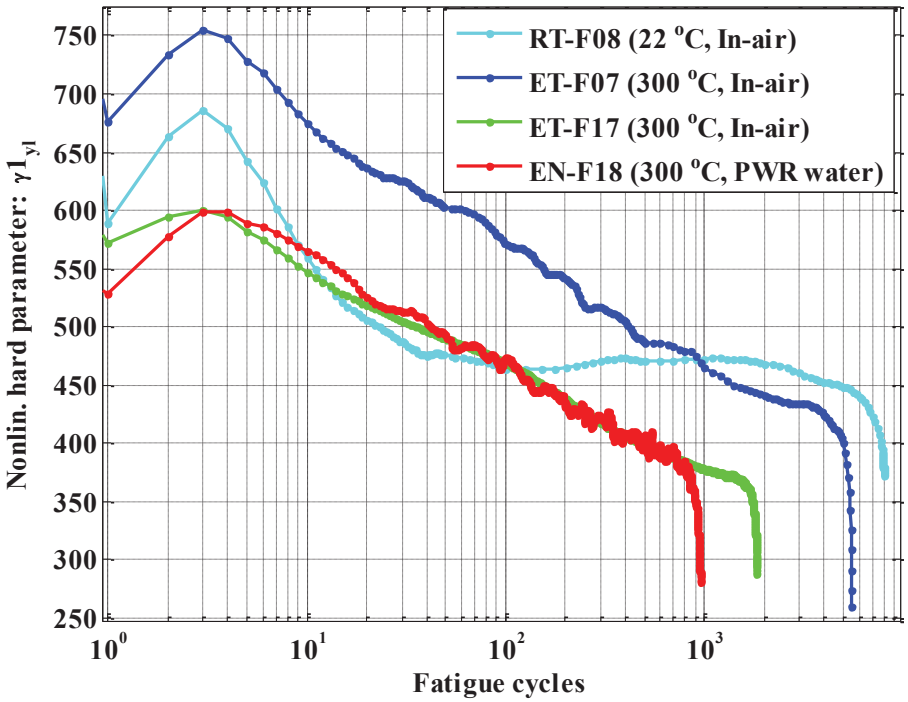

Figure 7. 21 Nonlinear kinematic hardening parameter γ1 (0.05% offset strain stress used as yield stress) for 316SS-316SS weld specimens fatigue tested under different conditions.

Table 7. 3 Material model parameters (0.05% offset strain stress used as yield limit stress)for 316 SS-316 SS weld specimens, at selected fatigue cycles and comparison with tensile test parameters.

Tensile test or fatigue test cycle no.		**Env. type**	**E (GPa)**	**σ_{YL} (MPa)**	**Lin. Model C_1 (MPa)**	**Nonlin. Model C_1 (MPa)**	**Nonlin. Model γ_1 (MPa)**
Tensile tests (RT→T06, and ET→T08 data)		RT	131.93	414.56	3223.3	5749.7	65.753
		ET	130.66	345.8	2593.6	4046.3	40.831
Selected fatigue cycles (RT-F08, ET-F17, and EN-F18)	Cy=1	RT	147.94	365.1	47990	72708	589.33
		ET	121.39	258.67	24275	51684	572.39
		EN	120.66	259.91	26157	52039	528.14
	Cy=20	RT	148.91	370.83	46930	66702	505.99
		ET	126.78	270.34	28864	53779	518.92
		EN	125.06	270.56	28964	53502	524.91
	Cy=40	RT	148.54	363.38	44019	61807	475.6
		ET	127.99	268.38	28764	52725	496.28
		EN	126.47	265.66	28551	52763	503.68
	Cy=N/4 for RT-F08=2001, ET-F17=460, and EN-F18=239	RT	143.29	302.62	32108	47037	468.34
		ET	125.87	235.41	24990	44971	402.13
		EN	124.55	242.4	25228	46059	432.1
	Cy=N/2 for RT-F08= 4001, ET-F17= 919, and EN-F18= 478	RT	141.67	294.03	31285	45555	452.69
		ET	123.58	228.88	23254	41336	379.9
		EN	122.21	236.28	22918	40859	399.59
	Cy=3N/4 RT-F08= 6001, ET-F17= 1379, and EN-F18= 717	RT	140.16	287.32	31115	45048	440.24
		ET	122.96	223.52	22950	40928	371.6
		EN	120.94	231.92	21957	39054	390.6

* RT, ET, and EN symbolize room temperature, elevated temperature, and PWR environment, respectively.

8 Summary and Future Study

This report presents tensile and fatigue test data for specimens of 508 LAS base metal, 508 LAS heat-affected zone metal (in 508 LAS-316 SS dissimilar metal weld), and 316 SS-316 SS similar metal weld. The tests were conducted in air at room temperature and 300 ^{o}C and in PWR primary loop water. Data are provided for time-independent tensile tests and time-dependent cyclic tests and include the following material properties: elastic modulus, elastic and offset strain yield limit stress, and linear and nonlinear kinematic hardening model parameters. From a comparison of experimental and model results under various test conditions, we concluded that:

1. The bulk fatigue lives of the 316 SS-316 SS weld specimens are sensitive to temperature, test method (indirectly to strain/stress amplitude), and PWR water environment at the tested strain rate of 0.01%/s.
2. The bulk fatigue lives of the 508 LAS specimens are sensitive to temperature and not to environment at the tested strain rate of 0.1%/s (note: the test method comparison was not made for the 508 LAS specimens).
3. The model parameters calculated for both 508 LAS and 316 SS-316 SS weld specimens are generally time/cycle dependent and broadly sensitive to temperature and test method (indirectly to strain/stress amplitude).

The overall objective of this report is to provide guidance for estimating hardening parameters based on tensile/fatigue tests. The material models and parameters reported in this report can directly be used by industry for FE fatigue and ratcheting evaluation of reactor components under in-air and PWR water conditions.

Suggested areas for the improvement of the discussed approach/models include the following:

1. Use FE models and perform parametric component-level stress and fatigue analysis to check the effect of time-dependent material parameters on overall fatigue lives.
2. Conduct tests under stress control and check how the related material properties compare to the corresponding fatigue parameters from stroke/strain control tests.
3. Conduct variable amplitude fatigue test and estimate material properties as a function of stress/strain amplitude and then compare results with random amplitude test results and material properties.
4. Conduct fatigue tests and material modeling under lower strain/stroke rates to study the effect of environment on material properties.
5. Conduct fatigue tests and material modeling under different hold conditions to study the effect of environment on material parameters due to different hold effects.

References

1. Mohanty, S., Soppet, W. K., Majumdar, S. and Natesan, K. "System-Level Heat Transfer Analysis, Thermal-Mechanical Cyclic Stress Analysis, and Environmental Fatigue Modeling of a Two-Loop Pressurized Water Reactor: A Preliminary Study," ANL/LWRS-15/1, http://www.osti.gov/scitech/biblio/1179020 (April 2015).
2. American Society of Mechanical Engineers, *ASME Boiler and Pressure Vessel Code*, Section III, Division 1 - Subsection NB (2013).
3. Nuclear Safety Standards Commission (KTA), "Components of the Reactor Coolant Pressure Boundary of Light Water Reactors," KTA 3201.2 Part 2, Design and Analysis, Salzgitter, Germany (2013).
4. Faidy, C., and Wazylyk, A., "Nuclear Fatigue Analysis Codified Design Rules Comparison of Cyclic Plasticity Effects," Proceedings of the ASME Pressure Vessels and Piping Conference, Paper No. PVP2015-45198 (2015).
5. Chopra, O. K., and Shack, W. J., "Effect of LWR Coolant Environments on the Fatigue Life of Reactor Materials," U.S. Nuclear Regulatory Commission Report No. NUREG/CR-6909 (2007).
6. Chopra, O., and Stevens, G., "Effect of LWR Coolant Environments on the Fatigue Life of Reactor Materials," U.S. Nuclear Regulatory Commission Report No. NUREG/CR-6909, Revision 1 (2014).
7. Japan Nuclear Energy Safety Organization, "Nuclear Power Generation Facilities Environmental Fatigue Evaluation Method for Nuclear Power Plants," Nuclear Energy System Safety Division, Japan Nuclear Energy Safety Organization Report No. JNES-SS-1005 (2011).
8. Kalnins, A., Rudolph, J., and Willuweit, A., "Using the Nonlinear Kinematic Hardening Material Model of Chaboche for Elastic–Plastic Ratcheting Analysis," *Journal of Pressure Vessel Technology*, *137*(3), 031006 (2015).
9. Rudolph, J., Kalnins, A., Götz, A., and Hilpert, R., "Local Ratcheting by Elastic-Plastic FEA — Criteria and Code Based Approaches," Proceedings of the ASME Pressure Vessels and Piping Conference, Paper No. PVP2011-57229 (2011).
10. Gilman, T., Weitze, W., Rudolph, J., Willuweit, A., and Kalnins, A., "Using Nonlinear Kinematic Hardening Material Models for Elastic-Plastic Ratcheting Analysis," Proceedings of the ASME Pressure Vessels and Piping Conference, Paper No. PVP2015-45674 (2015).
11. Shit, J., Dhar, S., and Acharyya S., "Modeling and Finite Element Simulation of Low Cycle Fatigue Behavior of 316 SS," 6th International Conference on Creep, Fatigue and Creep-Fatigue Interaction (Procedia Engineering), Vol. 55, pp. 774-779 (2013).
12. Yun, G. J., and Shang, S., "A Self-optimizing Inverse Analysis Method for Estimation of Cyclic Elasto-plasticity Model Parameters," *International Journal of Plasticity*, *27*(4), 576-595 (2011).
13. Pirondi, A., and Bonora, N., "Modeling Ductile Damage under Fully Reversed Cycling," *Computational Materials Science*, *26*, 129-141 (2003).
14. Chakherlou, T. N., and Ajri, M., "Strain Ratcheting and Stress Relaxation around Interference-Fitted Single-holed Plates under Cyclic Loading: Experimental and Numerical Investigations," *Fatigue & Fracture of Engineering Materials & Structures*, *36*, 327–339 (2013).
15. Mohanty, S., Soppet, W. K., Majumdar, S., and Natesan, K., "Environmental Effect on Evolutionary Cyclic Plasticity Material Parameters of 316 Stainless Steel: An Experimental & Material Modeling Approach," ANL/LWRS-14/1, http://www.osti.gov/scitech/biblio/1168233 (September 2014).

16. Mohanty, S., Soppet, W. K., Majumdar, S. and Natesan, K., "Pressurized Water Reactor Environment Effect on 316 Stainless Steel Stress Hardening/Softening: An Experimental Study," Proceedings of the ASME Pressure Vessels and Piping Conference, Paper No. PVP2015-45694 (2015).
17. Mohanty, S., Soppet, W. K., Majumdar, S., and Natesan, K., "Effect of Pressurized Water Reactor Environment on Material Parameters of 316 Stainless Steel: A Cyclic Plasticity Based Evolutionary Material Modeling Approach" Proceedings of the ASME Pressure Vessels and Piping Conference, Paper No. PVP2015-45701 (2015).
18. Mohanty, S., Soppet, W. K., Majumdar, S., and Natesan, K., "Report on Assessment of Environmentally-Assisted Fatigue for LWR Extended Service Conditions," ANL/LWRS-13/3, http://www.osti.gov/scitech/biblio/1168222 (September 2013).

This page intentionally left blank

Nuclear Engineering Division
Argonne National Laboratory
9700 South Cass Avenue, Bldg. 208
Argonne, IL 60439

www.anl.gov

Argonne National Laboratory is a U.S. Department of Energy laboratory managed by UChicago Argonne, LLC